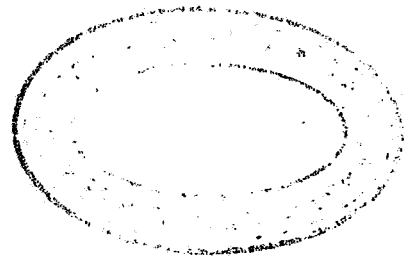# METAMORPHIC AND GEOCHRONOLOGICAL CONSTRAINTS ON THE KIMBAN OROGENY, SOUTHERN EYRE PENINSULA.

Betina R. Bendall B.Sc.

This thesis is submitted as partial fulfilment for the
Honours Degree of Bachelor of Science.
November 1994

The University of Adelaide
The Department of Geology and Geophysics

Australian National Grid Reference
Lincoln Sheet (SI 53-11) 1 : 250 000

Supervisors: M Sandiford, K Stuwe

TABLE OF CONTENTS

LIST OF TABLES AND FIGURES

Key to abbreviations used in text

amph	amphibole
bt	biotite
cd	cordierite
cpx	clinopyroxene
fspar	feldspar
gnt	garnet
kspar	potassium feldspar
hbl	hornblende
ilm	ilmenite
KMZ	Kalinjala Mylonite Zone
Ma	Mega anna ie. millions of years before present
my	million years
plag	plagioclase
qtz	quartz
REE	Rare Earth Elements

ABSTRACT

The Palaeoproterozoic Kimban Orogeny is responsible for widespread deformation throughout the Gawler Craton, but is best recorded in Hutchison Group metasediments and Lincoln Complex granitoids located near the east coast of southern Eyre Peninsula. Garnet-bearing granulite facies metabasic dykes of the Tournefort Dyke Swarm, emplaced during or prior to orogenesis, have been used to constrain the timing of peak metamorphism attributed to the Kimban Orogeny, via Sm-Nd mineral isochrons, at 1716 ± 14 Ma, approximately 100 Ma younger than previously believed. Estimates of P-T conditions recorded by the rocks were also calculated, in order to reconstruct a baric section across the Kimban Orogen. The dykes generally consist of the assemblages garnet-hornblende-plagioclase-ilmenite and garnet-hornblende-plagioclase-clinopyroxene-ilmenite. Peak assemblages involve garnet-orthopyroxene-clinopyroxene-plagioclase-hornblende-ilmenite. P-T estimates suggest a baric section across the Kimban Orogen is asymmetrical, and centred on the Kalinjala Mylonite Zone with metamorphic conditions of 840 ± 95°C and 10.1 ± 1.2 kbar adjacent to and within the Kalinjala Mylonite Zone, declining shallowly to the east to about 600°C and 5.4 ± 1.7 kbar about 24 kms across strike. This data in concert with structural evidence, suggests that the Kimban Orogen may have developed in an environment of oblique convergence, with associated strains partitioned between strike-slip movement along the Kalinjala Mylonite Zone, and a strike-normal component away from the zone, leading to the differential exhumation of granulite facies Lincoln Complex rocks east of the KMZ, and their juxtaposition against amphibolite-greenschist facies Hutchison Group rocks to the west.

1. INTRODUCTION

Convergent orogenesis involves the thickening of crust and burial of rocks with concomitant changes in the temperature and pressure conditions which are reflected in rocks by the growth of new equilibrium mineral assemblages (Thompson, 1992; Yardley, 1989). Individual rocks evolve along disparate P-T paths as they move through different parts of an orogenic belt in response to deformation and erosion, while spatial variations in metamorphic grade, reflect variation in the distribution of heat and strain associated with deformation at the orogenic scale (Winkler, 1979; Yardley, 1989). Importantly, in ancient orogenic belts, variations in pressure conditions recorded by rocks may provide a significant record of the distribution of crustal thickening strain. Reconstruction of baric sections through ancient orogenic belts should therefore provide substantial information about the crustal scale architecture of the orogen. This information provides an important data set independent of structural interpretation, which can be used to infer the nature of the orogenic environment. Moreover, spatial variation in P-T conditions will reflect in some manner, the nature of the heat sources responsible for metamorphism, whether they be transient, or regional and relating only to crustal thickening (Scholz, 1980; Winkler, 1979; Thompson, 1992).

In the southern Eyre Peninsula, the Kimban Orogeny (1845-1710 Ma) resulted in the formation of a fold belt which is exposed along the present east coast of the Eyre Peninsula (Parker, 1993). The dominant structural feature of this fold belt is the NNE trending Kalinjala Mylonite Zone (KMZ) (Figures 1 and 2). Juxtaposed across the KMZ are amphibolite facies metasediments of the Hutchison Group to the west and upper-amphibolite to granulite facies orthogneisses and granitoids of the Lincoln Complex to the east (Coin, 1976; Mortimer, 1984). The restriction of granulite facies metamorphism to Lincoln Complex rocks, including those incorporated in the KMZ, indicates there is a change in metamorphic grade across the zone. All previous workers have regarded the Kalinjala Mylonite Zone as a retrogressive feature representing the mid-crustal expression of a major lithospheric scale dextral strike-slip fault operative during the terminal stages of the orogeny (Parker and Lemon, 1982; Glen et al, 1977). However recent work at Pt Neill proposes that the KMZ is the locus of highest grade Kimban rocks (Oussa, 1993), and was certainly operative at peak metamorphic conditions. This suggests it may have been operative throughout the Kimban Orogeny, in which case formation of the Kalinjala Mylonite Zone may reflect partitioning of strain between strike-slip and strike-normal components in an obliquely convergent system. The evaluation of this hypothesis is the primary motivation for this study.

The aim of this study therefore, is to document spatial variations in metamorphic grade across the Kimban Orogen, and in particular the distribution of baric variations, in order to evaluate the gross architecture of the Kimban Orogen and the mechanical significance of the Kalinjala Mylonite Zone. Previous metamorphic studies have concentrated on the Hutchison

Group metasediments (Coin, 1976; Parker, 1978) and hence, this work will focus on the metamorphism of the Lincoln Complex in south eastern Eyre Peninsula. Exposures in the region are generally poor, with orthogneissic units predominantly exposed in narrow coastal platforms. Garnet-bearing mafic dykes which intrude the gneisses were targeted for study as these are widespread Kimban rocks which offer the best opportunity for determining peak metamorphic conditions (Bradley, 1972; Harley, 1988; Sengupta, 1993). The age of the Kimban Orogeny, and associated metamorphism in particular, are poorly constrained with most previous investigations concentrating on the description and interpretation of structure on the outcrop and map scales, and geochronology of the numerous granitic bodies intruding the area (Parker, 1978; Coin, 1976; Mortimer, 1984; Bradley, 1972). In order to evaluate the timing of peak metamorphism during the Kimban, Sm-Nd isotopic dating of mineral separates from two garnet-bearing mafic dykes was also undertaken. The dating of metamorphic assemblages rather than igneous minerals is potentially advantageous as it provides direct geochronological constraints on metamorphism rather than a range of dates during which metamorphism must have occurred (Cliff, 1985; Faure, 1986).
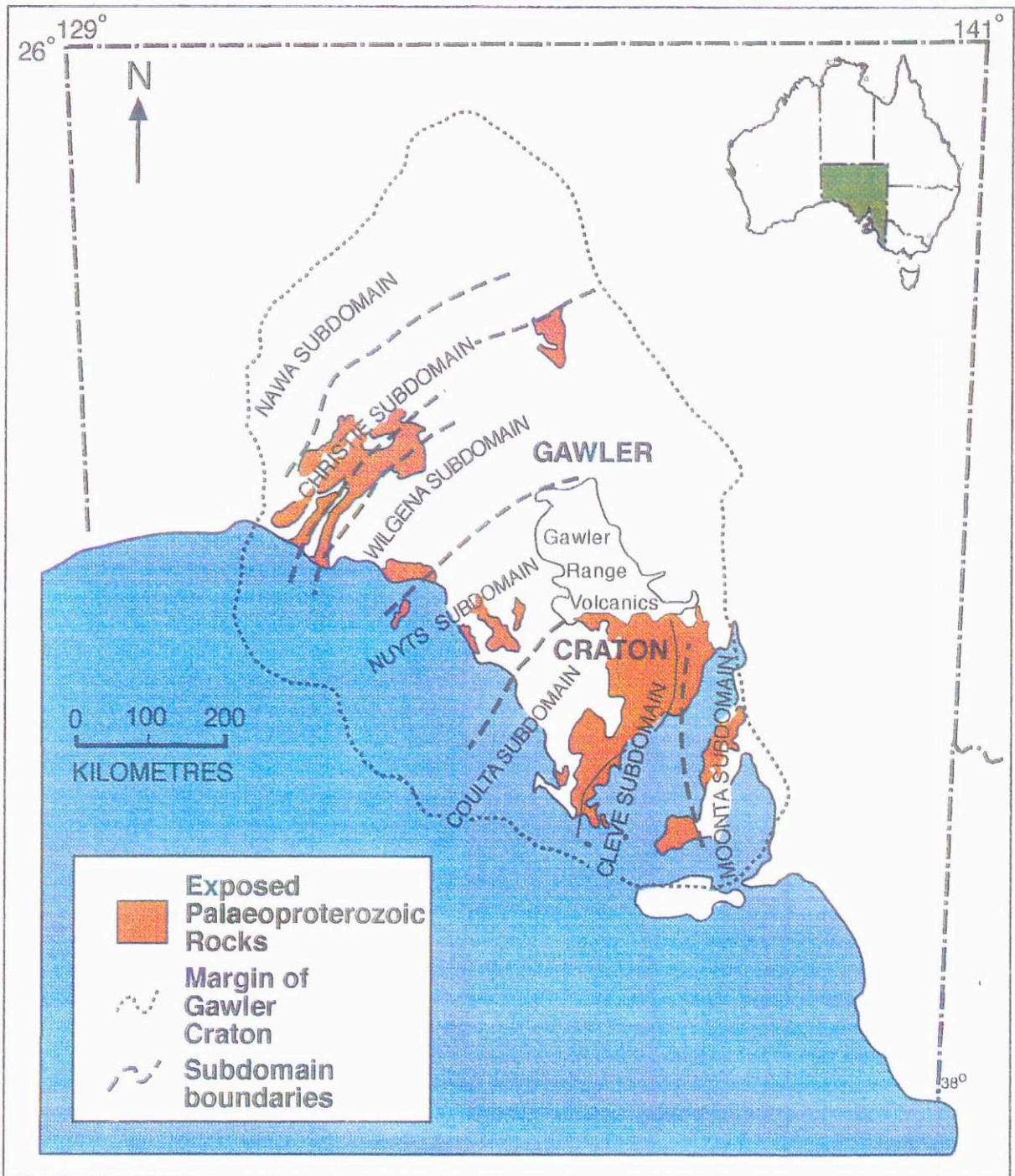
Figure 1. Locality Map of the Gawler Craton and subdomains.
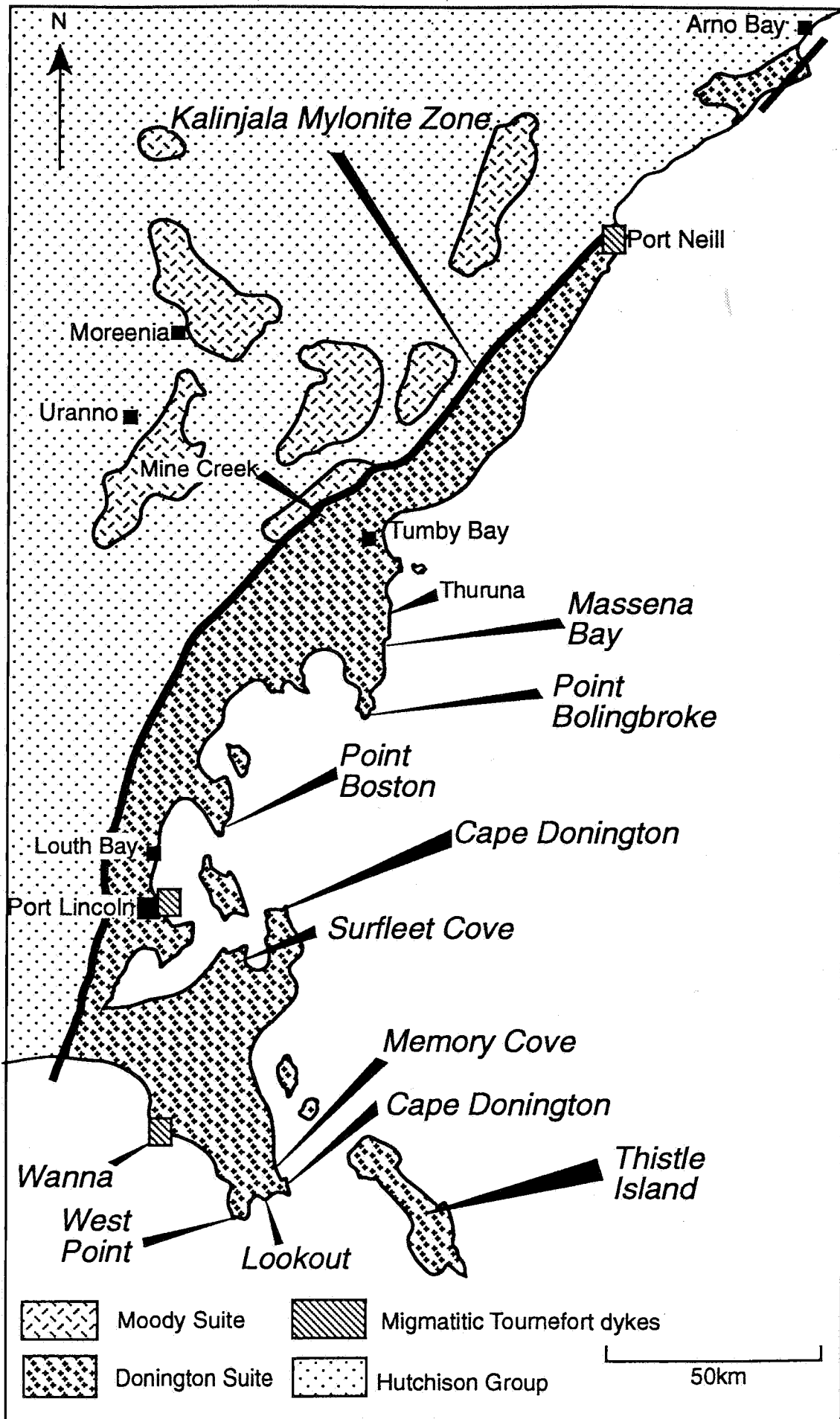
Figure 2. Locality Map and generalised geology of south eastern Eyre Peninsula

2. GEOLOGICAL BACKGROUND

2.1 The Kimban Orogen

The Kimban Orogen forms part of the Gawler Craton, a large region of Precambrian crystalline basement consisting of Archaean, Palaeo- and Mesoproterozoic granites, gneisses and metasediments (Fanning et al., 1986). The craton has been loosely divided into a series of subdomains, each of which is characterised by a distinctive and regionally homogeneous structural, metamorphic and stratigraphic style (Parker, 1990a) (Figure 1). The distribution of these subdomains and the successive younging of radiometric ages eastward across the craton, suggests progressive accretion of Proterozoic terrains (Parker, 1993). Two major periods of orogenesis have been experienced by the craton, namely the Sleaford Orogeny (2500-2300 Ma) whose effects are preserved predominantly in the Coulta subdomain and the Kimban Orogeny (1800-1700 Ma) which is best recorded in the Cleve subdomain (Parker et al., 1981).

The Cleve subdomain represents an orogenic belt extending the length of the Eyre Peninsula's east coast. The subdomain is dominated by the metasediments of the Hutchison Group derived from mixed shallow marine clastic and chemical sediments (including quartzites, schists, dolomites, iron formations and amphibolites) which unconformably overlie the Miltalie Gneiss and Sleaford Complex basement, and have been highly deformed and metamorphosed during the Kimban Orogeny (Parker et al., 1981; Webb et al., 1986; Fanning et al., 1988). These sequences are intruded by the voluminous granitoids of the Lincoln Complex which occur predominantly along the eastern margin of the domain and are juxtaposed against the Hutchison Group along the Kalinjala Mylonite Zone (Tilley, 1920; Parker and Lemon, 1982). However, the combined effects of extensive movement on the KMZ, together with Cainozoic cover largely obscures the stratigraphic relationship between the Lincoln Complex granitoids and the Hutchison Group, and the features produced by the Kimban Orogeny (Mortimer et al., 1988; Webb et al., 1986).

2.2 The Lincoln Complex and Tournefort Dyke Suite

In southern Eyre Peninsula, the Lincoln Complex is divided into three distinct granitoid suites, the Donington Granitoid Suite, the Colbert Suite and the Moody Suite which are temporally and geochemically distinct, (Table 1) although elsewhere the term Lincoln Complex, has been applied to many deformed intrusives of Kimban equivalent age (Parker, 1993; S. Daly pers comm.). These granitoids display various structural features considered by previous workers to be indicative of three discrete phases of tectonism associated with the Kimban Orogeny (Parker and Lemon, 1982; Fanning et al., 1988) and thus emplacement ages for these suites have been used to constrain timing of the orogeny.

Stratigraphic Unit	Description	Age
Lincoln Complex Equivalents	Symons Granite - foliated porphyritic granite and augen gneiss with feldspar augen.	1585 +/- 12 Ma 1700 - 1680 Ma
	Engenina Adamellite - weakly foliated adamellite with K feldspar phenocrysts	1641 +/- 38 Ma
	Carappee Granite - suspected Moody Suite equivalent. Coarse-grained granite, foliated.	1689 +/- 59 Ma
Moody Suite	Bungalow Granodiorite - foliated equigranular granite	1601 +/- 14 Ma
	Burkitt Granite - massive granite, unfoliated.	1655 +/- 61 Ma
	Moody Tank granite - massive granite believed to be syn-Kimban due to the presence of recrystallised quartz	1709 +/- 14 Ma (Rb-Sr: Mortimer et al, 1986a)
		1562 Ma (K-Ar biotite: Webb et al, 1986)
	Carpa Granite - unfoliated equigranular granite, considered as syn-Kimban.	1677 +/- 125 Ma (Rb-Sr: Webb et al, 1986)
Tournefort Dyke Swarm	Igneous textured dykes - fine grained doleritic dykes with relict igneous texture, intrude Lincoln Complex granitoids	1600 - 1550 Ma (Rb-Sr: Mortimer et al, 1988)
	Recrystallised dykes - massive to foliated hornblende-rich and pyroxene-rich transitional granulites, intrude Lincoln Comp granitoids.	>1710 Ma (Rb-Sr: Fanning, 1984a)
Middle Camp Granite	Granodiorite gneiss intruding Hutchison Group	1738 +/- 68 Ma (U-Pb zircon: Fanning, 1987a)
		1650 +/- 35 Ma (Rb-Sr: Webb et al, 1986)
Colbert Suite	Granite gneiss and hornblende granite	1757 +/- 14 Ma (Rb-Sr: Mortimer et al, 1986a)
Donington Granitoid Suite	Strongly foliated megacrystic granite gneiss and augen gneiss.	1794 +/- 40 Ma (Rb-Sr: Webb et al, 1986)
	Memory Cove Charnockite - locally foliated granite gneiss	1818 +/- 13 Ma (Rb-Sr: Mortimer et al, 1986a)
	quartz gabbronorite - massive to foliated gabbronorite.	1843 +/- 2 Ma (U-Pb zircon: (Mortimer et al, 1988)

Table 1. Summary of Lincoln Complex Lithologies (Modified after Parker, 1993)

Rocks of the Donington Suite (U-Pb zircon: 1843 ± 2 Ma) have D1, D2 and D3 foliations and occur as xenoliths in Colbert Suite granites (Rb-Sr whole rock: 1757 ± 14 Ma) which display the D2 fabric (Mortimer et al, 1988; Mortimer et al, 1986a). Therefore deformation is inferred to have a maximum age of 1845 Ma. The suggested minimum age for deformation is 1710 Ma, based on a Rb-Sr whole rock - mineral age from a little deformed pegmatite cross-cutting the Kalinjala Mylonite Zone at Pt Neill (Fanning, 1984a), however Rb-Sr and K-Ar ages on the Moody Suite, the Middle Camp Granite and other Lincoln Complex equivalents range between 1650 and 1562 Ma (Parker, 1993) (Table 1). This suggests either the Kimban Orogeny extends from 1845 to about 1600 Ma rather than 1710 Ma, or another heating event has reset the Rb-Sr and K-Ar systems at about 1600 Ma.

The Lincoln Complex granitoids are intruded by mafic dykes of the Tournefort Dyke Swarm (Bradley, 1972; Mortimer, 1984). These dykes occur either as deformed and recrystallised transitional granulites, or as relict igneous textured metabasites (Bradley, 1972). Parker (1993) suggests that the deformed dykes are syn-tectonic, and therefore must have been emplaced before 1710 Ma. A Rb-Sr age of 1600-1550 Ma has been calculated for the igneous textured dykes however, (Mortimer et al., 1986b) suggesting either a younger minimum age for the Kimban Orogeny (Webb et al., 1986), or resetting of the dykes' Rb-Sr system via a subsequent reheating event. Mortimer (1984) geochemically characterised the Tournefort Dyke Swarm as resulting from fractionation of a mantle derived magma with elemental signatures typical of Proterozoic mafic dykes. Using isotope geochemistry and model age calculations, previous workers have inferred that the Lincoln Complex represents the addition of new crustal material derived from a fractionated mafic source of similar composition to the Tournefort dykes, rather than a recycling of basement or Hutchison Group rocks (Mortimer et al., 1988).

2.3 Field Setting of the Tournefort Dyke Swarm

In the field, mafic dykes of the Tournefort Dyke Swarm commonly occur as massive or foliated, fine-grained dykes, layers or boudins which trend subparallel to the Kalinjala Mylonite Zone. The dykes occasionally include xenoliths of surrounding gneisses which clearly indicates that the dykes have intruded into the Lincoln Complex granitoids (Plate 1A). At locations within and adjacent to the Kalinjala Mylonite Zone such as Pt Neill and Kirton Point, the dykes and surrounding felsic gneisses are migmatised and highly strained (Plates 1B, 1C, 1D and Figure 2). However the fine-grained nature of these rocks means they often appear little or undeformed in hand specimen (Plate 1E), and contacts between the dykes and granitic gneisses are usually sharply defined (Plate 1F). Dykes may also occur as plagioclase phyric metabasalts which retain a relict igneous texture and may be discordant to the foliation in surrounding rocks (Plate 1G).

Plate 1.

A. Xenoliths of felsic gneiss within an igneous textured Tournefort mafic dyke clearly indicate the intrusive nature of the dyke. Surfleet Cove, Jussieu Peninsula.

B. A highly strained migmatitic mafic rock from Arno Bay.

C. The presence of two adjacent, yet distinctly different mafic dykes, demonstrates the disparity in the reaction of dykes to deformation and metamorphism. Both dykes are deformed, however one is migmatitic, while the other appears essentially undeformed. Wanna.

D. A migmatitic, deformed mafic dyke from Kirton Point.

E. A garnet-bearing mafic dyke from Lookout appears undeformed in hand specimen, but in thin section reveals a foliation.

F. Even in areas of high strain, contacts between felsic gneisses and mafic dykes are sharply defined. A photomicrograph of the contact between Memory Cove Charnockite and a mafic dyke at Cape Catastrophe indicates this relationship exists even at the microscopic scales. Field of view = 14 mm wide.

G. Mafic dyke retaining a doleritic texture, intruding felsic gneiss at Surfleet Pnt. The dyke cross-cuts the foliation in the felsic rock (indicated by the orientation of the pencil) suggesting intrusion has occurred late in the deformation history at this location.
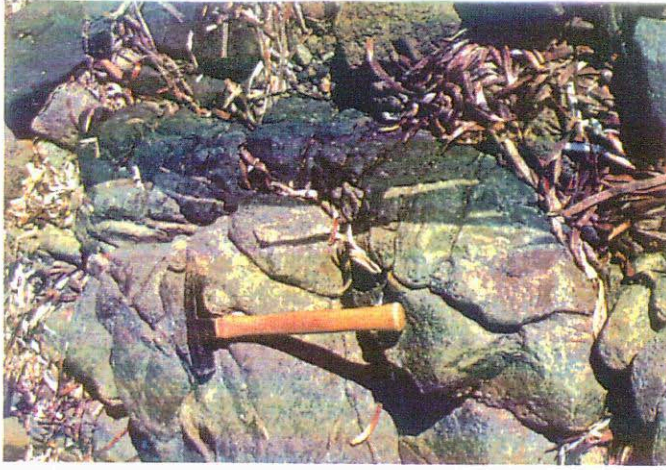
A
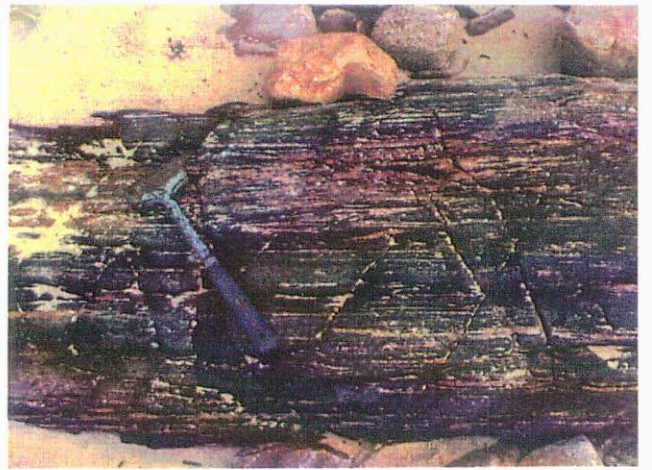
B

C
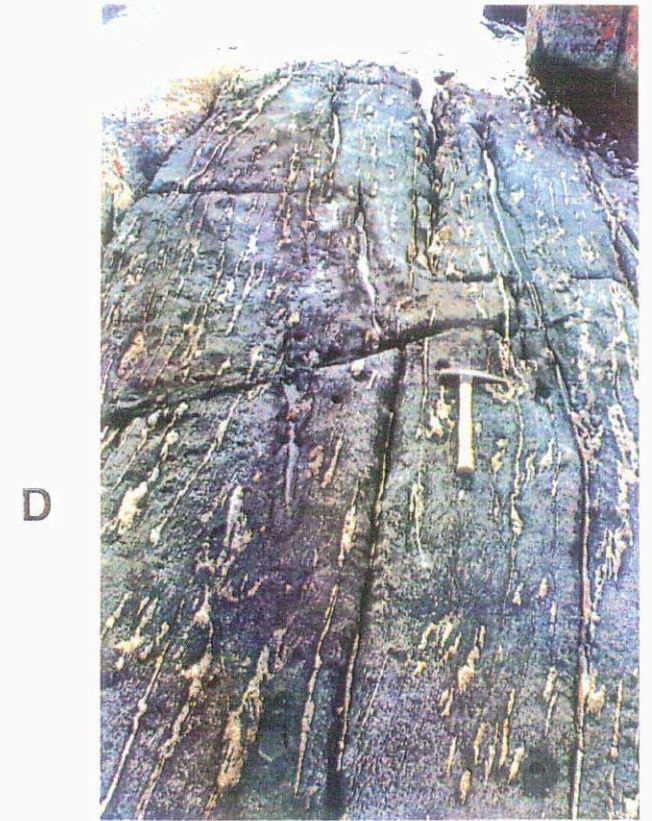
D

E

F
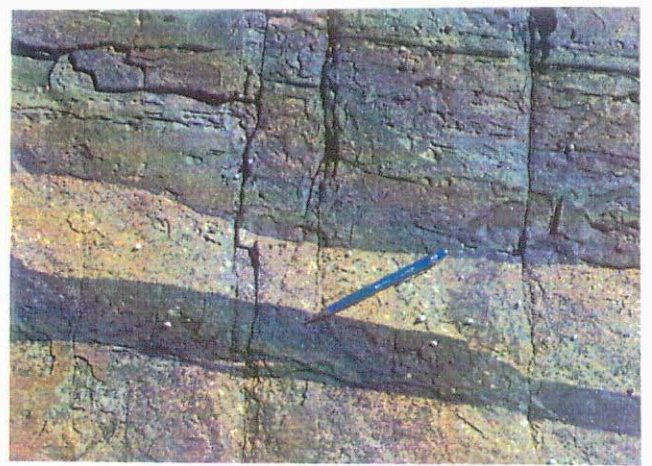
G

Despite the occurrence of both deformed and undeformed dykes in close proximity, cross cutting relationships between dykes are rarely observed, possibly because exposures are generally confined to narrow coastal strips. Superficially, the relict doleritic texture of the undeformed dykes and the Rb-Sr age of 1600-1550 Ma (Mortimer et al., 1986b) suggests emplacement of the dyke swarm may have occurred via multiple magmatic episodes which span a syn- to post-Kimban Orogeny period (Mortimer et al., 1988; Parker, 1993). However, deformation within the Lincoln Complex is heterogeneous, (Cohen and James, 1979) and therefore it can only be said that individual dykes were intruded late in the deformation history of the particular outcrop in which they occur, rather than post kinematic with respect to the entire orogenic episode.

2.4 Interpretations of Structural Evolution of the Kimban Orogen

The Kimban Orogeny has been characterised by previous workers (Parker, 1978; Parker and Lemon, 1982; Glen et al., 1977) in terms of three discrete, major tectonic events (D1, D2 and D3) responsible for the development of structures observed predominantly in Hutchison Group metasediments outcropping in the Cleve-Cowell area. These workers have described the initial phases of deformation and metamorphism (D1 and D2) as regional upper amphibolite facies metamorphic events throughout the Cleve subdomain and granulite facies locally (Parker, 1979; Parker and Lemon, 1982). The final stage (D3) has been interpreted as a major deformational event associated with retrogressive metamorphism to greenschist and amphibolite facies, and the formation of major shear zones including the Kalinjala Mylonite Zone (Parker, 1980a).

The Kalinjala Mylonite Zone is an important feature on Eyre Peninsula. It is a linear ductile deformational zone approximately 300 km long and up to 1 km wide, which trends subparallel to the present east coast of the Peninsula, cutting the coast at Pt Neill where it is best exposed (Parker et al., 1981; Parker, 1980a). Excellent exposures of the zone also occur in Mine Creek about 7 km west of Tumby Bay but apart from this, outcrop of the zone is largely obscured by cover sequences (Parker, 1980a). It has a well defined aeromagnetic signature and can be traced for most of its length between Sleaford Bay and the Middleback Ranges by this method (Parker, 1993). The KMZ includes a variety of lithologies from the Hutchison Group and the Lincoln Complex which have been variably deformed as gneiss through to ultramylonite (Plates 2A, B, C and D) (Coin, 1976; Parker et al., 1981). The asymmetry of porphyroclasts, pressure shadows and rhomboidal boudins indicates that movement along the zone is predominantly dextral and transcurrent (Parker, 1978; Clarke, 1976; Oussa, 1993) (Plate 2E) although occasional sinistral kinematic indicators are seen (Marmo, 1993; C. Simpson, 1994).

Plate 2.

A. Interlayered granite gneiss and felsic augen gneiss, approximately 2 km east of the Kalinjala Mylonite Zone in Mine Creek.

B. Sheared mafic dyke, approximately 1 km east of the Kalinjala Mylonite Zone, Mine Creek.

C. Felsic mylonite from within the Kalinjala Mylonite Zone, Mine Creek.

D. Cook Gap Schist (Hutchison Group) approximately 2 km west of the Kalinjala Mylonite Zone.

E. Asymmetrical feldspar porphyroclasts indicating a dextral sense of shear in a mylonitised pegmatite at Cape Catastrophe.

F. Complex deformation in a high strain zone on the west coast of Point Boston. Approximately 3m either side of this zone, rocks display simple planar fabrics, and about 10m east rocks appear essentially unstrained. The zone of complex deformation is bounded to the east and west by large (5m x 10m) mafic boudins.

G. The heterogeneity of deformation is demonstrated here by the presence of a local metre-scale shear zone concentrated at the contact between a mafic dyke and a granite. A smaller dyke intruding the granite indicates the unstrained nature of the rocks immediately adjacent to the shear zone, and the abrupt boundary between the deformed and undeformed rocks.

H. A boulder of mafic mylonite found on the beach between the high strain area of Lookout and the low strain area of West Point. Approximately 50m west of this boulder completely unstrained granites are located.
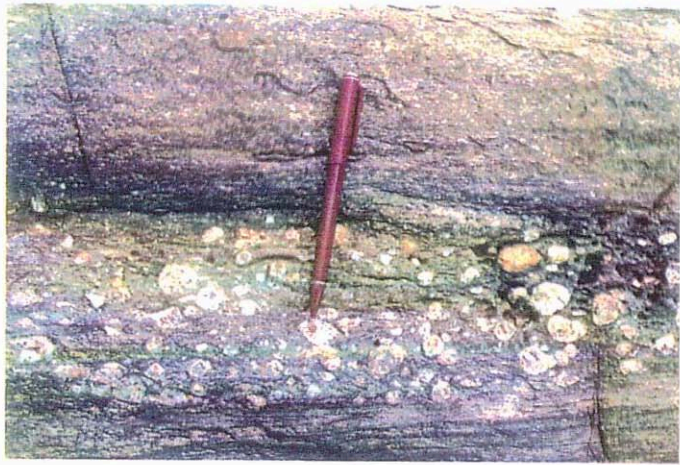
A
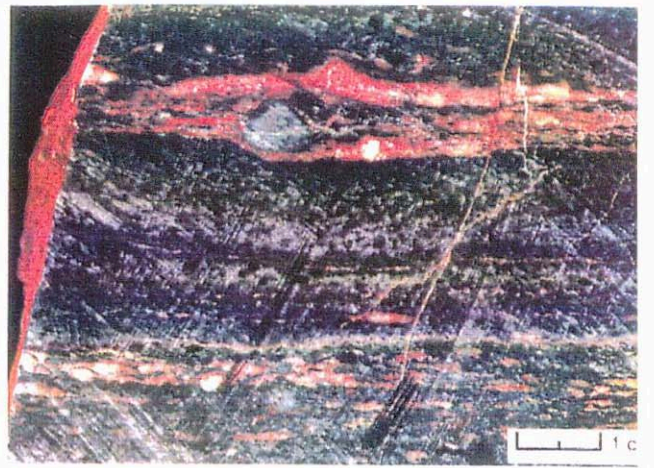
B
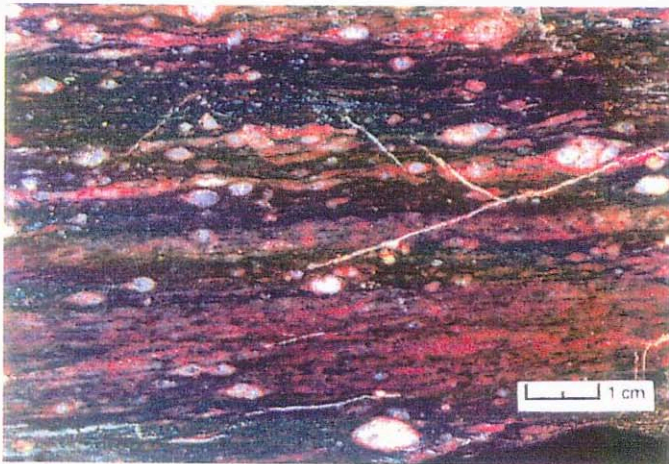
C
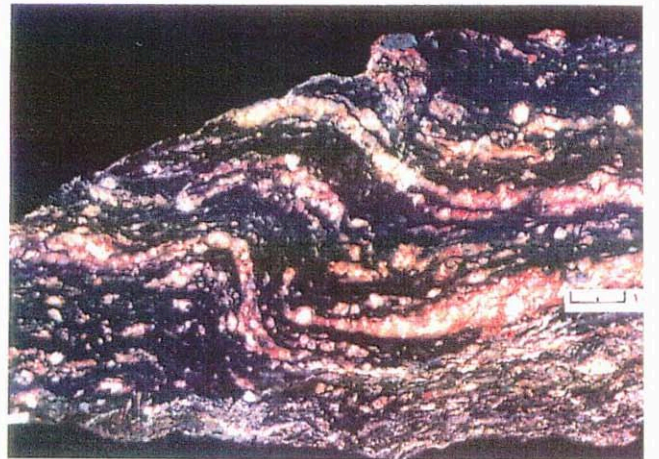
D
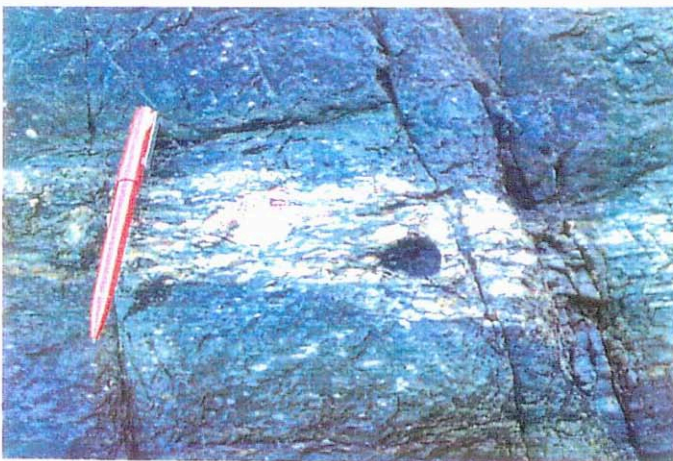
E

F

G

H

Plate 3.

A. Complex deformation at Lookout, an area of predominantly mafic rocks, intruded by pegmatities, located approximately 24 kms across-strike from the Kalinjala Mylonite Zone of the south coast of Jussieu Peninsula.

B. One of the few examples of a mafic dyke cross-cutting another dyke. This demonstrates the low-strain nature of West Point, approximately 2 km west of the high-strain zone at Lookout.

C. A local metre-scale shear zone cutting a garnet-bearing mafic dyke (sample no. A1028-98) at West Point.

D. Igneous textured mafic dykes intruding undeformed charnockite at West Point. This area is

located about 5m east of the deformed rock shown in Plate 2C.

E. A rare example of felsic rocks intruding mafics. Note the undeformed nature of the rocks. This outcrop occurs at West Point about 80 metres from the highly strained mafic rocks shown in Plate 2C.

F. In areas of high strain, strain often appears to be partitioned into felsic gneisses rather than mafic dykes which can often appear essentially undeformed or significantly less deformed.

A

B
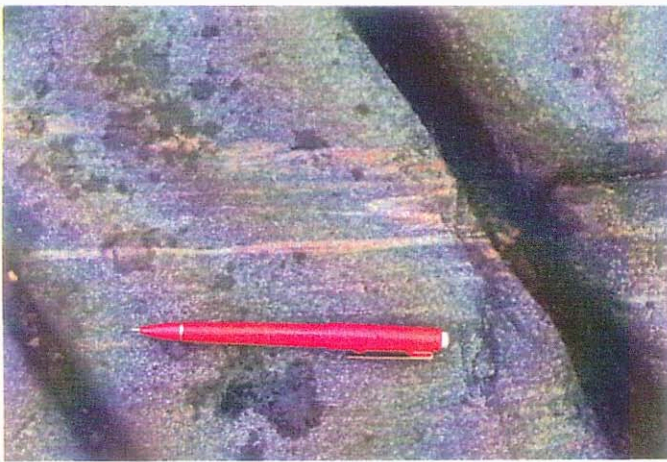
C
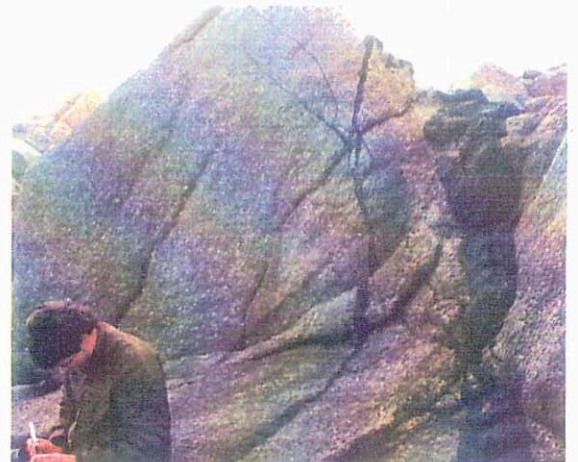
D

E

F

Although a series of discrete phases of deformation may be an appropriate structural interpretation for the Hutchison Group, recent work has indicated that deformation in the Lincoln Complex is associated with non-coaxial, progressive deformation (Oussa, 1993). The only substantial structural work undertaken on the Lincoln Complex rocks has been at Pt Neill by Clarke (1976) and Oussa (1993). Both workers suggest that the rocks in this area have undergone progressive deformation and that deformation is heterogeneous in nature. Clarke (1976) states that although various structures within the zone are able to be assigned to three deformational phases, no evidence exists to relate deformation in the mylonite zone to any single phase of deformation in the Hutchison Group. In the Kalinjala Mylonite Zone, the progressive nature of deformation is demonstrated by the consistent overprinting of dextral shear fabrics, while the co-linearity of all structures, across all lithological and structural boundaries, suggests discontinuities in planar fabrics result from progressive shearing rather than discrete overprinting events (Oussa, 1993; Ridley, 1986).

Areas of equally complex structure in Lincoln Complex rocks can also be observed at Pt Boston, Tumby Bay and Lookout. The heterogeneity of strain in these areas is evident by the occurrence of high-strain domains within generally low-strain regions (Plates 2F, 2G, 2H and 3A, 3B, 3C, 3D, 3E). These discrete high-strain zones undergo complex deformation including interference folding and appear to be localised by the presence of numerous mafic dykes (Plate 3F). Figures 3 and 4, and Plate 2B, show complex foliations form in the pressure shadows behind the mafic boudins, and areas of heterogeneous flow in felsic rocks between mafic dykes. These foliations are commonly tight to isoclinally folded, and the folds often propagate into the surrounding felsic gneiss. In contrast, adjacent areas of low-strain may be unfoliated, or have a simple linear or planar fabric with the same general orientation as structures in the areas of complex deformation. Fabrics in these regions of overprinting structures are defined by metamorphic assemblages recording the same metamorphic conditions (e.g. Oussa, 1993) suggesting these structures are essentially contemporaneous. If this is the case, then correlation of structures across the Lincoln Complex is not possible as complex deformation producing several foliations in a high-strain area may be concomitant with development of a weak foliation or single fabric in a low-strain area. Therefore an interpretation of the structural development of the Lincoln Complex in terms of progressive deformation rather than punctuated phases of deformation may be more applicable (Molnar, 1992).

The scheme outlined by previous workers (Parker and Lemon, 1982; Glen et al., 1977) for the structural evolution of the Kimban Orogeny, implies a regime of convergent orogenesis dominated initially by strike-normal partitioning of strain associated with NW-SE convergence, followed by dextral strike-slip movement along the KMZ during the terminal stages of tectonic development, as a consequence of the creation of topography in the region of maximum thickening (Figure 5). At Pt Neill, lineations within the KMZ are subhorizontal and defined by
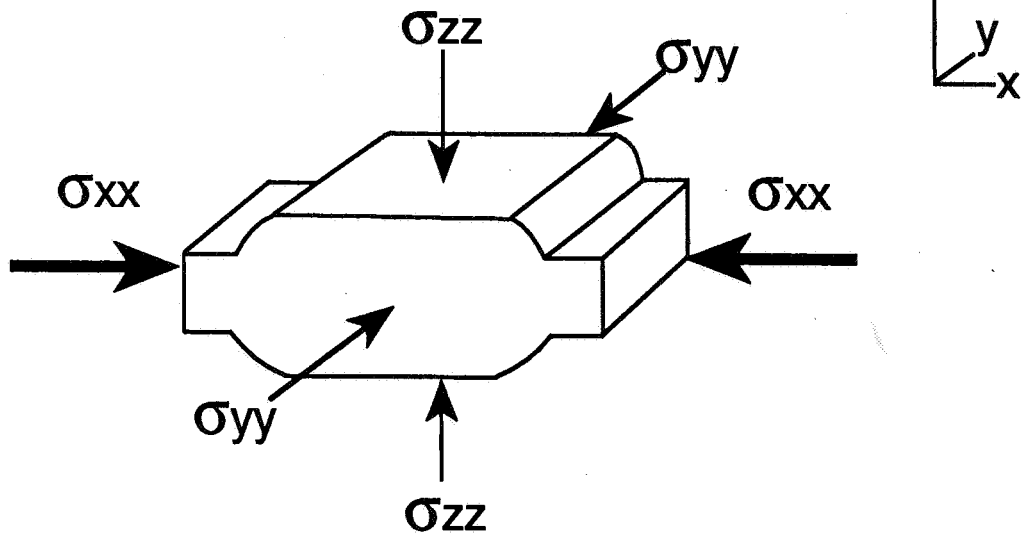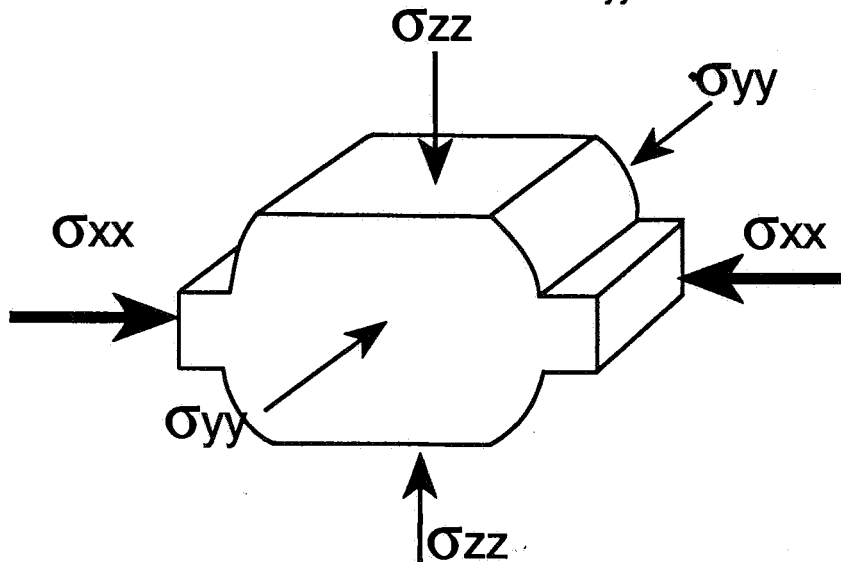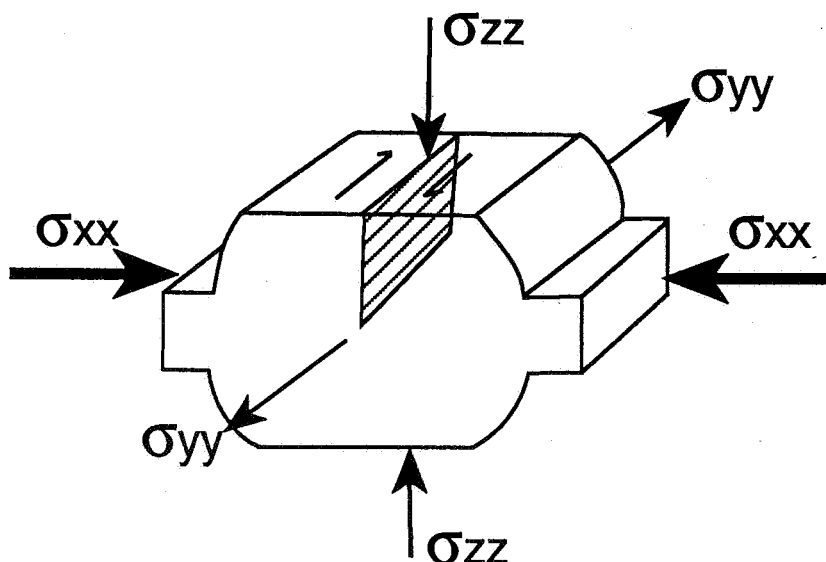
Figure 5. Formation of late stage strike-slip faulting during convergent orogenesis, resulting from the creation of topography.
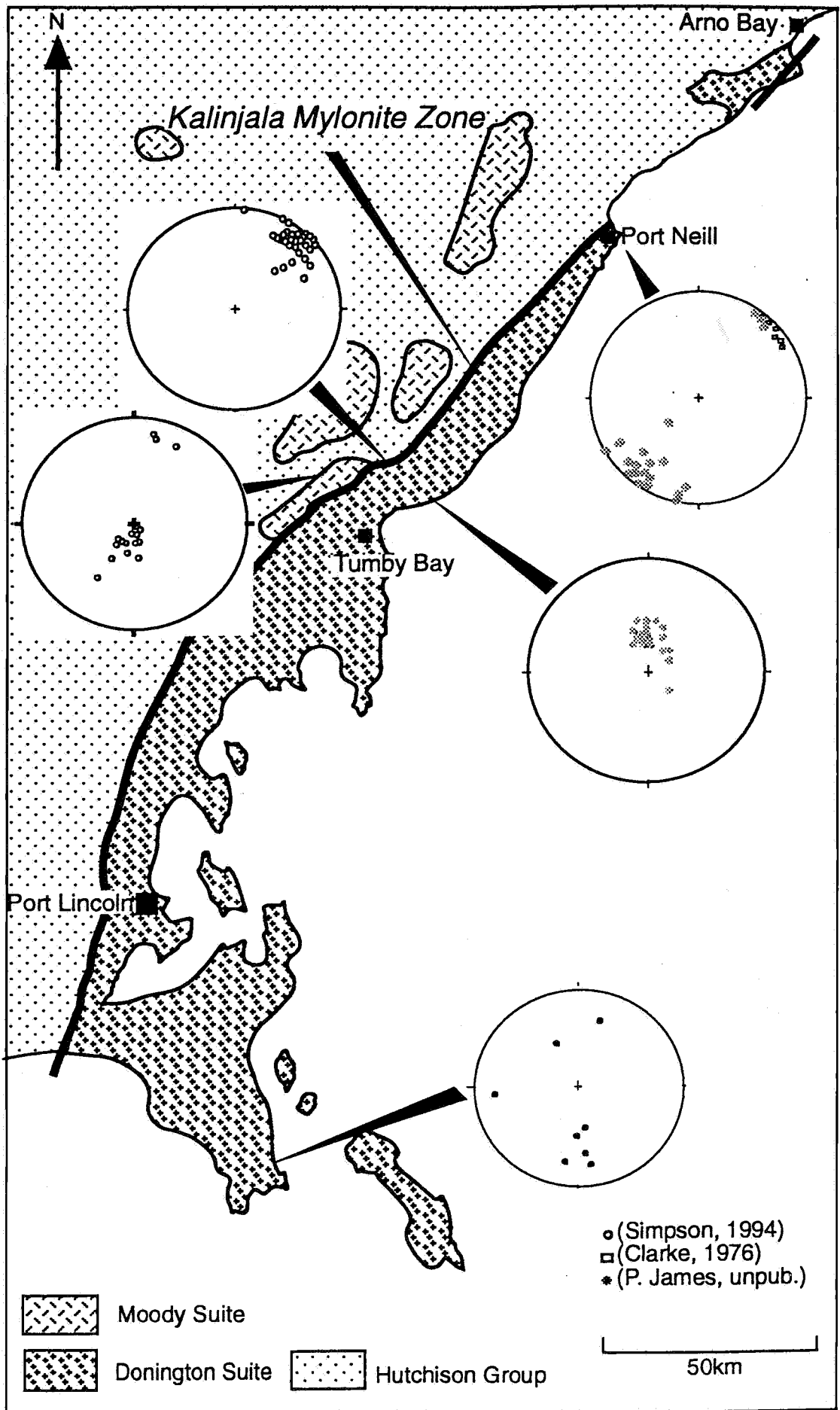
Figure 6. Distribution of lineations in the Cleve Subdomain

Map labels:
- N
- Arno Bay
- Kalinjala Mylonite Zone
- Port Neill
- Tumby Bay
- Port Lincoln

Legend:
- o (Simpson, 1994)
- □ (Clarke, 1976)
- ✳ (P. James, unpub.)
- Moody Suite
- Donington Suite
- Hutchison Group
- 50km

the highest grade mineral assemblages (Oussa, 1993). In Mine Creek, lineations within and adjacent to the shear zone are also shallowly plunging. Away from the KMZ, lineations also defined by high grade assemblages are steeply plunging and convergent, trending obliquely to the shear zone. These steep lineations are preserved in rocks within 2 to 5 km from the KMZ in the Tumby Bay and Mine Creek areas (Coin, 1976; Simpson, 1994) (Figure 6). These observations suggest that a transpressional regime operated during formation of the orogen, with oblique convergence partitioned into strike-normal and strike-slip components. The plausibility of such a regime is supported by many theoretical and empirical studies (Platt, 1993; Richard and Cobbald, 1990; Molnar, 1992).

3. METAMORPHIC GEOLOGY OF THE LINCOLN COMPLEX

3.1 Introduction

This section describes an investigation of the P-T conditions recorded in rocks east of the Kalinjala Mylonite Zone, in order to reconstruct a baric section across the Kimban Orogen. Metamorphism of the Hutchison Group has been investigated by previous workers and therefore a collation of their data will be used to constrain P-T conditions west of the KMZ (Coin, 1976; Parker, 1978). Although a minor component of the Lincoln Complex volumetrically, this study focuses on garnet-bearing mafic dykes of the Tournefort Dyke Swarm which intrude the Lincoln Complex granitoids, as these contain the most pressure sensitive mineral assemblages (Bradley, 1972). Additionally, since they are geographically widespread, they enable assessment of changes in pressure and temperature over a wide region. Calculations constraining P-T conditions for these rocks were performed using garnet-pyroxene (Powell, 1985) and garnet-hornblende (Graham and Powell, 1984) geothermometery, and the computer program THERMOCALC (Powell and Holland, 1988). Mineral analyses were performed on the Cameca SX 51 Camebax electron microprobe at the Centre for Electron Microprobe and Microscopic Analysis (CEMMSA) operating with an acceleration voltage of 15 kV and a beam width of 3 μm.

3.2 Petrography

Field relations of textural features of the mafic dykes allows division of the dykes into two groups. Those dykes retaining a relict igneous texture, and those which have been completely recrystallised during the Kimban Orogeny. Geochemical data for selected samples is presented in Appendix B, but cursory examination of this data reveals no obvious correlations between differences in bulk geochemistry and mineralogy.

3.2.1 Igneous textured mafic dykes

These dykes retain relict doleritic textures defined by randomly oriented grains of relict pyroxene with interstitial plagioclase. Moats of fine grained recrystallised metamorphic minerals surround these relict igneous grains implying they have undergone metamorphism in a low strain environment (Plates 4A and 4B). The dykes typically have hbl-plag-bi ± cpx ± gnt as metamorphic phases and relict igneous crystals of cpx-plag ± opx ± ilm (Plate 4B), which make up about 40-50% of the rock. Relict pyroxenes retain typical igneous compositions (Appendix C, Figure 2) and frequently display exsolution lamellae. Exsolution lamellae are never seen in metamorphic pyroxenes. Garnets occur typically in planar or linear arrangements, suggesting that garnet growth is associated with metasomatic activity (Plates 4C and 4D).

8

Plate 4.

A. Sample No. A1028-117, an igneous textured mafic dyke from Peake Point. The relict doleritic texture is defined by the random orientation of plagioclase and pyroxenes. Metamorphic minerals include fine-grained clinopyroxene, hornblende and plagioclase which form moats around the relict pyroxenes. Exsolution lamellae are present in the relict pyroxenes but do not occur in the metamorphic pyroxenes. Field of view = 4mm.

B. Sample No. A1028-6 from Memory Cove. Another igneous textured mafic dyke with the igneous mineral assemblage opx-cpx-plag-ilm. Exsolution lamellae are common in the relict pyroxenes. Metamorphic assemblages are very fine grained and form moats around the igneous pyroxenes. Field of view = 3mm.

C. Sample No. A1028-100, an igneous textured, garnet-bearing mafic granulite from West Point. This dyke contains the igneous assemblage opx-cpx-plag-ilm, and the metamorphic assemblage cpx-plag-hbl-gnt-qtz. Garnets occur in linear, vein-like arrangements suggesting a metasomatic origin. Field of view = 8mm.

D. Identical view as Plate 4C under crossed-polars.

E. Sample No. A1028-27, a recrystallised mafic dyke from Louth Bay, a low strain environment. This dyke has the mineral assemblage plag-cpx-hbl-gnt-bt-qtz, and displays a typical equigranular, granoblastic texture. Field of view = 8mm

F. Identical view as Plate 4E under crossed polars.

G. Sample No. A1028-98, a deformed mafic dyke from West Point, shown in hand specimen in Plate 3C. This rock occurs adjacent to A1028-99 (Plate 4H), and has the same assemblage of cpx-plag-hbl-gnt-qtz-ilm. Garnets in this rock occur in plagioclase-rich veins, in a similar manner to that observed in igneous textured dykes and pyroxene-rich recrystallised dykes. Field of view = 6mm

H. Sample No. A1028-99, a low-strain equivalent of A1028-98, with an identical mineral assemblage. This rock has a weak foliation defined by the preferred orientation of plagioclase and hornblende. Again, garnet occurs in linear arrangements suggesting metasomatic activity. Field of view = 6mm
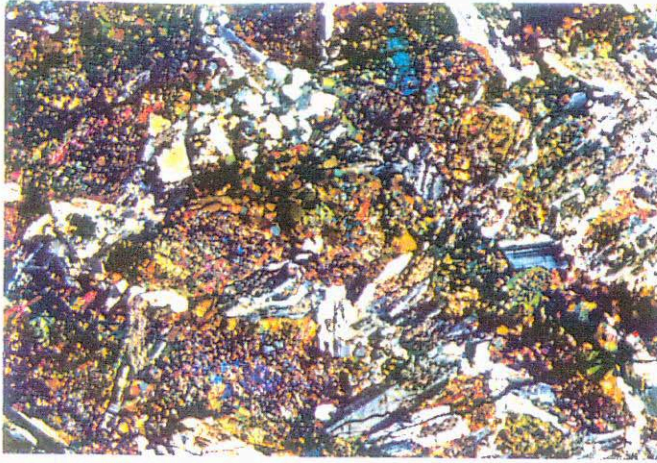
A
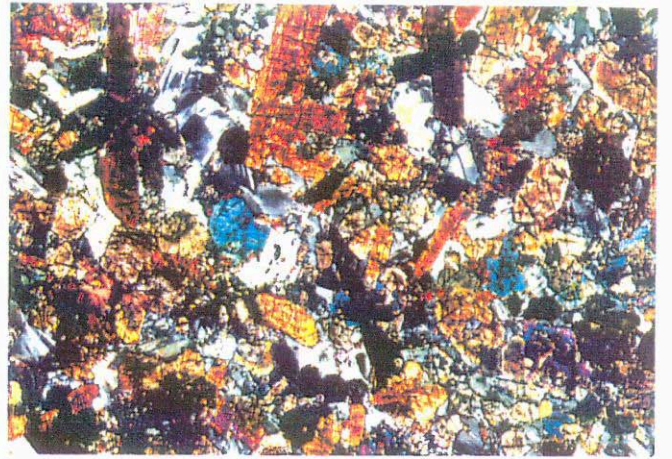
B
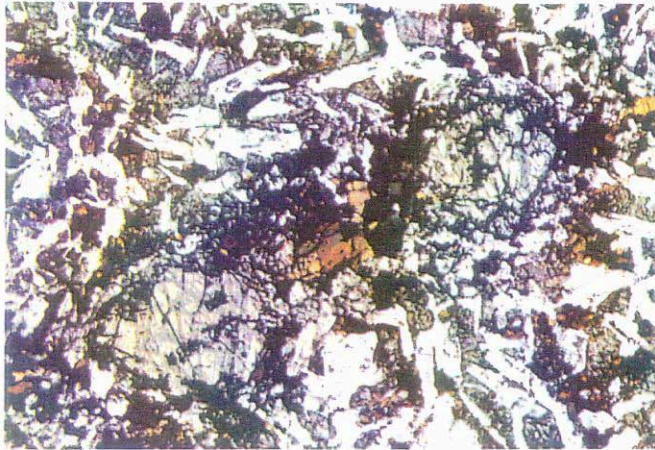
C
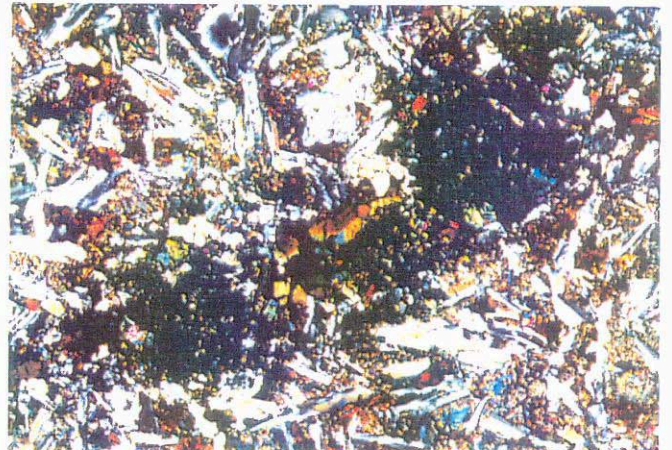
D
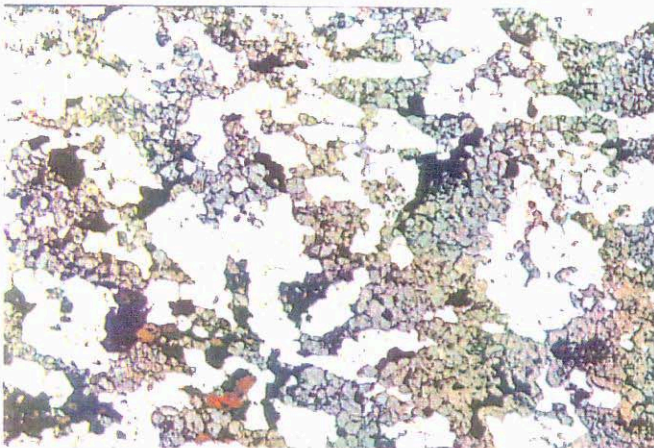
E
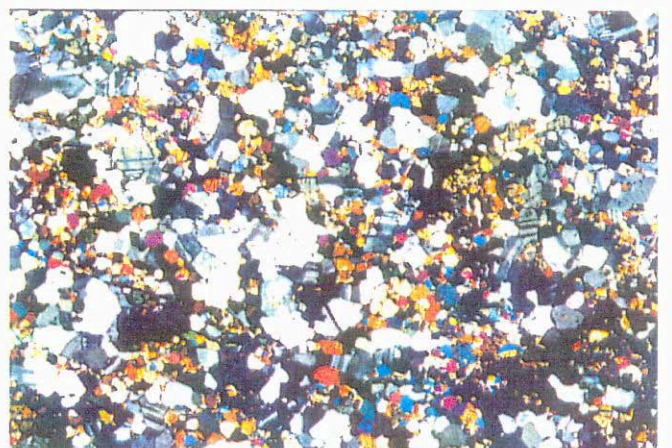
F
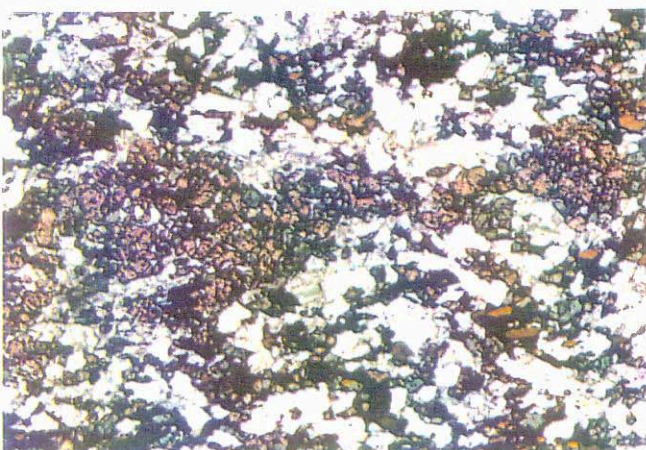
G
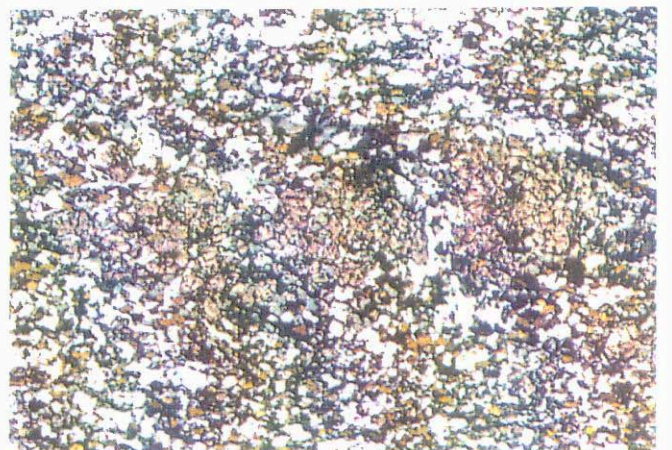
H

3.2.2 Recrystallised mafic dykes

These dykes contain texturally equilibrated assemblages consisting of the pyroxene-rich transitional granulite facies assemblage cpx-plag-ilm ± hbl ± opx ± gnt ± qtz, or hornblende-rich transitional granulites with the assemblage hbl-plag-bi-ilm-qtz ± cpx ± gnt (Green and Ringwood, 1967; Bradley, 1972; Harley, 1988; Spear, 1993). The pyroxene-rich dykes generally have an equigranular, granoblastic texture, but occasional relict pyroxenes can exist in these rocks (Plates 4E and 4F). Far from the KMZ, these dykes usually have a weak fabric, however some dykes are cut by local metre-scale shear zones and therefore are strongly foliated (Plate 3C). At Pt Neill these dykes occur within the shear zone, and are highly deformed. In garnet-bearing examples, garnet typically grows in linear or planar arrangements in association with plagioclase-rich veins (Plates 4G and 4H), similar to garnets occurring in igneous textured dykes.

Hornblende-rich mafic dykes intrude both the Lincoln Complex granitoids and the Hutchison Group metasediments. They form a wide band adjacent to the Kalinjala Mylonite Zone, and in the Lincoln Complex are always associated with relatively high strain zones, occasionally occurring as mylonites in minor shear zones cross cutting mafic granulite dykes (Plate 5A). As with the pyroxene granulites and igneous textured dykes, the garnet in hornblende-rich dykes is again associated with veins which are usually quartz and plagioclase-rich. In places these gt-plag-qtz segregations truncate the foliation defined by hornblende and biotite, but are themselves elongate parallel to the foliation suggesting syn-tectonic growth (Plate 5B). In hornblende-rich dykes intruding the Hutchison Group metasediments adjacent to the KMZ, garnet is prolific and predates the foliation, forming porphyroblasts around which the fabric wraps. The fabric is defined by the preferred orientation of hornblende, biotite and plagioclase (Plates 5C and 5D).

Reaction textures are uncommon in the recrystallised dykes, with typically only one textural generation of each mineral type. However in one mylonitized sample (sample no. A1028-12) from Lookout, very fine-grained second generation garnet has grown around porphyroclasts of primary garnet. The secondary garnet occurs in equilibrium with a recrystallised assemblage containing the same mineral phases as the sample's original mineral assemblage which are present as porphyroclasts (Plate 5E). This indicates that while grainsize reduction occurred during shear zone development, the P-T conditions were still within the stability field of the original assemblage. In a less deformed mafic dyke adjacent to the mylonite (sample no. A1028-13), a similar textural feature occurs, where fine-grained second generation garnet has grown around porphyroclasts of primary garnet. This secondary garnet is also interpreted to be in equilibrium with a mineral assemblage equivalent to the primary assemblage (Plate 5G). The mylonitic sample has the typical hornblende-rich assemblage of

Plate 5.

A. Sample A1028-21 a garnet-bearing hornblende-rich dyke from Kirton Point. This dyke has the mineral assemblage hbl-plag-gnt-bt-ilm-qtz, and displays a fabric typical of these dykes, defined by the preferred orientation of plagioclase and hornblende. Field of view = 8mm.

B. Garnets in hornblende-rich dyke A1028-21 typically occur in plagioclase and quartz-rich veins, in a similar style to those in igneous textured and recrystallised pyroxene-rich dykes. The veins commonly occur parallel to the foliation, but occassionally truncate it. Field of view = 15 mm.

C. Sample No. A1028-110 is a mafic rock interlayered with Hutchison Group metasediments approximately 3 kms west of the Kalinjala Mylonite Zone, in Mine Creek. This rock also has the assemblage hbl-plag-bt-gnt-qtz. However garnet is a common phase in the rock, and is evenly distributed throughout the rock, occurring as porphyroblasts around which the fabric wraps. Field of view = 8 mm.

D. Identical view to Plate 5C under crossed polars.

E. Sample No. A1028-12 a mafic mylonite from Lookout. This rock has an equilibrium mineral assemblage of hbl-plag-bt-qtz-gnt. These minerals are present in the matrix and as porphyroclasts. Around porphyroclasts of garnet however, very fine-grained secondary gnt-hbl-plag have crystallised. Field of view = 4mm.

F. Sample No. A1028-13 is a pyroxene-rich recrystallised dyke without a fabric, which occurs adjacent to A1028-12. This rock has the primary metamorphic assemblage of cpx-plag-hbl-gnt-ilm-qtz, and similar to A1028-12, a secondary assemblage crystallised around porphyroblastic primary garnets. In this instance however, the secondary assemblage is also cpx-plag-hbl-gnt. This suggests that deformation associated with formation of the mylonite occurred under metamorphic conditions equivalent to peak metamorphism. Field of view = 12mm.
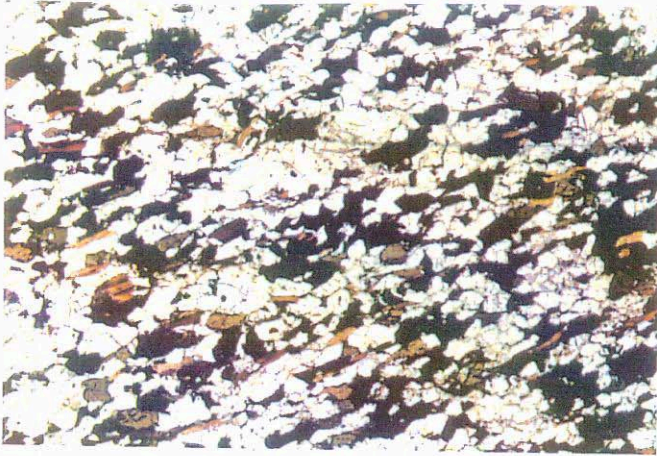
A

B
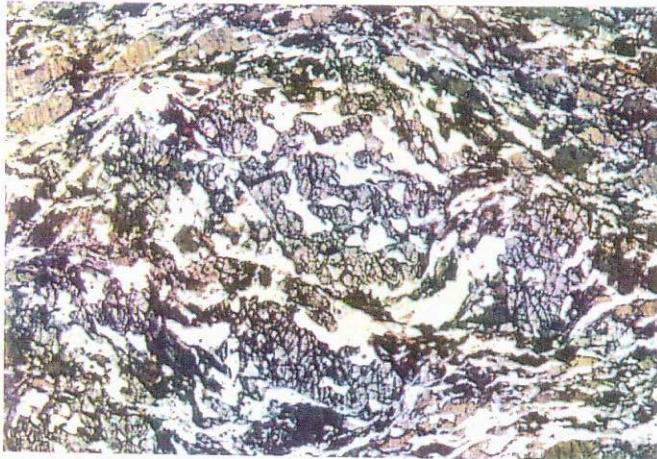
C

D
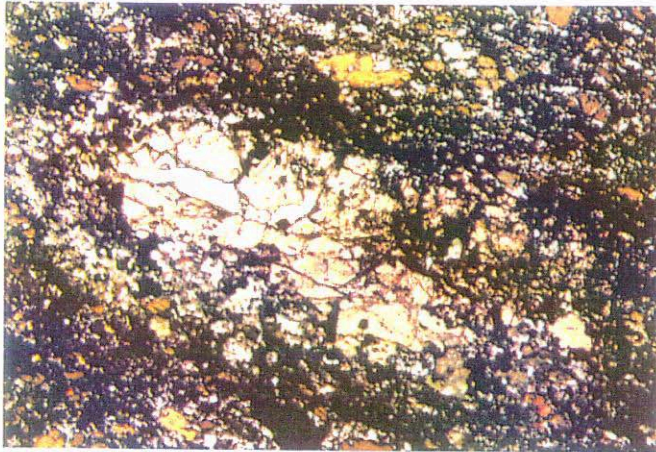
E
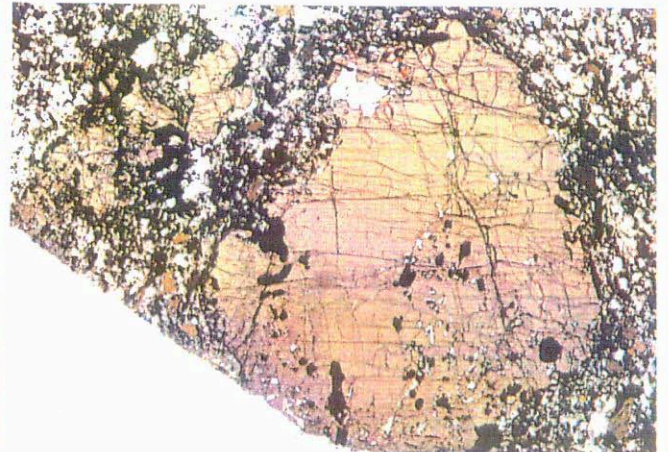
F

hbl-plag-bi-ilm-qtz-cpx-gnt described above, while the less deformed dyke is a pyroxene-rich mafic with the assemblage cpx-plag-ilm-hbl-gnt-qtz. The shear zone is a late stage feature which cross cuts another garnet-bearing granulite mafic dyke. This indicates that deformation was occurring under P-T conditions of at least transitional granulite facies.

The rarity of high-grade reaction textures and the fine-grained nature of the rocks are interpreted as indicative of rapid cooling (Ellis and Green, 1985; Harley, 1989; Barker, 1990). Alternatively the anhydrous nature of the rocks might indicate that paucity of a fluid phase during the cooling history inhibited further reaction. Overall these observations suggest that the mineral assemblages present in the mafic dykes record near peak metamorphic conditions, and deformation during the orogeny was associated with high grade metamorphic conditions. This implies that deformation attributed to D3 and movement along the Kalinjala Mylonite Zone was not retrogressive only.

3.3 Mineral Chemistry

Garnet in the mafic dykes is generally an almandine-grossular-pyrope mixture showing a relatively limited range of compositions within individual samples, and across the suite of samples as a whole. XFe, XMg and XCa of sampled garnets range from 0.695 to 0.645, 0.105 to 0.084 and 0.217 to 0.188 respectively (Appendix C, Figure 1). Exceptions to this are samples 1028-21 which is particularly almandine-rich (XFe = 0.668, XMg = 0.037) and 1028-100 which is pyrope-rich (XFe = 0.541, XMg = 0.254). The XCa values of the garnets in these dyke samples separates them from the almandine-rich garnets found in the pelites of the Hutchison Group (e.g. A1028-67). Garnets are generally unzoned, however garnets in samples A1028-100, A1028-119, and A1028-67, display a measurable rimward increase of XFe accompanied by slight decreases in XMg and XCa (Appendix C, Figures 4-7). The zoning profiles in the mafic rocks are similar to those reported for retrograde zoning in iron-rich, high-grade rocks elsewhere (Harley, 1988; Boullier & Barbey, 1988), but the rarity of such zoning in the dykes sampled suggests rapid cooling relative to diffusion (Thost et al., 1991). Two garnets in sample A1028-12 have decreasing XFe toward the rim, however these are adjacent to composite grains of ilmenite ($FeTiO_3$) (Appendix C, Figure 6). Other garnets in this sample do not display rimward zoning.

The lack of compositional zoning is also generally reflected in amphiboles and pyroxenes, with the exception of those samples which contain zoned garnets. Amphibole compositions are more diverse, but variation in their chemistry does not appear to reflect mineralogical differences, as amphiboles from granulite mafics or hornblende-rich mafics do not consistently plot together (Appendix C, Figure 3). The typical pyroxene in the mafics is clinopyroxene with orthopyroxene absent or only a minor component. As previously indicated, relict igneous pyroxenes often contain exsolution lamellae and have an igneous chemistry

(Appendix C, Figure 2). Interestingly relict igneous pyroxenes from sample A1028-100 do not display lamellae and have sub-calcic augite compositions.

3.4 P-T Estimates

Garnet-bearing mafic dykes were specifically selected for P-T work since the formation of garnet in mafic rocks is well known to be pressure sensitive (Schumacher et al, 1990; Vance and O'Nions, 1990; Mezger et al., 1992) enabling more accurate determination of baric variation across the Kimban Orogen. P-T estimates were derived using garnet-clinopyroxene and garnet-hornblende Fe-Mg exchange geothermometers (Powell, 1985; Graham and Powell, 1984), and the average P-T or average P routines in the computer program THERMOCALC (Powell & Holland, 1988).

3.4.1 THERMOCALC

The critical information required for use of THERMOCALC is the identification of an equilibrium mineral assemblage. The end members which constitute this assemblage are incorporated in a set of independent reactions whose P-T locations are constrained by the internally consistent data set of Holland and Powell (1990). These independent reactions are combined to produce a weighted pressure-temperature estimate. The calculated answer is then subjected to a chi squared test which is expressed as a σ_{fit} value. If the σ_{fit} is below a given value for the number of independent reactions, the calculated answer is passed at 95% confidence. A well constrained answer is generally achieved if an equilibrium assemblage is preserved, and sufficient independent reactions with favourable P-T slopes can be generated.

End member activities have been calculated using the computer program AX (T. Holland pers comm). This utilises the site mixing model for hornblende from Holland and Powell (1990) and Fe^{3+} calculation from Holland and Blundy (1994). The mixing model for garnet is from Newton and Haselton (1981) and for biotite, the site mixing model of Holland and Powell (1990) is used with activity coefficients from Eugster et al (1972). Feldspar activities are calculated from Holland and Powell (1992) and pyroxene activities assumed ideal 2-site mixing. Examples of P-T calculations are shown in Appendix C (Figures 8-16).

3.4.2 Methodology

In rocks that appear to have been migmatitic during peak metamorphism, THERMOCALC calculations were performed for a range of water activities on a selection of samples from varying distances across strike from the Kalinjala Mylonite Zone. Variations in water activity were applied in order to assess the dependence of the calculated P-T on aH_2O.

This approach was employed since precise determination of aH_2O in rocks is difficult (Green and Ringwood, 1967; Phillips, 1980). In samples where garnets clearly grew in veins, calculations were performed assuming a fluid was present during metamorphism. In these cases, calculations were done for a range of H_2O-CO_2 mixtures, since fluid inclusions in high grade rocks are commonly composed of this mixture (Harley, 1989). Additionally where samples permitted, calculations were performed on anhydrous sub-assemblages within the complete assemblages. P-T estimates from such assemblages are not hampered by the lack of knowledge of the metamorphic fluid composition.

In the calculated assemblages, pressures are essentially isobaric over a range of temperatures and water activities (aH_2O) or fluid compositions (XH_2O) (Appendix C, Figures 8-16). This indicates that although temperature is poorly constrained for these rocks, the assemblages are pressure sensitive. Thus in order to produce a coherent baric section from this data, a number of broad but geologically reasonable rationalisations were made to constrain the variables of temperature, water activity and XH_2O. In the field, a decline in temperature away from the mylonite zone is suggested from the distribution of migmatisation, mentioned in section 2.2 (Figure 2). Schumacher et al (1990) determined that melting can be initiated in mafic rocks at metamorphic temperatures as low as 660^oC at pressures of ~ 5-6 kbars, however most of the mafic rocks in this study can be described as transitional granulites as they commonly contain both pyroxenes and amphiboles (Harley, 1989; Spear, 1993; Green and Ringwood, 1967). Transitional granulites frequently occur at temperatures of 700 - 750^oC without melting (Harley, 1989) therefore it is apparent that the mafic dykes intruding the Lincoln Complex could have experienced temperatures in the range of 650^oC to 700^oC during the Kimban, without significant melt production. In an attempt to corroborate these inferences, temperature estimates were calculated using garnet-pyroxene (Powell, 1985) and garnet-hornblende (Graham and Powell, 1984) geothermometers (Appendix C, Figure 17). The results of these calculations are generally within the expected temperature range for most of the samples, however estimates for some samples lying close to the Kalinjala Mylonite Zone are lower than expected for the migmatitic character of rocks in the vicinity of the sample site.

A feature of the migmatitic rocks is their hornblende-rich composition. Therefore in these rocks it is concluded that $aH_2O>0.2$, since hornblende would undergo dehydration reactions to form pyroxene (Phillips, 1980; Green and Ringwood, 1967) below this value. As no evidence of such reactions are observed in thin section, water activities must have been above this value, however activities greater than 0.75 tended to produce unreasonably high pressure estimates. Therefore an $aH2O = 0.5$ was taken as a reasonable estimate of water activity in hydrated rocks and $aH2O \leq 0.25$ in hornblende-poor rocks.

In rocks where the occurrence of veins suggested that a fluid phase existed during metamorphism, calculations with pure water or near-pure $CO2$ as fluid phases also consistently
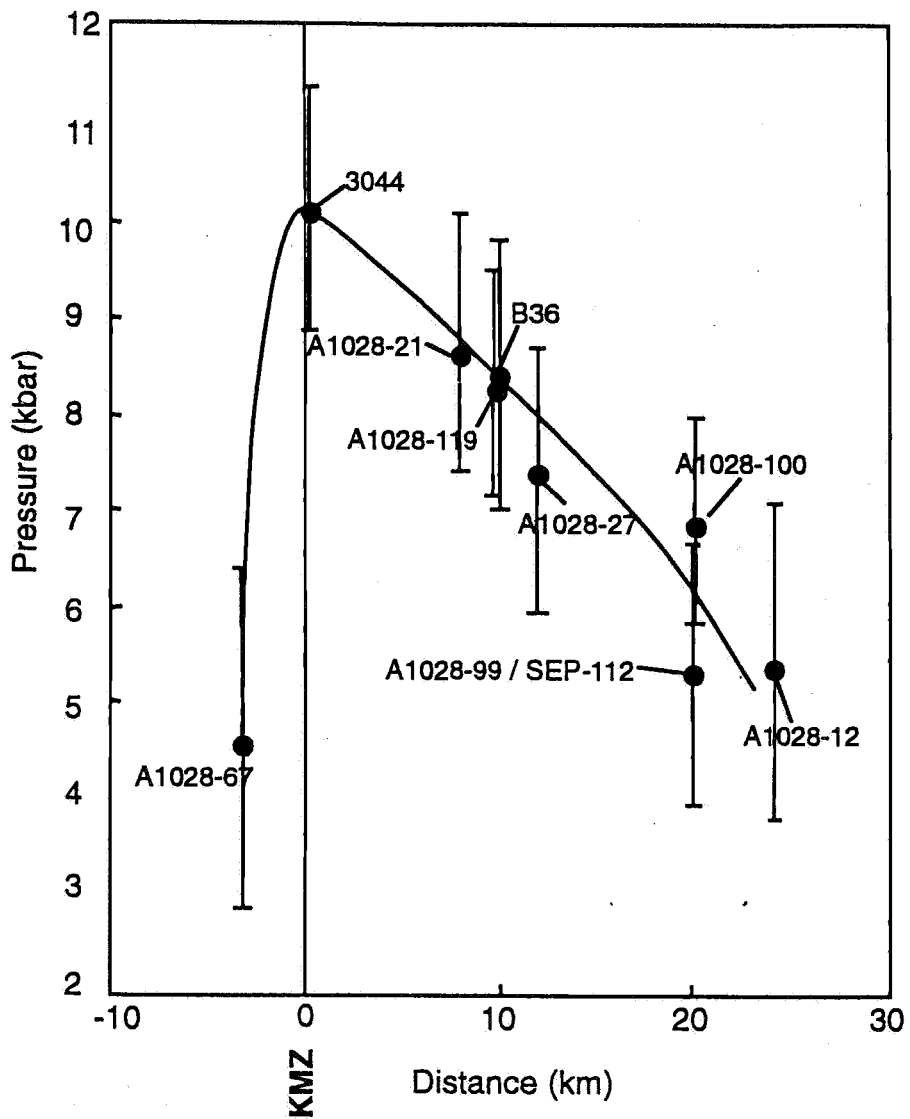
Figure 7. A baric section across the Kalinjala Mylonite Zone.

produced geologically unreasonable pressures and frequently failed the chi-squared statistical test. However fluids in high grade rocks are commonly inferred to be CO_2-bearing (Newton et al, 1980; Touret, 1985, 1986). At Lookout the presence of calcite in close spatial association with the garnet-bearing veins implies this fluid was CO_2 rich (sample A1028-13). Calcite is rarely present in samples from the other locations, however evidence is often available to support the existence of a fluid. At Surfleet Cove dehydration reactions involving the break down of biotite to produce garnet and water, require the presence of a fluid phase to transport K out of the system. This is required to explain the absence of K feldspar in the rock. Calcite is absent from this rock suggesting the fluid may have been water-rich compared to that at Lookout. In circumstances where the fluid composition is uncertain, an intermediate composition of XH2O = 0.5 was used. Where estimated pressures were calculated for a range of temperatures using the average pressure sub-routine of THERMOCALC, pressures determined for low temperatures often occurred within the kyanite stability field. In these cases, pressures within the sillimanite field at higher temperatures were accepted as no kyanite has yet been identified in Hutchison Group or Lincoln Complex rocks on Eyre Peninsula (Bradley, 1972; Coin, 1976; Parker, 1978).

Table 2 provides a synopsis of the inferred PT conditions for a number of selected samples, derived using the rationalisations discussed above. From this data and Figure 7, it is apparent that a positive pressure gradient exists across the Lincoln Complex as the Kalinjala Mylonite Zone is approached. The highest pressure rocks of ~10 kbars exist within the shear zone at Pt Neill, and pressure subsequently declines eastwards at about 0.2 kbar/km, to ~ 5.4 kbar rocks at Lookout approximately 24 km across strike. The use of virtually constant temperature across the zone in order to constrain pressure obviously does not mimic naturally occurring metamorphic environments as intuitively, increasing pressures should be accompanied by increases in temperature. Nonetheless the near isobaric nature of the pressure estimates from each sample with respect to changing temperature means that pressures calculated in this way are within error of those calculated under a declining temperature regime. The fact that a pressure gradient exists using a fixed, but geologically plausible temperature demonstrates this gradient is genuine, since pressure estimates made assuming decreasing temperatures eastward would result in even lower pressures for rocks far from the Kalinjala Mylonite Zone.

Sample number SEP-112 is the only non-mafic rock within the Lincoln Complex, on which P-T calculations were performed. This pelitic xenolith occurs within a charnockite exposed in a coastal outcrop about 10 kms south of Tumby Bay. The sample was included for P-T work as an independent test on the accuracy of P-T estimates made on the mafic assemblages, since the mafic assemblages have a wide stability field (Spear, 1993). Sample A1028-12 from Lookout is approximately equivalent in distance from the Kalinjala Mylonite Zone to SEP-112 and pressures calculated for both rocks correlate well.

13

Sample No.	Water Activity aH$_2$O	Fluid Composition XH$_2$O	Estimated Temperature (^{o}C)	Estimated Pressure (kbar)	Geothermometer * gnt-hbl # gnt-pyx	Distance from KMZ (km)
3044 (Oussa)			840 ± 95	10.1 ± 1.2		0-1
1028-21	0.5		700 - 750	8.8 ± 1.3	550 - 650 *	8
1028-27	0.5	0.5	650 - 700	7.35 ± 1.4	605 - 640 #	12
1028-119	0.5	0.5	650 - 700	8.3 ± 1.2	650 - 745 *	10
B36 (Mortimer)		0.5	650 - 700	8.4 ± 1.4		10
1028-99	0.5	0.5	650 - 700	5.3 ± 1	590 - 715 #	20
1028-100			725 ± 85	6.9 ± 1.1	670 - 730 #	20
1028-12		0.5	650 - 700	5.4 ± 1.7	600 -615 *	24
SEP-112	0.5	0.5	600 - 650	5.3 ± 1.4		20
1028-67		0.5	600 - 650	4.6 ± 1.7		3

Table 2. Synopsis of P-T estimates for selected samples, constituting a transect across the Kimban Orogen.

3.5 Metamorphism in the Hutchison Group

Parker (1978) recorded the presence of a migmatised zone in Hutchison Group rocks in the Cleve Hills adjacent to the Kalinjala Mylonite Zone, which graded westward into non-migmatised pelitic schists. The schists in both zones were biotite, sillimanite and garnet-bearing but contained no cordierite, staurolite or other AlSiO$_2$ polymorphs. He concluded the absence of staurolite reflected a deficiency in bulk composition rather than unfavourable metamorphic conditions, and used the pressure sensitive relationship between cordierite and almandine to constrain the lower limits of pressure for these rocks. Parker (1978) described metamorphism in these rocks as lower pressure Barrovian style metamorphism and concluded that they had experienced pressures of 5-7 kbars and 600-675°C for the migmatites and 600-650°C for the non-migmatites.

Coin (1976) investigated the metamorphism of Hutchison Group rocks of similar composition to the pelitic schists of Parker, located in the Tumby Bay area between the Yunta Well Leucogranite and the Kalinjala Mylonite Zone. Adjacent to the leucogranite, schists are

garnet, sillimanite and K feldspar-bearing with no evidence of staurolite, cordierite or andalusite. East of these rocks, andalusite with included sillimanite and rare staurolite, occur within 3 kms of the mylonite zone. Coin (1976) concluded that the distribution of the sillimanite-andalusite boundary reflected contact metamorphism of the schists by intrusion of the leucogranite, and calculated metamorphic conditions in the sillimanite-grade rocks as 570 ± 80°C and about 3.4 kbar. These assemblages however are syn-tectonic (Coin, 1976) and if equivalent to those pelitic schists in the Cleve Hills are also apparently widespread. The Yunta Well Leucogranite is also considered as pre or syn-tectonic as it is variably foliated (Parker, 1993), suggesting that these P-T conditions may reflect regional metamorphism rather than contact metamorphism, as they do not overprint a previous metamorphic assemblage.

Sample 1028-67 is a pelite from the Hutchison Group metasediments located in Mine Creek approximately 3 kms west of the Kalinjala Mylonite Zone. This sample contains a mylonitic foliation associated with the KMZ and was included to gain some insight into the metamorphic conditions experienced by the Hutchison Group rocks immediately adjacent to the shear zone. The rock records pressures of about 4.6 kbars which is slightly lower than that recorded at Lookout about 24 kms from the zone.

3.6 Synopsis

The general lack of obvious high grade reaction textures and mineral zoning in most of the mafic dykes studied implies these rocks experienced rapid cooling (Ellis and Green, 1985; Barker, 1990), and therefore should provide constraints on near-peak metamorphism during the Kimban Orogeny. This is a powerful observation, especially considering the lack of retrograde, high P-T reaction textures in the highest grade rocks from Pt Neill, which would be those most likely to display such retrograde features (Oussa, 1993). The P-T estimates calculated from these rocks are therefore considered to represent peak metamorphic conditions which occurred during the Kimban Orogen.

The P-T estimates demonstrate that a significant pressure gradient existed across the orogen with Hutchison Group rocks never experiencing the higher pressures recorded by the Lincoln Complex. The highest grade rocks currently observed are ~10 kbar Lincoln Complex orthogneisses occurring within the Kalinjala Mylonite Zone, while adjacent exposed Hutchison Group metasediments experienced maximum pressures of 5 to 7 kbar. Lincoln Complex rocks of equivalent pressure occur 15-20 kms from the mylonite zone illustrating the distinct asymmetry of a baric section through the orogen (Figure 7). This implies that Lincoln Complex rocks were differentially exhumed along the Kalinjala Mylonite Zone and therefore must have had undergone significant vertical movement in addition to strike slip motion.

4. ISOTOPE GEOCHRONOLOGY

The age of the Kimban Orogeny has been constrained primarily by Rb-Sr and U-Pb zircon emplacement ages of granitic intrusives on Eyre Peninsula (Parker, 1980; Parker, 1993). This data has failed to adequately establish the duration of orogenesis or timing of metamorphism, although it provides an upper limit of 1845 Ma (Parker, 1993). Nevertheless, there has been no previous attempt to directly date Kimban metamorphic rocks to constrain timing of the orogen. The garnet bearing mafic dykes of the Tournefort Dyke Swarm are particularly suitable for this task as they have an obvious association with Kimban age Lincoln Complex granitoids and have amenable mineralogy for Sm-Nd dating. Additionally the general absence of retrograde reaction textures overprinting their high grade mineral assemblages suggests that Sm-Nd systematics of metamorphic minerals in these mafic dykes should relate directly to peak metamorphism.

With this in mind, two garnet bearing mafic dykes were selected for analysis. One sample (A1028-99) was taken from West Point (Appendix A, Figure 1) on the Jussieu Peninsula, south of Pt Lincoln and approximately 20 km east across-strike from the Kalinjala Mylonite Zone. This is one of the most easterly garnet bearing mafic granulites on the mainland. The other sample (A1028-110) is a garnet bearing mafic taken from Mine Creek approximately 7 km west of Tumby Bay. This rock occurs as a dyke interlayered with Hutchison Group metasediments, directly adjacent to mylonites and ultramylonites of the KMZ, which the creek cross-cuts. Therefore the dyke may not strictly be a Tournefort dyke. Whole rock, garnet and hornblende mineral separates define a three point isochron for each sample. The results are shown in Figures 8-11 and summary of the data gathered is presented in Appendix D.

4.1 Sm - Nd in metamorphic mineral systems

Samarium (Sm) and neodymium (Nd) are rare earth elements (REE) which occur as minor components in many major rock forming minerals and accessory phases. The radioactive ^{147}Sm isotope decays to its radiogenic daughter of ^{143}Nd, a stable isotope of neodymium (Faure, 1986; DePaolo, 1988). The variable partitioning of rare earth elements into different minerals leads to variable parent/daughter element ratios in mineral phases. Providing this variation is large enough to define an isochron, dating of mineral separates can be used to provide very precise ages from single rocks rather than requiring whole rock analysis of co-genetic suites of rock (DePaolo, 1988). Garnet bearing rocks offer the greatest opportunity for gaining geochronological information using the Sm-Nd system as garnet is one of the few minerals which partitions Sm much more strongly than Nd (Cliff, 1985; Faure, 1986).

16

The Sm-Nd system is a powerful dating method particularly suited for dating metamorphism as the general immobility of REE, suggests that this system is relatively more robust to regional metamorphism, fluid interaction and weathering than other isotopic systems, although this is still a contentious issue (Black, 1988; Vance & O'Nions, 1990). In a metamorphic rock, interpretation of age data is complicated by the recognition that mineral isochrons may represent either closure temperatures or crystallisation ages. Temperature is considered the dominant process determining if a mineral remains closed to the exchange of major elements and isotopes (Cliff, 1985). If temperature remains below that which will enable isotopic re-equilibration then the mineral will retain its initial isotopic signature. On the other hand, if re-equilibration occurs, the isotopic system will record the age at which the mineral became a closed system again following cooling from the metamorphic event. This critical temperature has been termed the mineral's closure or blocking temperature (T_c) (Dodson, 1973). The reputed immobility of Sm-Nd suggests closure temperatures for these elements are high, and therefore may be useful in constraining ages on medium and high grade metamorphic events (Black, 1988; McCulloch & Black, 1984). Other factors such as composition, cooling rate and grain size also influence closure temperature, and in metamorphic rocks in particular, fluid movement and strain are likely to have significant effects (Black, 1988; McCulloch & Black, 1984). Evidence for correlation between major element and isotope diffusion is still inconclusive however and so isotopic distribution in minerals can not yet be directly equated with that of major elements (Vance & O'Nions, 1990). As a result the closure temperature can really only be empirically determined.

Humphries and Cliff (1982) concluded that the closure temperature for the Sm-Nd system in garnets is in the range of 500 - 700°C using experimental diffusion data from Harrison and Wood (1980), while Cohen et al (1988) suggested that garnets preserved their Sm-Nd signature up to 900°C. Mezger et al (1992) calculated garnet closure temperature is in the range of 600°C - 650°C, while in Enderby Land granulites McCulloch and Black (1984) inferred that the Sm-Nd system had been reset on a mineral scale during metamorphism of 650°C and 7 kbar. Thus timing of peak metamorphism to about mid-amphibolite facies should be directly recorded by crystallisation of garnets, whereas if higher grade metamorphism is achieved they will only record the timing of cooling through the closure temperature.

4.2 Interpretation of Eyre Peninsula data

Sample No. A1028-99

The garnet-hornblende-whole rock three point isochron from this sample gives a very precise age of 1716 ± 14 Ma, (an error of 0.85%) (Figure 8). This date would appear to represent the age of near-peak metamorphism, as the equilibrium mineral assemblage in this rock has crystallised under transitional granulite facies conditions. In light of the above discussion on
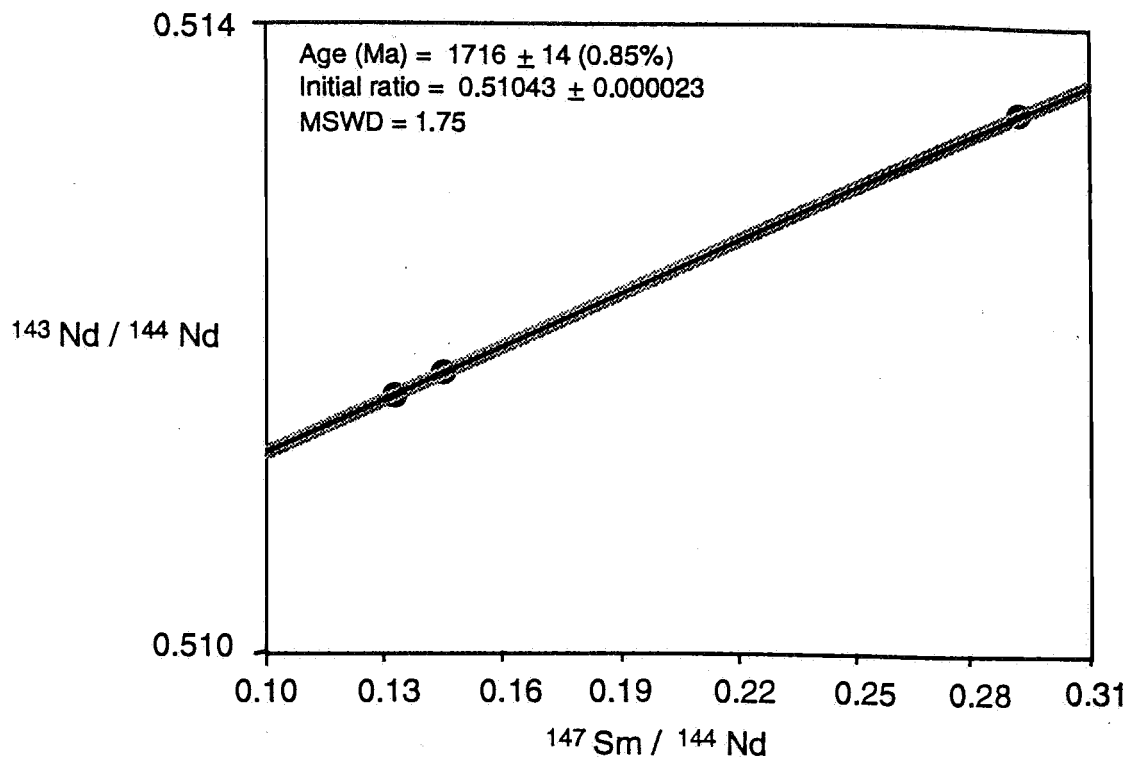
Figure 8. Sample A1028-99 whole rock - garnet - hornblende isochron
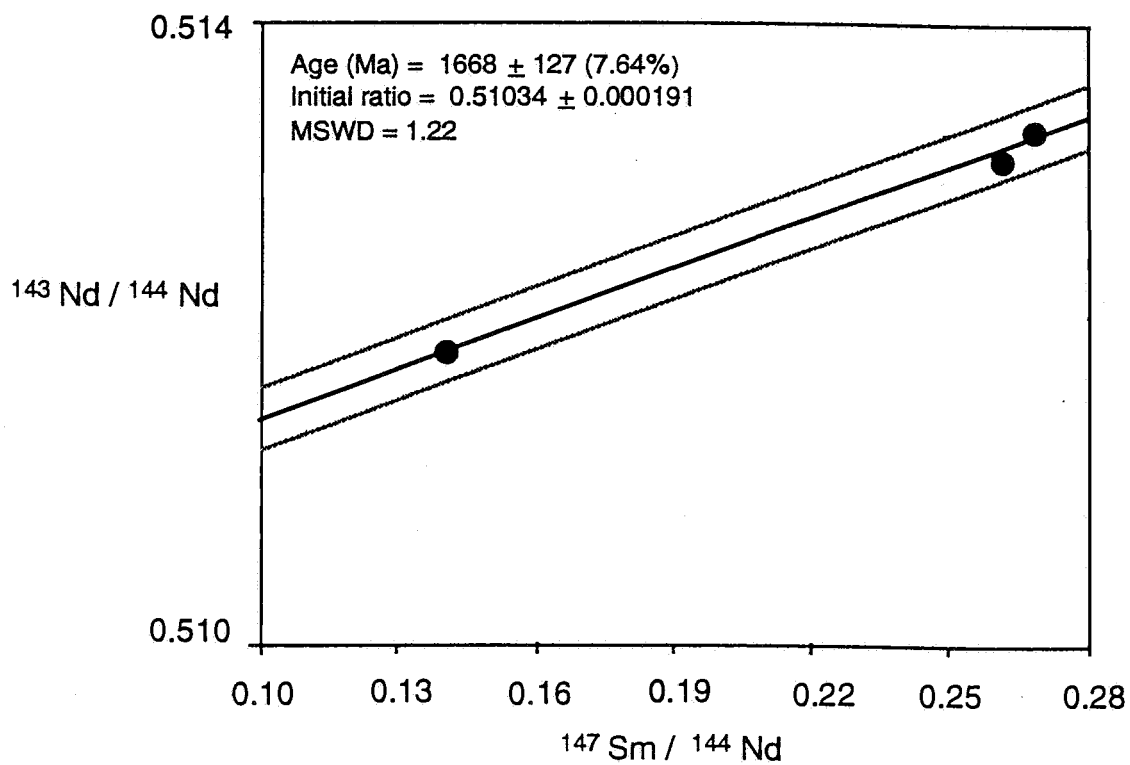
Figure 9. Sample A1028-110 whole rock-garnet-horneblende mineral isochron

the closure temperatures of minerals, it could also be argued that this date may represent re-equilibration of the Sm-Nd isotope system during the retrogressive amphibolite facies D3 event of previous workers (Parker and Lemon, 1982). However the D3 event is associated with high strain deformation allied to large scale movement along the KMZ (Parker, 1978; Glen et al, 1977). As this rock is undeformed, the former interpretation is the favoured option.

Sample No. A1028-110

The age gained for sample A1028-110 is problematic as the three point (garnet-hornblende-whole rock) isochron yields an age of 1668 ± 127 Ma, (an error of 7.6%) (Figure 9). Of more concern is the position of the hornblende point on the isochron. Rather than lying close to the whole rock point, as would be expected, the $^{147}Sm/^{144}$ Nd ratio of hornblende places it close to the garnet point. In comparison, a garnet - whole rock two point isochron yields an age of 1576 ± 7 Ma, (an error of 0.46%) (Figure 10), while a hornblende - whole rock isochron yields an age of 1744 ± 6 Ma, (an error of 0.35%) (Figure 11). All three ages could be geologically meaningful, however it is apparent that the isotopic ratio of at least one component of the isochron has been modified.

Regardless of specific closure temperatures, isotopic ages from mineral separates usually form a trend of decreasing age with decreasing parent to daughter values. In the Sm-Nd system, zircon, pyroxene and garnet typically close before hornblende, biotite and plagioclase, and therefore record older ages (Vance & O'Nions, 1990; Cliff, 1985; Mezger et al., 1992). That the hornblende in this sample has an uncharacteristically high $^{147}Sm/^{144}$ Nd ratio, suggests either the analysis is poor or the ratio reflects interference by inclusions within the hornblende, or disturbance of hornblende due to alteration.

Petrographically, the hornblende appears unaltered, but does contain a significant amount of zircon present as inclusions. Zircon has a very high Sm/Nd ratio, well above that of garnet, so minor amounts of zircon present in the hornblende sample may in effect displace hornblende toward the garnet point on the isochron. Interpolation calculations indicate about 10% of the hornblende sample needs to be zircon for such a displacement to occur. If indeed hornblende has been displaced by the presence of zircon, then the age obtained from the three point isochron is unreliable. As discussed previously the T_C for zircon is greater than that of garnet, however garnet and hornblende are believed to record near-peak metamorphic conditions, therefore one can not be confident that zircon is an equilibrium phase. Nonetheless, although zircon inclusions within the hornblende are prevalent, they appear to compose less volume than is required to account for displacement of the hornblende.

It is also apparent that this rock has undergone some degree of alteration. This is evident by the complete retrogression of plagioclase to sericite. The presence of sericite requires the introduction of a fluid, transporting sufficient potassium into the rock to form this mineral. The surrounding pelites could have acted as a source for this element. Indeed, geochemical
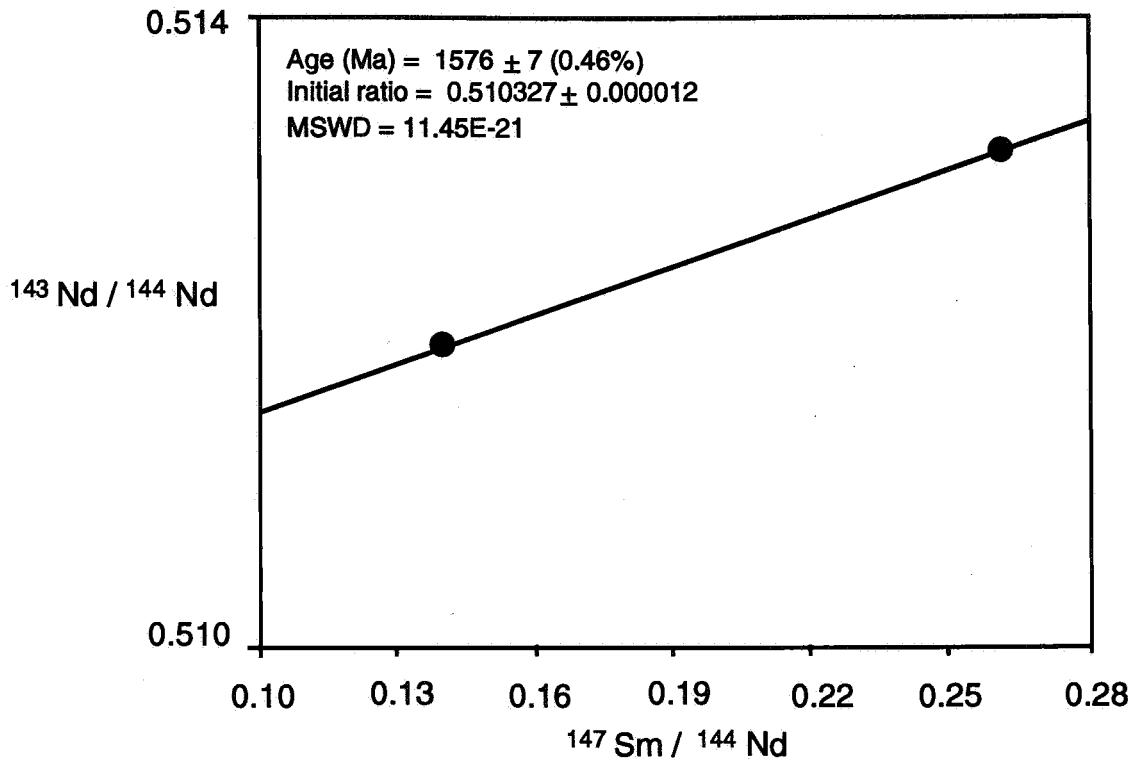
Figure 10. Sample A1028-110 whole rock - garnet mineral isochron
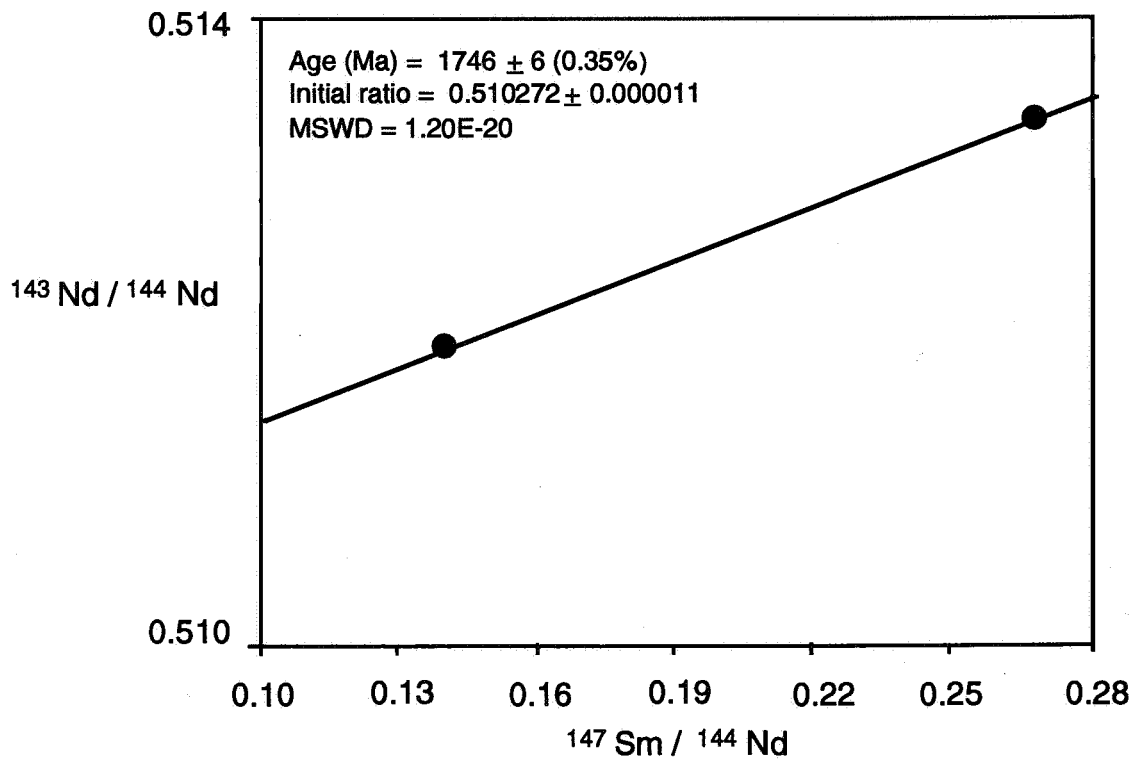
Figure 11. Sample A1028-110 whole rock-hornblende mineral isochron

analysis of an adjacent mafic dyke indicates the dyke has the geochemical signature of a sedimentary rock (B. Schaefer pers. comm.). Petrographically the hornblende and garnet appear unaffected by this alteration. During fluid flow induced alteration, Sm - Nd may have been mobilised in the rock, thereby producing spurious isotopic ratios in the whole rock while hornblende and garnet have remained unaffected.

An unlikely scenario might consider all the data points to be valid and simply interpret the relative position of hornblende and garnet to be reversed. In this case the garnet may have been reset due to reheating above its closure temperature which in this rock is lower than that of hornblende. If so the hornblende-whole rock age is a record of peak metamorphism, and the garnet - whole rock isochron is not geologically meaningful other than to indicate that a subsequent reheating event has occurred and temperatures during this event exceeded the closure temperature of the garnet.

It is most likely that fluid flow induced alteration of the rock has led to some disruption of the Sm-Nd isotopic system in either the whole rock, or the garnet and hornblende mineral separates. As a result of this disruption, the age derived from the three point isochron for this sample is poorly constrained and of dubious merit. Additional disturbance of the Sm-Nd system in the rock as a result of thermal perturbation is supported by the calculation of a hornblende Ar/Ar age of 1580 Ma from Pt Neill (K. Ehlers pers comm.). If this is the case, the data determined from the isochron may represent a resetting of the Sm-Nd system consistent with a reheating event at about 1570 - 1600 Ma.

Evidence for another orogenic event, referred to as the Wartaken Orogeny, at about 1550 - 1600 Ma is manifold. Numerous granitic intrusives from Eyre Peninsula yield Rb-Sr and K-Ar dates within this range and yet are regarded as Kimban because they are variably deformed. Examples of such intrusives are the Bungalow Granodiorite (Rb-Sr: 1601 ± 14 Ma, Webb et al. 1986), the Symons Granite (Rb-Sr: 1585 ± 12, Webb et al. 1986; U-Pb zircon: 1700-1680 Ma, Parker, 1993) and igneous textured mafics of the Tournefort Dyke Swarm (Rb-Sr: 1550-1600 Ma, Webb et al, 1988). The most compelling evidence for the reality of another major orogeny however is the existence of the St Peter Suite granitoids at Streaky Bay. These granitoids have previously been described as syn-Kimban as they are foliated and sheared. However they yield U-Pb zircon ages of 1620 ± 4 Ma (Flint et al., 1990), significantly younger than the Lincoln Complex (Parker, 1993). Given that the Pt Neill orthogneisses and the Moody Tank granite, a Lincoln Complex granitoid, both record a reheating event at about 1550-1600 Ma (K-Ar hornblende: 1562 Ma, Webb et al., 1986) it appears reasonable that sample A1028-110 is also recording this event as a resetting of its Sm-Nd system.

4.3 Synthesis

An Rb-Sr whole rock-biotite-plagioclase isochron from a little deformed pegmatite cross cutting the Kalinjala Mylonite Zone at Pt Neill has been used to constrain the minimum age for

the Kimban Orogeny at 1710 Ma (Fanning 1984a), while initiation of deformation is constrained at 1845 - 1745 Ma based on the intrusive ages of pre-tectonic granitoids. Given that a transitional granulite facies mafic dyke from the Lincoln Complex (sample A1028-99) recording near-peak metamorphic conditions yields a Sm-Nd age of 1716 ± 14 Ma however, it is evident that peak metamorphism during the Kimban Orogeny occurred about 50 - 100 m.y. later than previously expected, coincident with movement along the Kalinjala Mylonite Zone. Subsequently at 1550 - 1600 Ma Lincoln Complex rocks such as the Moody Tank granite and the Bungalow Granite experienced resetting of their R-Sr and K-Ar systems in response to heating during the Wartaken Orogeny. Contemporaneous ages gained from Sm-Nd dating of a hornblende-rich mafic dyke from Tumby Bay adjacent to the Kalinjala Mylonite Zone and Rb-Sr dating of igneous textured mafic dykes from near Pt Lincoln, are consistent with this observation.

5. DISCUSSION

5.1 Overview of main findings

Previous workers have used structural data to interpret the Kimban Orogeny in terms of three tectonic events (Parker, 1978; Coin, 1976; Glen et al, 1977). Under this system, prograde metamorphism is attributed to D1 and D2 which produced characteristic structural features discussed above in section 2.4. D3 is considered the event responsible for retrogressive metamorphism, activation of strike-slip movement along the Kalinjala Mylonite Zone and concomitant exhumation juxtaposing high-grade Lincoln Complex against lower grade Hutchison Group metasediments (Parker, 1978; Parker and Lemon, 1982; Fanning et al., 1988). This interpretation invokes a regime of convergent orogenesis with strain initially accommodated by shortening normal to the strike of the KMZ, resulting in prograde metamorphism as a manifestation of crustal thickening only, followed by a discrete episode of strike-slip movement along the Kalinjala Mylonite Zone.

In a tectonic environment such as discussed above, movement would be initially strike normal with a major vertical component, followed by subsequent horizontal movement along the strike of the orogen (Figure 5). In such a regime, overprinting of steep lineations by shallow strike-slip lineations would be expected. Within, and adjacent to the Kalinjala Mylonite Zone, shallow lineations are observed and are defined by the maximum grade assemblages developed during the Kimban Orogeny (Cohen and James, 1979; Oussa, 1993). Further away from the zone, lineations are predominantly steep-plunging and trend obliquely to the strike of the Kalinjala Mylonite Zone (Figure 6). There is little evidence that either of these lineations overprints the other. While these observations do not preclude orogenesis via normal convergence, they suggests that strike-slip movement has occurred along the shear zone during peak metamorphism (therefore the KMZ is not a retrogressive structure only), and are consistent with formation of the orogenic belt in a transpressive regime.

Estimates of P-T conditions recorded by transitional granulite facies garnet-bearing mafic dykes of the Lincoln Complex, demonstrate that a significant pressure gradient exists eastwards, across strike from the Kalinjala Mylonite Zone. The deepest level (and highest temperature) Lincoln Complex rocks outcrop at Pt Neill (Oussa, 1993) within the mylonite zone. These rocks have experienced pressures of 10.1 ± 1.2 kbar. Pressure declines eastward at about 0.2 kbar/km to 5.4 ± 1.7 kbar about 24 km across strike from the shear zone. In contrast, Hutchison Group metasediments about 3 km west of the Kalinjala Mylonite Zone record pressures of 4.6 ± 1.7 kbars. The distinct asymmetry of this baric section (Figure 7) and the dramatic pressure contrast between the two lithologies centred upon the shear zone, implies that movement along this feature enabled differential exhumation of Lincoln Complex orthogneiss relative to the Hutchison Group during the Kimban Orogeny.

5. DISCUSSION

5.1 Overview of main findings

Previous workers have used structural data to interpret the Kimban Orogeny in terms of three tectonic events (Parker, 1978; Coin, 1976; Glen et al, 1977). Under this system, prograde metamorphism is attributed to D1 and D2 which produced characteristic structural features discussed above in section 2.4. D3 is considered the event responsible for retrogressive metamorphism, activation of strike-slip movement along the Kalinjala Mylonite Zone and concomitant exhumation juxtaposing high-grade Lincoln Complex against lower grade Hutchison Group metasediments (Parker, 1978; Parker and Lemon, 1982; Fanning et al., 1988). This interpretation invokes a regime of convergent orogenesis with strain initially accommodated by shortening normal to the strike of the KMZ, resulting in prograde metamorphism as a manifestation of crustal thickening only, followed by a discrete episode of strike-slip movement along the Kalinjala Mylonite Zone.

In a tectonic environment such as discussed above, movement would be initially strike normal with a major vertical component, followed by subsequent horizontal movement along the strike of the orogen (Figure 5). In such a regime, overprinting of steep lineations by shallow strike-slip lineations would be expected. Within, and adjacent to the Kalinjala Mylonite Zone, shallow lineations are observed and are defined by the maximum grade assemblages developed during the Kimban Orogeny (Cohen and James, 1979; Oussa, 1993). Further away from the zone, lineations are predominantly steep-plunging and trend obliquely to the strike of the Kalinjala Mylonite Zone (Figure 6). There is little evidence that either of these lineations overprints the other. While these observations do not preclude orogenesis via normal convergence, they suggests that strike-slip movement has occurred along the shear zone during peak metamorphism (therefore the KMZ is not a retrogressive structure only), and are consistent with formation of the orogenic belt in a transpressive regime.

Estimates of P-T conditions recorded by transitional granulite facies garnet-bearing mafic dykes of the Lincoln Complex, demonstrate that a significant pressure gradient exists eastwards, across strike from the Kalinjala Mylonite Zone. The deepest level (and highest temperature) Lincoln Complex rocks outcrop at Pt Neill (Oussa, 1993) within the mylonite zone. These rocks have experienced pressures of 10.1 ± 1.2 kbar. Pressure declines eastward at about 0.2 kbar/km to 5.4 ± 1.7 kbar about 24 km across strike from the shear zone. In contrast, Hutchison Group metasediments about 3 km west of the Kalinjala Mylonite Zone record pressures of 4.6 ± 1.7 kbars. The distinct asymmetry of this baric section (Figure 7) and the dramatic pressure contrast between the two lithologies centred upon the shear zone, implies that movement along this feature enabled differential exhumation of Lincoln Complex orthogneiss relative to the Hutchison Group during the Kimban Orogeny.

20

Sm-Nd dating of peak metamorphic phases in a transitional granulite facies mafic dyke from West Point approximately 20 km across strike from the Kalinjala Mylonite Zone yields an age of 1716 ± 14 Ma. The sample dated is regarded as recording the timing of near-peak metamorphism as no high-temperature retrograde reaction textures or structures overprint the high-grade equilibrium assemblage. The age of this rock, correlates with a Rb-Sr age of 1710 Ma from a little deformed pegmatite cutting the shear zone at Pt Neill which is considered to constrain the termination of the Kimban Orogeny (Fanning, 1984a). Thus it is evident that peak metamorphism was essentially contemporaneous with deformation along the shear zone, which ceased shortly after 1710 Ma. This reduces the age of the Kimban Orogeny by about 100 m.y. from that estimated by previous workers (1845-1710 Ma) (Parker, 1993), and shortens its duration from a period spanning about 135 m.y. to about 30 m.y. or less.

5.2 Implications for evolution of the orogen

The distribution of different P-T conditions in the orogen, may provide information indicating whether observed changes in metamorphic grade are a local phenomena, or regional and relating to crustal thickening (Winkler, 1979; Yardley, 1989). One possible cause of local heating is shear heating arising from movement along the Kalinjala Mylonite Zone and subsidiary mylonite zones such as that at Lookout (Scholz, 1980). Shear heating developed from movement on a strike-slip fault, such as the KMZ, would be associated with a symmetrical distribution of heat about the fault (Scholz, 1980; Molnar, 1992). However this style of faulting typically lacks extensive topographic expression (Reading 1980), therefore only minor pressure changes would probably result from such a regime, producing essentially isobaric heating and cooling histories in the rocks affected by the faulting. Thus, although shear heating provides an potential heat source from metamorphism during the Kimban Orogeny, it is unlikely to have played a major role since a baric section across the orogen does not reflect this geometry. In contrast, a regime involving conductive heating on a regional scale in response to crustal thickening will have attendant changes in pressure due to thickening strain (Winkler, 1979; Yardley, 1989). In this case, changes in metamorphic grade may be symmetrically or asymmetrically disposed about a fault, as metamorphic conditions will, in some manner, mimic the geometry of crustal thickening (Roure et al, 1989; Norris et al, 1990). The metamorphic data described in this thesis imply that the latter scenario is more applicable to the Kimban Orogen, and that the style of metamorphism is suggestive of a large-scale obliquely convergent system.

Controversy continues over the manner in which oblique convergence at plate boundaries is partitioned into strike-slip and strike-normal components, however observational evidence favours a high degree of partitioning (Molnar, 1992), and seizmicity from modern examples suggests that strike-slip movement is concentrated at plate boundaries (Scholz, 1977; Sylvester

strike-slip movement partitioned
into shear zone at rear of wedge

velocity of strike-slip movement
decreases exponentially toward the
wedge front

strike-normal convergence at
wedge front

deformation by corner flow
leads to the circulation of
material through the
wedge
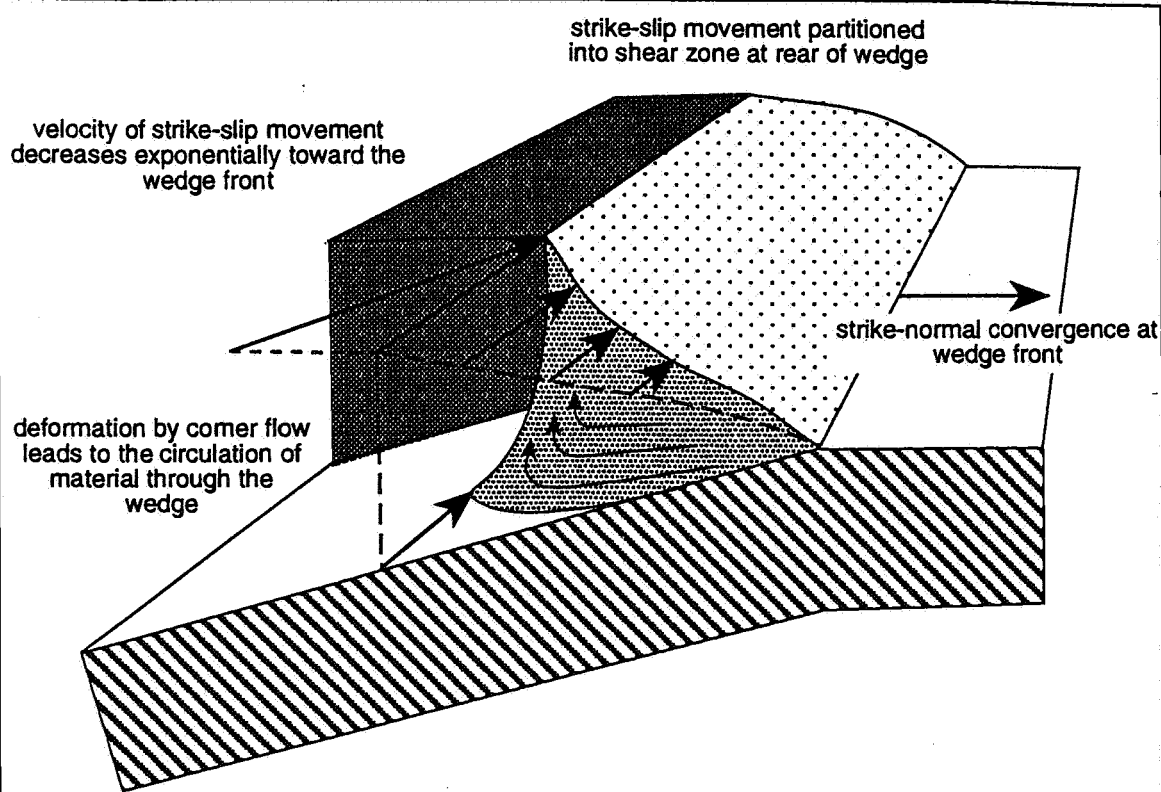
Figure 12. Schematic representation of the partitioning of strike-slip and
strike-normal movement in an obliquely convergent viscous wedge. (Modified
after Platt, 1993)

and Smith, 1976; Platt, 1993). Lineations on faults accommodating strike-slip movement can lie between the convergent and strike-slip vectors, or show a bimodal distribution. In contrast, lineations may have a radial or near normal trend in the areas of the terrain where crustal thickening is less, and parallel to strike in the internal areas where crustal thickening is greatest (Platt, 1993). Platt (1993) investigating the degree of partitioning between strike-slip and dip-slip components in an obliquely convergent system, found that in a linear viscous wedge, strike-slip motion exponentially decreases away from the internal part of the orogen (ie the plate boundary) (Figure 12). Additionally, he found strike-slip motion was confined to a shear zone at the rear of the wedge, with the width of this shear zone relating to the vertical thickness of the orogenic wedge. The wedge deformed by corner flow resulting in the circulation of material through the wedge in the X-Z plane. These findings agree with the analysis of England et al (1985) which predicted an exponential increase in the strike-slip component of motion toward the plate boundary using a thin viscous sheet model. Molnar (1992) suggests that partitioning of oblique convergence in the manner described above, manifests as continuous, ductile deformation in the upper mantle and lower crust. Coupling between the upper and lower crust leads to the creation of principle stresses in the upper crust, which are directly derived from this partitioning, however the style of deformation observed in the upper crust is distinct from that of the lower crust, due to rheological differences (Molnar, 1992). This hypothesis may explain the distictly different styles of deformation observed in the Lincoln Complex and Hutchison Group rocks. The models discussed above appear to be consistent with observations made in southern Eyre Peninsula and support metamorphic evidence suggesting the Kimban Orogen was an obliquely convergent regime.

5.3 Modern analogues of the Kimban Orogeny

The San Andreas Fault system of California and the Alpine Fault of New Zealand are recognised as obliquely convergent plate margins associated with differing styles of exhumation (Scholz, 1977). In California movement is distributed among a series of block faults, while exhumation in New Zealand is accomplished by thrusting along the Alpine Fault. Bearing in mind the removal of about 10 kbar of overburden required to expose granulite facies Lincoln Complex rocks at the surface, and the existance of numerous smaller shear zones subparallel to the Kalinjala, it is possible that the Californian scenario was operative during the Kimban Orogeny. However the abrupt discordance in lithology and metamorphic grade immediately across the KMZ and the asymmetrical distribution of pressure within the Lincoln Complex centred on the Kalinjala Mylonite Zone, as discussed in section 3.4, suggests the New Zealand Alpine Fault may be a more appropriate modern analogue of processes which occurred during the Kimban Orogeny.

The Alpine Fault is a major terrane boundary accommodating the bulk of interplate displacement caused by the oblique collision of the Australian and Pacific plates (Norris, 1994). Displacement is achieved along the fault without large scale partitioning into

convergent or strike-slip components in discrete zones and deformation is concentrated along the fault (Scholz, 1980). Typically a zone of mylonite up to one kilometre thick is developed in the Alpine Schists in the hangingwall block east of the fault, with strain increasing toward the fault, and to the east of the fault convergence has led to the rapid uplift of the Southern Alps (Norris and Koons, 1977). The Alps are asymmetrically arranged about the fault with short steep metamorphic gradients west of the fault and more gradual gradients east. The highest grade amphibolite facies rocks occur immediately adjacent to the fault, as a result of differential uplift during the Cainozoic, with metamorphic gradients declining to prehnite-pumpellyite facies about 20 kms eastward across-strike from the Alpine Fault (Norris et al, 1990). The asymmetry of metamorphic gradients and topography centred on the Alpine Fault is certainly suggestive of the scenario proposed for the Kalinjala Mylonite Zone and the Kimban Orogen.

5.4 Recommendations

Due to time limitations this study is necessarily a reconnaissance view of the Kimban Orogen and would benefit from further multidisciplinary research. Valuable future investigations of the Kimban Orogeny are,

-a parallel investigation to this study based on the western margin of the Cleve subdomain to constrain the P-T conditions experienced by the Hutchison Group,

-mapping of the Lincoln Complex outcropping on Yorke Peninsula and calculation of metamorphic conditions experienced by those rocks,

-further isotopic investigation to confirm the contemporaneity of metamorphic assemblages and provide additional constraints on the timing of the orogeny,

-computer modelling of the shear stresses and strain rates required to produce the temperature increases implied by the calculated metamorphic conditions and consequently,

-modelling of the effect of such a regime, through thermal perturbation and strain rate, on lithospheric strength.

ACKNOWLEDGMENTS

REFERENCES

Barker, A.J. (1990) 'Introduction to metamorphic textures and microstructures' (Blackie and Son, Ltd: Glasgow.)

Black, L.P. (1988) Isotopic resetting of U-Pb zircon and Rb-Sr and Sm-Nd whole rock systems in Enderby Land, Antarctica: implications for the interpretation of isotopic data from polymetamorphic and multiply deformed terrains. *Precambrian Research, 38* : 355-365.

Bouillier, A.M. and Barbey, P. (1988) A polycyclic two - stage corona growth in the Iforas Granulite Unit (Mali). *J. Metamorphic Geol., 6* : 235 - 254.

Bradley, G.M. (1972) The geochemistry of a medium pressure granulite terrain at southern Eyre Peninsula, Australia. Unpublished Ph.D. Thesis, the University of Adelaide.

Clarke, N.G. (1976) Structural analysis of the Port Neill Mylonite Zone and its country rocks, Pt Neill, South Australia. Unpublished Honours Thesis, The University of Adelaide.

Cliff, R.A. (1985) Isotopic dating in metamorphic belts. *J. Geol. Soc. London, 142* : 97-110.

Cohen, A.S., O'Nions, R.K., Siegenthaler, R., and Griffin, W.L. (1988) Chronology of the pressure-temperature history recorded by a granulite terrane. *Contrib. Min. Petr., 98* : 303-311.

Cohen, P.H. and James, P.R. (1980) Some structural aspects of the Lincoln Complex from Tumby Bay to Port Neill. Symposium on the Gawler Craton, 1979. *J. Geol. Soc. Aust., 27* : 45-53.

Coin, C.D.A. (1976) A study of the Precambrian rocks in the vicinity of Tumby Bay, southern Eyre Peninsula. Unpublished Ph.D. Thesis, The University of Adelaide.

Cooper, A.F. and Norris, R.J. (1994) Anatomy, structural evolution, and slip rate of a plate-boundary thrust: The Alpine Fault at Gaunt Creek, Westland, New Zealand. *Geol. Soc. Amer. Bull., 106* : 627-633.

DePaolo, D.J. (1988) 'Neodymium isotope geochemistry: an introduction.' (Springer-Verlag: New York)

Dodson, M.H. (1973) Closure temperature in cooling geochronological and petrological systems. *Contr. Mineral. and Petrol., 40* : 259-274.

Ellis, D.J. and Green, D.H. (1985) Garnet-forming reactions in mafic granulites from Enderby Land, Antarctica-Implications for geothermometry and geobarometry. *J. of Petrology, 26* (3): 633 - 662.

England, P., Houseman, G and Sonder, L. (1985) Length scales for continental deformation in convergent, divergent and strike-slip environments: Analytical and approximate solutions for a thin viscous sheet model. *J. Geophys Res., 90* : 3551-3557.

Fanning, C.M. (1984a) Rb-Sr geochronology of a pegmatite intrusive into the Kalinjala Mylonite Zone. *Amdel report*, GS6102/84 (unpublished).

Fanning, C.M., Blissett, A.H., Flint, R.B., Ludwig, K.R. and Parker, A.J. (1986) A refined geological history for the southern Gawler Craton through U-Pb zircon dating of acid volcanics, and correlations with Northern Australia. *In* 8th Australian Geological Convention, Adelaide, 1986. *Geol. Soc. Aust. Journal, 24* : 125-150.

Fanning, C.M., Flint, R.B., Parker, A.J., Ludwig, K.R. and Blissett, A.H. (1988) Refined Proterozoic evolution of the Gawler Craton, South Australia, through U-Pb zircon geochronology. *Precambrian Research, 40/41* : 363 - 386.

Faure, G. (1986) 'Principles of Isotope Geology'. 2nd Edn. (John Wiley & Sons: New York).

Flint, R.B, Rankin, L.R. and Fanning, C.M. (1990) Definition of the Palaeoproterozoic St Peter Suite of the western Gawler Craton, South Australia. *Sth. Aust. Geol. Surv. Q. Notes., 114* : 2-8.

Glen, R.A., Laing, W.P., Parker, A.J. and Rutland, R.W.R. (1977) Tectonic relationships between the Proterozoic Gawler and Willyama Orogenic Domains, Australia. *Geol. Soc. Aust. Journal, 24* : 125 - 150.

Graham, C.M. and Powell, R. (1984) A garnet - hornblende geothermometer: calibration, testing and application to the Pelona Schist, Southern California. *J. Metamorphic Geol., 2* : 13 - 31.

Green, D.H. and Ringwood, A.E. (1967) An experimental investigation of the gabbro to eclogite transformation and its petrological applications. *Geochimica et Cosmochimica Acta, 31* :767 - 833.

Harley, S.L. (1988) Proterozoic granulites from the Rauer Group, East Antarctica. I. Decompressional pressure - temperature paths deduced from mafic and felsic gneisses. *J. of Petrology, 29* : 1059 - 1095.

Harley, S.L. (1989) The origin of granulites; a metamorphic perspective. *Geol. Mag., 126* (3): 215-247.

Harrison, W.J. and Wood, B.J. (1980) An experimental investigation of the partitioning of REE between garnet and liquid with reference to the role of defect equilibria. *Contrib. Min. Petr., 72* : 145-155.

Holland, T.J.B. and Powell, R. (1990) Plagioclase feldspars; activity-composition relations based upon Darken's quadratic formalism and Landau theory. Amer. Min., 77 (1-2): 53-61.

Holland, T.J.B. and Blundy, J. (1994) Non-ideal interactions in calcic amphiboles and feldspars - bearing on amphibole-plagioclase thermometry. *Contr. Min. Petr., 116* : 433-337.

Mezger, K., Essene, E.J. and Halliday, A.N. (1992) Closure temperatures of the Sm-Nd system in metamorphic garnets. *Earth and Planetary Science Letters, 113* : 397-409.

McCulloch, M.T. and Black, L.P. (1984) Sm-Nd isotopic systematics of Enderby Land granulites and evidence for the redistribution of Sm and Nd during metamorphism. *Earth and Planetary Science Letters, 71* : 46-58.

Molnar, P. (1992) Chapter 18. Brace-Goetze strength profiles, the partitioning of strike-slip and thrust faulting at zones of oblique convergence, and the stress-heat flow paradox of the San Andreas Fault. In 'Fault mechanisms and transport properties of rocks.' (Eds. B. Evans and T. Wong) pp 435-459. (Academic Press: London).

Mortimer, G.E. (1984) Early to Mid Proterozoic granitoids, basaltic dykes and associated layered rocks of S.E. Eyre Peninsula, South Australia. Unpublished Ph.D Thesis, The University of Adelaide.

Mortimer, G.E., Cooper, J.A. and Oliver, R.L. (1986a) The geochronological and geochemical evolution of the Proterozoic Lincoln Complex, Eyre Peninsula, South Australia. *In* 8th Australian Geological Convention, Adelaide, 1986. *Geol. Soc. Aust. Journal, 15* : 142 - 143.

Mortimer, G.E., Cooper, J.A. and Oliver, R.L. (1986b) The geochemistry of basaltic dykes in the Proterozoic Lincoln Complex, southeastern Eyre Peninsula, South Australia. *Abst. Geol. Soc. Aust., 15* : 142 -143.

Mortimer, G.E., Cooper, J.A. and Oliver, R.L. (1988) The geochemical evolution of Proterozoic granitoids near Port Lincoln in the Gawler Orogenic Domain of South Australia. *Precambrian Research, 40/41* : 387 - 406.

Newton, R.C. and Haselton, H.T. (1981) Thermodynamics of the garnet-plagioclase-Al2SiO5-quartz geothermobarometer. In 'Thermodynamics of minerals and melts' (Eds. R.C. Newton, A. Navrotsky and B.J. Wood) pp 131-147 (Springer-Verlag: New York.)

Newton, R.C, Smith, J.V. and Windley, B.F. (1980) Carbonic metamorphism, granulites and crustal growth. *Nature, 288* : 45-50.

Norris, R.J. (1994) The significance of the Alpine Fault for crustal deformation during oblique collision. *Abs. Geol. Soc. Aust., 36* : 116-117.

Norris, R.J. and Koons, P.O. (1977) Tectonics of the modern obliquely convergent plate boundary in the South Island, N.Z., with implications for the interpretation of older terrane boundaries. *Abs. Geol. Soc. Aust., 24* : 108-109.

Norris, R.J., Koons, P.O. and Cooper, A.F. (1990) The obliquely - convergent plate boundary in the South Island of New Zealand: Implications for ancient collision zones. *J. Structural Geol., 12* : 715 - 725.

Oussa, S. (1993) Description of a granulite facies shear zone (Kalinjala Mylonite Zone) and inferred cooling rates following granulite facies metamorphism. Unpublished Honours thesis, The University of Melbourne.

Parker, A.J. (1978) Structural, stratigraphic and metamorphic geology of Lower Proterozoic rocks in the Cowell/Cleve district, eastern Eyre Peninsula. Unpublished Ph.D. Thesis, The University of Adelaide.

Parker, A.J. (1980a) The Kalinjala Mylonite Zone, eastern Eyre Peninsula, South Australia. *S. Aust. Geol. Surv. Q. Notes, 76* : 6-11.

Parker, A.J. (1990a) Gawler Craton and Stuart Shelf-regional geology and mineralisation. *In* 'Geology of the mineral deposits of Australia and Papua New Guinea.' *AusIMM, Monograph series, 14* : 999-1008.

Parker, A.J. (1993) Chapter 4. Palaeoproterozoic *In* 'The Geology of South Australia Vol. 1 The Precambrian'. (Ed: Drexel, J.F., Preiss, W.V. and Parker, A.J.) *Sth Aust. Geol. Surv. Bull. 54* : 51-106.

Parker, A.J. and Lemon, N.M. (1982) Reconstruction of the Early Proterozoic stratigraphy of the Gawler Craton, South Australia. *Geol. Soc. Aust. J., 29* : 221-238.

Parker, A.J., Fanning, C.M. and Flint, R.B. (1981) Archaean to Middle Proterozoic geology of the southern Gawler Craton, South Australia. Excursion Guide. *SADME Report Book, 81/91.*

Platt, J.P. (1993) Mechanics of oblique convergence. *J. Geophysical Research, 98* : 16,239-16,256.

Phillips, G.N. (1980) Water activity changes across an amphibolite - granulite facies transition, Broken Hill, Australia. *Contrib. Mineral. Petrol., 75* : 377 - 386.

Powell, R. (1985) Regression diagnostics and robust regression in geothermometer/ geobarometer calibration: the garnet-clinopyroxene geothermometer revisited. *J. Metamorphic Geol., 3* :231 -243.

Powell, R. and Holland, T.J.B. (1988) An internally consistent dataset with uncertainties and correlations: 3. Applications to geobarometry, worked examples and a computer program. *J. Metamorphic Geol., 6* : 173 - 204.

Reading, H.G. (1980) Characteristics of strike-slip fault systems. *Spec. Publ. int. Ass. Sediment., 4* : 7-26.

Richard, P. and Cobbald, P. (1990) Experimental insights into partitioning of fault motions in continental convergent wrench zones. *Annales Tectonicae, 4* (2); 35-44.

Ridley, J. (1986) Parallel stretching lineations and fold axes oblique to a shear displacement direction - a model and observations. *J. Structural Geol., 8* (6): 647-653.

Roure, F., Choukrounne, P., Berastegui, X., Munoz, J.A., Villien, A., Matheron, P., Bareyt, M., Seguret, M., Camara, P. and Deramond, J. (1989) ECORS deep seismic data and balanced cross sections: geometric constraints on the evolution of the Pyrenees. *Tectonics, 8* (1): 41-50.

Scholz, C.H. (1977) Transform fault systems of California and New Zealand: similaries in their tectonic and seizmic styles. *J. Geol. Soc. Lond. 133* : 215-229.

Scholz, C.H. (1980) Shear heating and the state of stress on faults. *J. Geophys. Res., 85* : 6174 - 6184.

Schumacher, K.C., Hollocher, K.T., Robinson, P. and Tracy, R.J. (1990) Progressive reactions and melting in the Acadian metamorphic high of central Massachusetts and southwestern New Hampshire, USA. *In* 'High-temperature metamorphism and crustal anatexis.' (Eds J.R. Ashworth and M. Brown) pp 198-234. (Unwin Hyman: London).

Schumacher, R. Schenk, V., Raase, P. and Vitanage, P.W. (1990) Granulite facies metamorphism of metabasic and intermediate rocks in the higland series of Sri Lanka. *In* 'High-temperature metamorphism and crustal anatexis.' (Eds J.R. Ashworth and M. Brown) pp 235-271. (Unwin Hyman: London).

Sengupta, S. (1993) Tectonothermal history recorded in mafic dykes and enclaves of gneissic basement in the Schirmacher Hills, East Antarctica. *Precambrian Research, 63* : 273-291.

Sibson, R.H. (1977) Fault rocks and fault mechanisms. *J. Geol. Soc. Lond., 133* :191-213.

Simpson, C. A. (1994) Constraints on Proterozoic crustal evolution from an isotopic and geochemical study of clastic sediments of the Gawler Craton, South Australia. Unpublished Honours Thesis, The University of Adelaide.

Sylvester, A.G. and Smith, R.R. (1976) Tectonic transpression and basement-controlled deformation in San Andreas Fault Zone, Salton Trough, California. *Amer. Assoc. Petr. Geol. Bull., 60* (12): 2081-2102.

Tilley, C.E. (1920) The metamorphism of the Precambrian dolomites of southern Eyre Peninsula, South Australia. *Geol. Mag., 57* : 449 - 462, 492 - 500.

Thompson, A.B. (1992) Metamorphism and fluids. *In* 'Understanding the Earth.' (Eds. G.C. Brown, C.J. Hawkesworth and R.C.L. Wilson) pp 222-248. (Cambridge University Press: Cambridge.)

Thost, D.E., Hensen, B.J. and Motoyoshi, Y. (1991) Two-stage decompression in garnet-bearing mafic granulites from Sostrene Island, Prydz Bay, East Antarctica. *J. Metamorphic Geol., 9* : 245-256.

Touret, J. (1985) Fluid regime in southern Norway: the record of fluid inclusions. *In* 'The deep Proterozoic crust in the North Atlantic provinces.' (Eds. A.C. Tobi and J.L.R. Touret) pp 517-549 (Reidel: Dordrecht)

Touret, J. (1986) Fluid inclusions in rocks from the lower continental crust. *In* 'The nature of the lower continental crust' (Eds J.B. Dawson, D.A. Carswell, J. Hall, and K.H. Wedepohl) *Soc. Lond. Spec. Publ., 24* : 161-172.

Vance, D. and O'Nions, R.K. (1990) Isotopic chronometry of zoned garnets: growth kinetics and metamorphic histories. *Earth and Planetary Science Letters, 97* : 227-240.

Webb, A.W., Thomson, B.P., Blissett, A.H., Daly, S.J., Flint, R.B. and Parker, A.J. (1986) Geochronology of the Gawler Craton, South Australia. *Aust. J. of Earth Sciences, 33* : 119 - 143.

Wendt, J.I., Kröner, A. Fiala, J. and Todt, W. (1994) U-Pb zircon and Sm-Nd dating of Moldanubian H*P/HT* granulites from South Bohemia, Czech Republic. *J. Geol. Soc. London, 151* : 83-90.

Winkler, H.G.F, (1979) 'Petrogenesis of metamorphic rocks'. 5th Edn. (Springer-Verlag: New York.)

Yardley, B.W. (1989) 'An introduction to metamorphic petrology.' (Longman Scientific and Technical: London.)

APPENDIX A

SAMPLE LOCATION MAP AND LIST OF SAMPLES
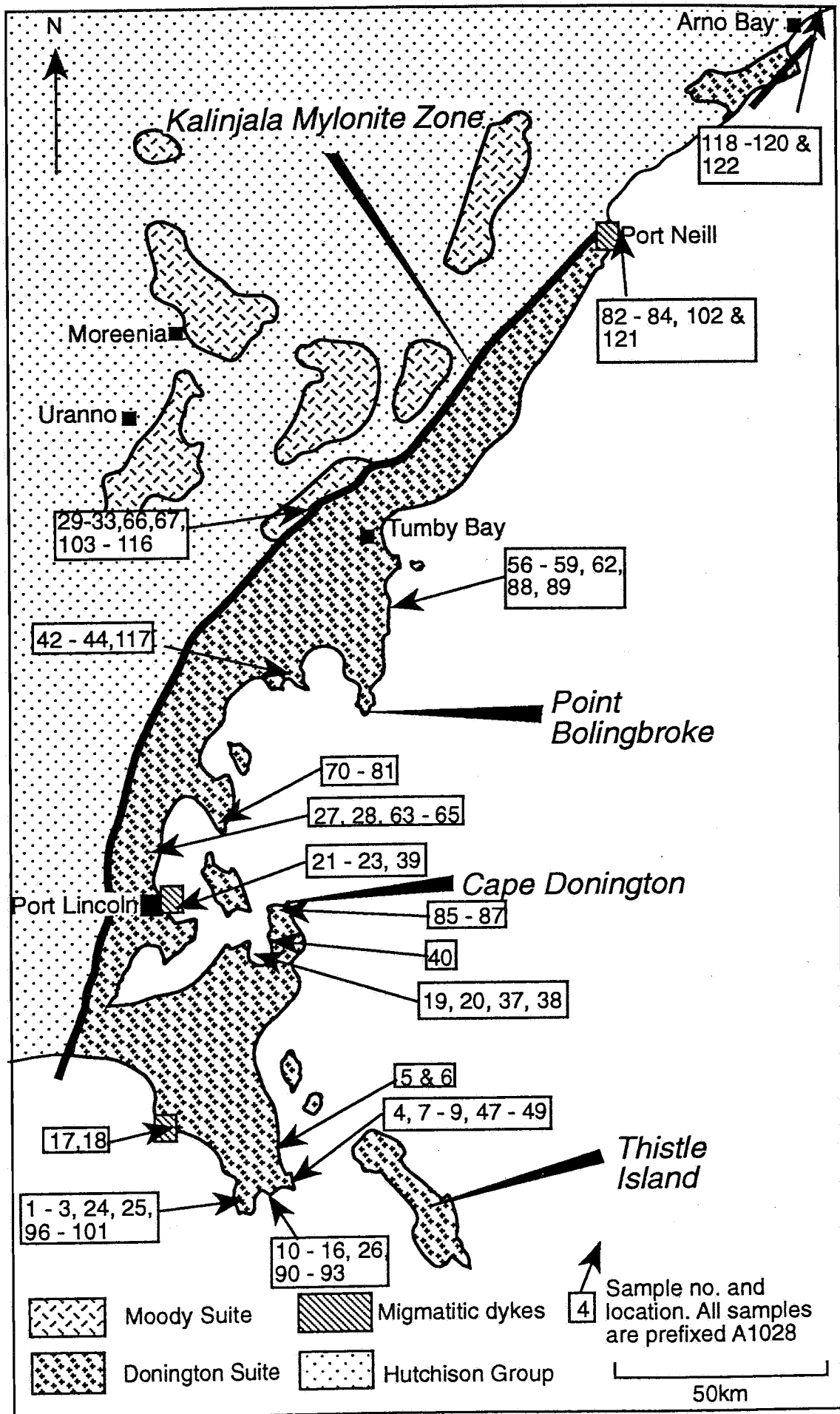
Figure 1. Sample Location Map.

SAMPLE LIST

Sample No.	Description	Location
A1028-1	Garnet -bearing calc silicate xenolith	West Point
A1028-2	Undeformed mafic dyke, trends 055	West Point
A1028-3	Deformed mafic dyke occupying shear zone. Gnt, hbl, pyx, trends 140. Deformed equiv. of A1028-2?	West Point
A1028-4	Large mafic dyke trends north	Cape Catastrophe
A1028-5	Undeformed mafic dyke trends north	Memory Cove
A1028-6	As per A1028-5	Memory Cove
A1028-7	Hbl bearing quartzofeldsp. mylonite, north trending	Cape Catastrophe
A1028-8	Sheared hbl bearing host of mylonite (1028-7)	Cape Catastrophe
A1028-9	Contact between MC Charnockite (1028-8) & a deformed mafic dyke.	Cape Catastrophe
A1028-10	Gnt-bearing coarse grained mafic unit intruded by megacrystic dykes	Lookout
A1028-11	Gnt-bearing mafic adjacent to mylonite cross cutting 1028-10	Lookout
A1028-12	Gnt bearing rock from shear zone which cuts 1028-10	Lookout
A1028-13	Relatively low strain domain gnt-bearing mafic S1 trends 160	Lookout
A1028-14	• Contact between gnt-free mafic & gnt-bearing mafic intruding it. Med strain	Lookout
A1028-15	Gnt- bearing mafic as per 1028-14	Lookout
A1028-16	Gnt-bearing mafic from shear zone	Lookout
A1028-17	Gnt-bearing felsic augen gneiss adjacent to 2 mafic dykes.	Wanna
A1028-18	Mafic dyke intruding 1028-17	Wanna
A1028-19	Gnt-bearing mafic	Surfleet Cove
A1028-20	Cpx veins in mafic dyke, highly sheared	Surfleet Cove
A1028-21	Three samples collected. Gnt-bearing mafic dyke adjacent to foliated felsic	Kirton Pnt (Boat Ramp)
A1028-21	As per 1028-21 but gnt free	Kirton Pnt
A1028-23	Coarse grained migmatitic mafic with hbl	Kirton Pnt
A1028-24	Coarse grained plag phyric dyke	West Pnt
A1028-25	Fine grained mafic dyke	West Pnt
A1028-26	Gnt-bearing mafic, gnt in veins	Lookout
A1028-27	Gnt-bearing mafic dyke with symplectic rims	Louth Bay
A1028-28	Non gnt bearing mafic	Louth Bay
A1028-29	Mafic dyke w random xtals coarse plag, pyx	Mine Creek
A1028-30	Ultramylonite oriented sample	Mine Creek
A1028-31	Ultramylonite oriented sample	Mine Creek
A1028-32	Gnt bearing rock in Quarry adjacent to Hutchison Grp	Mine Creek
A1028-33	Gnt bearing mafic dyke within Hutchison Grp, West of Falls	Mine Creek
A1028-35	Mafic dyke trends 040 L 080 S	Cape Euler
A1028-36	Calc silicate	Bolingbroke
A1028-37	Mafic dyke fine grnd trend 160	Surfleet Pnt
A1028-38	Mafic dyke cutting felsic fabric apparent undeformed trends 080	Surfleet Cove
A1028-35	Mafic dyke trends 040 L 080 S	Cape Euler
A1028-36	Calc silicate	Bolingbroke
A1028-37	Mafic dyke fine grnd trend 160	Surfleet Pnt

Sample No.	Description	Location
A1028-38	Mafic dyke cutting felsic fabric apparent undeformed trends 080	Surfleet Cove

Sample No.	Description	Location
A1028-39	Highly recrstallised mafic adjacent to leucosomes contains large hbl	Kirton Point
A1028-40	Mafic dyke with rxn texture	Engine Point (Nthn End)
A1028-41	Calc-silicate/marble with 2 green & 1 reddish minerals west of quarry.	Mine Creek
A1028-42	Opx bearing mafic from low strain area	Peake Point
A1028-43	Low strain cpx bearing coarse plag mafic	Peake Point
A1028-44	Mafic dyke associated with mylonites at western end of Peake Pnt	Peake Point
A1028-45	Cpx bearing mafic 30m E of Thuruna gate	Massena Bay
A1028-46	Gnt - sill gneiss 60m S of point	Massena Bay
A1028-47	Contact tween mafic & felsic host	Cape Catastrorphe
A1028-48	Migmatised mafic dyke (5m wide) foliated	Cape Catastrorphe
A1028-49	Less deformed mafic dyke cut by (48) oriented sample	Cape Catastrorphe
A1028-50	Granite bt schist possibly sedimentary	Bolingbroke
A1028-52	Gnt - bt schist w/in migmatite	Bolingbroke
A1028-53	As per SEP-019 Gnt schist w/in fold axis South of Red Point	Pnt Bolingbroke
A1028-54	Mafic bouding w foliation w/in GG1	Bolingbroke
A1028-55	Non gnt bearing mafic w no apparent foliation	Bolingbroke
A1028-56	Mafic w rxn textures (cf Kirton)	Red cliff
A1028-57	Contact of (56) & enclosing boudin of another mafic	Red Cliff
A1028-58	Mafic dyke intruding GG1 as per SEP-??	Thuruna
A1028-59	Mafic dyke intruding Grey Gneiss 2, possibly cpx bearing	Thuruna (Nthn tip)
A1028-60	Gnt sill gneiss (same as 46)	Massena Bay
A1028-61	Reaction rims of sill about spinel/ilmenite? (same as 46 & 60) 2 Samples	Massena Bay
A1028-62	gnt bt schist?? (cf Bolingbroke samples 50 &52) 2 samples	Thuruna (sth)
A1028-63	not obviously gnt bearing mafic (same as A1028-27)fresher sample for geochem.	Louth Bay
A1028-64	cpx bearing large mafic dyke	Louth Bay
A1028-65	small mafic dyke	Louth Bay
A1028-66	gnt bearing mafic dyke w/in Cook Gap Schist, same as SEP-047	Mine Creek
A1028-67	gnt sill gneiss 30m E of dolomite quarry	Mine Creek
A1028-68	oriented sample of migmatised/recryst. mafic dyke upper surface S-022/004E	Higgins Rd Crk
A1028-69	oriented sample of mafic S-134/080N	Higgins Rd Crk
A1028-70	Mafic dyke w/in Dalmatian Rock? (2 samples)	Pnt Boston (West coast)
A1028-71	mafic dyke with more random plag crystals Oriented	Point Boston
A1028-72	Mafic dyke, 1st in a series of 5 within close proximity (followed by 71) appear different	Pnt Boston (West coast)
A1028-73	Large sample of (oriented) mafic dyke S- 014/77W	Point Boston
A1028-74	Large oriented sample of mafic dyke S- 001/078W	Point Boston
A1028-75	Most likely candidate for gnt where Bruce found gnts	Point Boston
A1028-76	Isoclinally folded dyke at cross cutting dyke location	Point Boston
A1028-77	The mafic dyke cross cutting 76	Point Boston
A1028-78	Oriented sample of mafic dyke with random crystal arrangement S-160/082E	Point Boston
A1028-79	Very pristine mafic dyke oriented 338/001E	Point Boston
A1028-80	Oriented sample of mafic equivalent to Donington Dolerite	Point Boston

A1028-81	Curved mafic at Beacon, most likely candidate for Mortimer's gnt mafic	Point Boston
A1028-82	Gnt bearing mafics (3 samples)	Pt Neill Boat

Sample No.	Description	Location
A1028-83	Gnt bearing mafic c cpx (3 samples + 2 samples w/out gnt for geochem) last mafic	Cape Burr
A1028-84	garnetiferous calc silicate about 10 m W of 83 mafic dyke	Cape Burr
A1028-85	Gnt bearing calc silicate (6 samples)	Cape Donington
A1028-86	Oriented sample of metadolerite S-100/059S (large dyke on Mortimer's map)	Cape Donington
A1028-87	Another smaller metadolerite (opx bearing) East of beacon.	Cape Donington
A1028-88	Opx bearing? mafic	Trinity Haven
A1028-89	simplectic rim about gnt in mafic xeno Sample in 3 parts (See Bruce)	Trinity haven
A1028-90	gnt bearing mafic near white boulder gnt	Lookout
A1028-91	gnt bearing mafic near Lookout descentlinearly arranged, metasomatic.	Lookout
A1028-92	Gnt bearing mafic from scree at Lookout (2 samples) strong fabric	Lookout
A1028-93	gnt bearing mafic from scree at Lookout (no gnt in C&P)	Lookout
A1028-94	Mafic dyke from Nthn head at Corny Pnt cuts foliation	Corny Point
A1028-95	Gnt sill bt gneiss E of 94 (also Bookendite)	Corny Point
A1028-96	Gnt bt gneiss Same as SEP-106 -leave for Bruce	West Point
A1028-97	(ABC) 3 samples taken across strain gradient in mafic trending 340/070NE	West Point
A1028-98	Drawn mafic w mylonitised gnt (numerous samples)	West Point
A1028-99	gnt mafic trending 030 couplet to 98	West Point
A1028-100	gnt mafic dyke trending 040	West Point
A1028-101	mislabelled in notebook as 98. Mafic dyke cut by 97 (same as 100) No gnts	West Point
A1028-102	gnt bearing mafic (excellent gnts)	Pt Neill Boat Ramp
A1028-103	gnt bt sill schist within sequence of non retrogresses marbles ie before asbestos mine	Mine Creek
A1028-104	closer to Waterfall in retrogressed region with shallow lineations	Mine Creek
A1028-105	As above	Mine Creek
A1028-106	Last Calc-silicate layer before waterfall	Mine Creek
A1028-107	Pelite w steep lineation adjacent to calc-silicate 106	Mine Creek
A1028-108	Pelite just West of waterfall with steep lineation South	Mine Creek
A1028-109	Gnt bearing mafic dyke from just above waterfall	Mine Creek
A1028-110	Gnt bearing mafic dyke , further West of 109	Mine Creek
A1028-111	non gnt bearing mafic West of 110	Mine Creek
A1028-112	(as above) further West	Mine Creek
A1028-113	gnt bearing mafic (v mafic) furthest West	Mine Creek
A1028-114	Mafic mylonite (recystall) with non apparent or weak foliation	Mine Creek
A1028-115	Pelitic mylonite	Mine Creek
A1028-116	Mafic? ultramylonite (2 samples)	Mine Creek
A1028-117	Pristine igneous textured mafic dyke	Peake Point
A1028-117B	Pristine igneous textured mafic dykes	Peake Point
A1028-118	Clalc silicate	Arno Bay
A1028-119	gnt bearing mafic	Arno Bay
A1028-120	interlayered gnt bearing calc-silicate & mafic	Arno Bay
A1028-121	gnt hbl felsic gneiss	Cape Burr
A1028-122	Coarse cpx-hbl mafic	Arno Bay

APPENDIX B

TABLES OF WHOLE ROCK GEOCHEMICAL ANALYSIS

APPENDIX B

This appendix consists of tables of whole rock trace and major element chemistry of selected samples, derived from X-ray fluorescence analysis. The samples represent a range mafic dykes of the Tournefort Dyke Swarm from southern Eyre Peninsula, which include members of all the distinct dyke types discussed in Section 3.2.

	1028-1	1028-2	1028-4	1028-5	1028-6	1028-8	1028-10	1028-11	1028-12	1028-13	1028-15	1028-21	1028-27	1028-28	1028-29	1028-33	1028-36	1028-46
SiO2 %	62.68	48.94	49.72	46.16	50.68	53.87	48.10	47.09	47.28	48.51	48.47	58.32	48.84	49.47	48.27	51.92	78.54	70.77
Al2O3 %	13.04	16.83	13.61	8.11	9.54	15.04	14.72	12.66	12.77	12.39	12.16	12.67	14.56	15.63	14.62	14.60	11.43	14.96
Fe2O3 %	7.73	12.49	17.01	11.78	11.36	12.01	16.66	19.12	18.65	18.44	19.47	13.94	15.33	12.15	12.83	15.97	0.19	2.40
MnO %	0.44	0.17	0.23	0.18	0.18	0.16	0.21	0.24	0.24	0.25	0.26	0.15	0.21	0.18	0.19	0.25	0.00	0.01
MgO %	0.35	8.16	4.93	24.13	18.26	3.82	6.27	4.63	4.68	3.74	4.30	1.50	6.75	8.07	7.67	3.45	0.22	0.28
CaO %	13.47	10.74	8.95	6.25	7.30	7.99	8.68	7.93	8.43	8.13	7.65	4.80	10.61	11.66	10.31	7.17	0.57	0.69
Na2O %	1.34	2.08	2.62	1.00	1.24	2.76	2.73	2.26	2.32	2.44	2.02	2.54	2.14	1.87	1.79	1.52	2.43	1.86
K2O %	0.30	0.53	1.41	0.44	0.52	2.05	1.09	0.83	0.94	1.52	1.49	3.08	0.43	0.25	1.65	1.94	5.41	7.01
TiO2 %	0.29	0.77	2.08	0.50	0.59	1.23	1.81	3.46	3.56	3.13	3.31	1.60	1.49	1.04	1.09	2.44	0.10	0.25
P2O5 %	0.06	0.11	0.26	0.07	0.08	0.31	0.20	0.69	0.71	0.79	0.67	0.66	0.11	0.08	0.08	0.28	0.01	0.04
SO3 %	0.01	0.02	0.03	0.01	0.02	0.01	0.01	0.01	0.05	0.05	0.03	0.03	0.02	0.03	0.04	0.04	0.00	0.00
LOI %	0.28	-0.08	-0.54	0.44	-0.24	0.43	-0.52	0.77	0.48	0.81	0.47	0.03	-0.04	0.06	1.49	0.47	0.38	0.68
TOTAL	99.99	100.75	100.31	99.08	99.53	99.69	99.95	99.73	100.09	100.18	100.29	99.32	100.48	100.50	100.01	100.04	99.28	98.95
(ppm)																		
Rb	13.3	11.6	57.4	16.8	18.6	82.5	40.8	20.3	19.8	63.5	48.2	169.9	13.7	8.3	109.6	107.1	337.4	285.6
Ba	104	239	502	147	173	776	358	285	314	441	414	1188	126	95	134	446	150	1497
Th	12.8	1.3	5.1	2.2	2.9	9.5	3.4	5.1	5.7	6.7	4.6	14.3	1.1	1.1	17.2	17.2	6.1	21.4
U	5.1	2.3	2.9	2.5	0.9	3.8	2.2	3.8	2.9	2.3	2.7	4	1.2	0.9	1.1	3.5	2	3.9
Nb	9.6	3.9	11.8	3.4	3.3	11.1	9.6	14.8	14.7	16.4	14.1	16.6	8.3	5.3	5	18.8	8	14.5
K	2490.4	4399.8	11705.1	3685.9	4316.8	17018.1	9048.6	6890.2	7803.4	12618.3	12369.2	25568.6	3569.6	2075.4	13697.5	16104.9	44911.1	58193.4
La	53	7	26	9	9	17	19	28	35	5	73	73	7	6	3	109	-2	76
Ce	93	21	69	10	22	100	47	69	74	83	39	147	33	24	24	109	-2	76
Pb	25.2	4.4	12.5	5	2.3	12.5	5.7	7.5	8.1	10.5	4.6	25.4	4.7	1.2	3.4	18.2	39.8	34.7
Sr	151.4	177.6	164.6	88.5	89.5	270.2	183.1	142.2	143.1	143.3	145.2	256.4	184.3	168.9	150.3	146	40.4	149
P	261.9	480.1	1134.7	305.3	349.1	1352.9	872.8	3011.3	3098.6	3447.7	2924	2880.4	480.1	349.1	349.1	121.9	43.6	174.6
Nd	41	5	26	11	10	40	20	33	37	38	22	64	9	7	7	46	4	36
Zr	218.8	55.3	170.3	60.3	68.7	208	144.2	180	183	221	185	281.1	66.8	43.4	50.8	286.8	58.8	255.1
Sm																		
Ti	1738.5	4614.1	12469.6	2997.5	3537	7373.8	10850.9	2074.7	21342.2	18764.3	19843.4	9591.9	8932.5	6234.8	6534.5	14627.8	599.5	1498.7
Y	39.9	19.6	41.8	12.3	14.5	41.9	31.6	56.5	59.8	60.2	52.3	49.7	22.1	24.2	16	56.1	2.7	21.3
Sc	12.3	32.1	40.8	22	28.1	37.1	32.4	48.1	49.1	41.2	45.4	32.4	45.8	39.8	43.9	37.6	0.9	8.7
Cr	20	135	148	4166	3261	52	94	28	28	27	38	14	175	276	306	395.1	2	8
V	15	231.8	350.5	168.4	208.4	214	267.1	484.3	476.1	332.8	435.1	0.4	400.9	319.3	324.2	395.1	4.2	14
Co	98.5	70.9	76.3	105.9	92.6	59.6	80.9	68.5	68.5	55.1	46.8	47.9	76.7	93.4	82.2	50.6	107.7	88.2
Ga	22.3	17.9	22.5	9	12.2	16.5	23	22.3	23.4	20.7	22	18.7	20	15.4	16.9	24.3	16.1	18
Cu	-1	66	172	46	62	144	445	218	241	69	44	52	109	218	99	236	3	7
Zn	97	96	167	84	82	111	135	115	136	179	154	140	121	93	89	157	6	19
Ni	-1	234	63	1228	724	48	104	58	73	34	38	5	72	239	117	137	-5	-4

	1028-48	1028-49	1028-53	1028-71	1028-78	1028-79	1028-80	1028-84	1028-85	1028-85B	1028-87	1028-99	1028-100	1028-110	1028-117	1028-117B	1028-118
SIO2 %	49.53	48.97	54.65	51.48	49.26	49.34	48.75	71.30	68.49	67.12	52.76	51.00	48.71	56.71	50.21	49.52	45.95
Al2O3 %	13.65	15.13	12.60	12.93	15.95	14.58	16.31	14.45	13.61	14.30	13.38	14.40	16.90	14.84	14.44	14.24	10.86
Fe2O3 %	17.00	14.22	14.17	10.62	12.72	15.54	10.93	2.94	3.56	4.24	10.75	18.02	12.73	11.73	14.54	14.54	12.78
MnO %	0.23	0.18	0.20	0.17	0.18	0.22	0.17	0.05	0.07	0.12	0.17	0.22	0.18	0.17	0.20	0.20	0.24
MgO %	4.96	7.21	2.18	12.10	8.03	6.38	8.69	0.25	0.71	0.83	9.81	4.62	7.89	3.89	6.70	6.24	2.28
CaO %	8.89	9.49	9.10	9.86	10.48	10.45	12.49	8.32	12.00	8.90	10.05	8.80	10.49	7.06	8.75	9.63	23.90
Na2O %	2.58	2.47	0.69	1.87	2.15	2.46	2.03	1.85	0.49	1.44	2.02	2.29	2.33	0.65	2.15	2.33	0.42
K2O %	1.39	1.18	1.09	0.56	0.70	0.43	0.24	0.30	0.05	0.94	0.86	1.73	0.54	1.57	1.13	0.68	0.50
TIO2 %	2.10	1.23	1.55	0.72	0.92	1.51	0.95	0.18	0.46	0.59	0.74	1.76	0.77	1.40	1.42	1.95	2.68
P2O5 %	0.25	0.20	0.18	0.10	0.16	0.15	0.08	0.04	0.10	0.13	0.10	0.35	0.11	0.19	0.14	0.18	0.28
SO3 %	0.02	0.01	0.05	0.00	0.01	0.01	0.01	0.00	0.03	0.08	0.00	0.02	0.03	0.02	0.01	0.01	0.01
LOI %	-0.56	-0.20	3.37	-0.12	-0.20	-0.66	-0.29	0.30	0.20	0.69	-0.21	-2.94	-0.04	1.91	0.50	0.61	-0.03
TOTAL	100.05	100.08	99.82	100.29	100.36	100.40	100.34	99.97	99.77	99.38	100.44	100.26	100.63	100.14	100.19	100.12	99.86
Rb	56.8	43.3	50.3	19	21	14.7	8.6	7.6	4.6	59.1	34.8	59.7	11.3	97.9	83.9	38.6	52.4
Ba	479	456	472	213	303	148	65	42	135	604	245	671	243	234	234	244	71
Th	4.9	3	8.2	2.3	2.1	1.7	1.9	50.6	21.8	20.7	5.3	3.9	0.9	9.1	1.9	2.8	6.7
U	2.7	2.2	3.7	1.4	1.1	1.7	0.4	10.7	7	4.6	1.4	1.9	1.4	4.2	1.3	2.4	8.5
Nb	12.4	10.4	8.3	4.9	6.1	7.3	3.7	12.7	14	16.1	6.2	11	3.8	10.1	8.5	11.1	26.5
K	11539.1	9795.8	9048.6	4648.8	5811	3569.6	1992.4	2490.4	415.1	7803.4	7139.3	14361.6	4482.8	13033.3	9390.7	5645	4150.7
La	67	54	35	25	11	10	2	66	51	61	19	34	7	19	8	20	22
Ce	67	54	75	25	35	39	18	128	91	110	42	79	25	54	36	55	54
Pb	6.1	7.5	9.6	3.7	2.3	0.9	1.8	23.1	10.5	14.3	7.1	10.6	4.5	5.5	2.9	4.4	5.3
Sr	162.2	204.9	235.5	148.9	199.7	170.6	165.1	144.5	121.5	145	145.4	208.7	172	150.3	188.5	226.1	58.5
P	1091.1	872.8	785.6	436.4	698.3	654.6	349.1	174.6	436.4	567.3	436.4	1527.5	480.1	829.2	610.9	785.6	1221.9
Nd	26	21	27	14	12	13	5	53	39	47	14	31	6	22	8	28	23
Zr	175.4	118.7	154.2	89.2	73.1	95.9	45.9	137.4	267.3	269.2	105.4	167.1	58.6	169.3	105.6	126	163.6
Sm																	
TI	12589.5	7373.8	9292.2	4316.4	5515.4	9052.4	5695.2	1079.1	2757.7	3537.1	436.3	10551.1	4616.1	8392.9	8512.9	11690.2	16066.6
Y	40.4	29.2	27.3	18.4	21.2	27.7	16.6	44.5	26.5	31	20.8	42.2	20.1	32.8	31.5	71.3	73.1
Sc	42.1	32.5	33.4	29.1	32.4	39.6	33.7	7.1	8.7	10.4	29.4	39.5	32.7	35.8	40.8	45.3	31.3
Cr	142	330	16	1504	304	145	375	7	11	30	889	67	113	25	197	187	15
V	345.5	246	447.6	228.5	240.7	355.2	252.8	26.7	25.2	33.4	240.8	307.5	238.8	295.8	354.8	430.8	411.7
Co	76.1	71.3	67.6	62.7	68.3	81.4	85.1	87.9	89.2	90.5	61.2	100.2	80.6	69.5	84.5	63	70.2
Ga	22.5	18.1	20.5	15.5	17.9	18.8	17.1	22.9	15.3	18.2	15.7	22.2	16.3	21.2	19.8	19.7	21.4
Cu	165	108	27	82	112	200	130	5	32	26	80	132	245	9	6	36	3
Zn	139	115	129	75	96	114	73	10	57	58	75	162	98	121	117	119	201
NI	49	216	28	389	206	84	277	0	0	4	220	84	221	16	86	75	22

Garnet bearing hornblende-rich dykes- Trace Element Chemistry

Non garnet bearing hornblende-rich dykes- Trace Element Chemistry

Sample (ppm) Chondrite normalised

Trace Element

Rb Ba Th U Nb K La Ce .Pb Sr P Nd Zr Sm Ti Y

1028-33
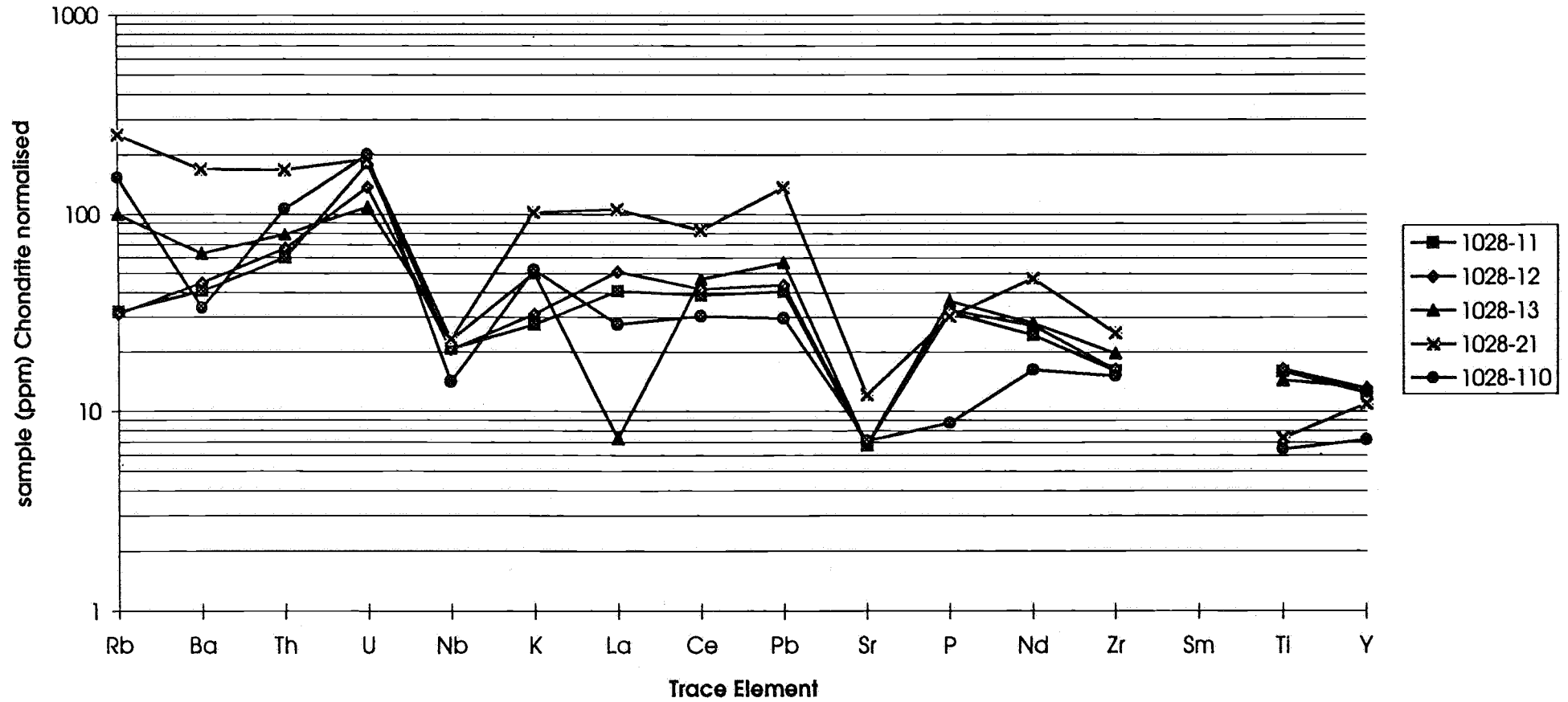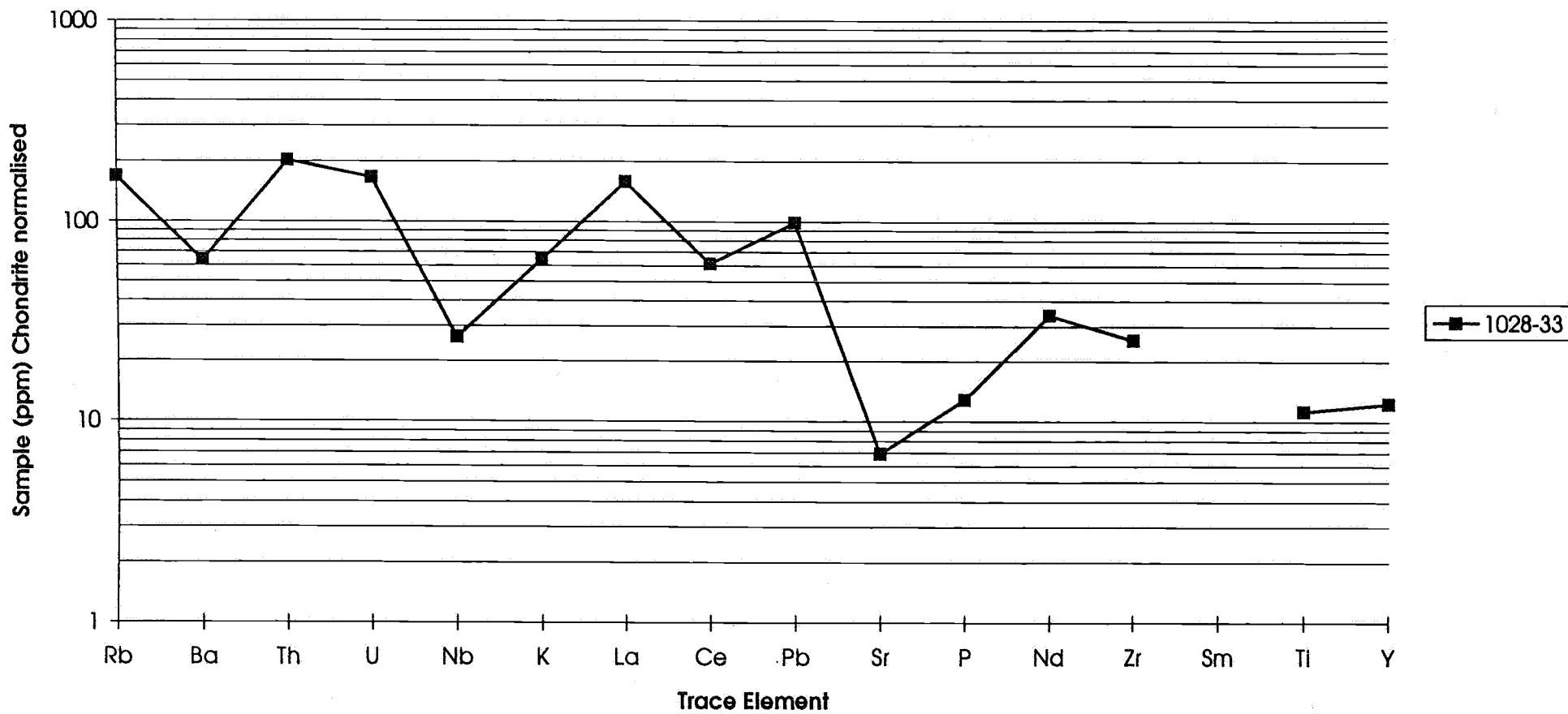
Pyroxene-rich granulites - major element chemistry
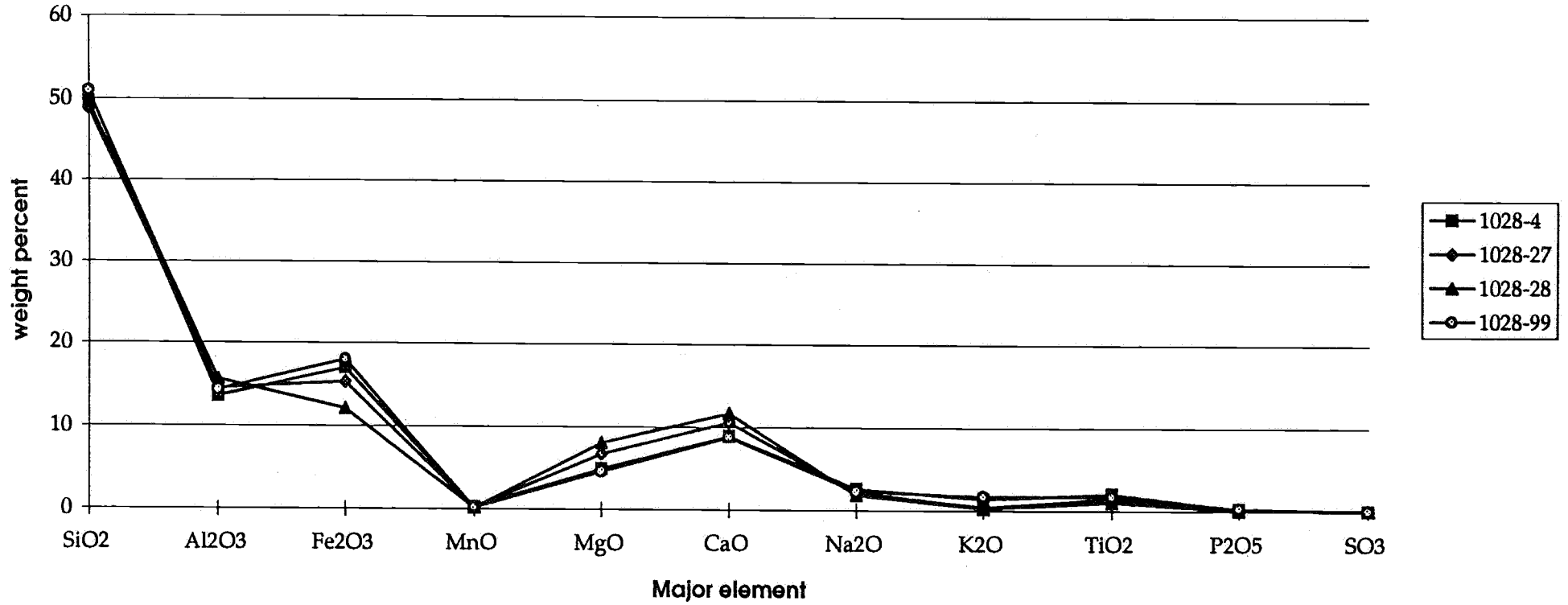
Igneous Textured dykes -Trace Element Chemistry

Legend:
- 1028-2
- 1028-10
- 1028-29
- 1028-49
- 1028-71

X-axis: Trace Elements (Rb, Ba, Th, U, Nb, K, La, Ce, Pb, Sr, P, Nd, Zr, Sm, Tl, Y)

Y-axis: Sample (ppm) Chondrite normalised

Igneous Textured dykes-Trace Element Chemistry

Legend:
- 1028-79
- 1028-80
- 1028-87
- 1028-100
- 1028-117
- 1028-117B

Y-axis: Sample (ppm) Chondrite normalised
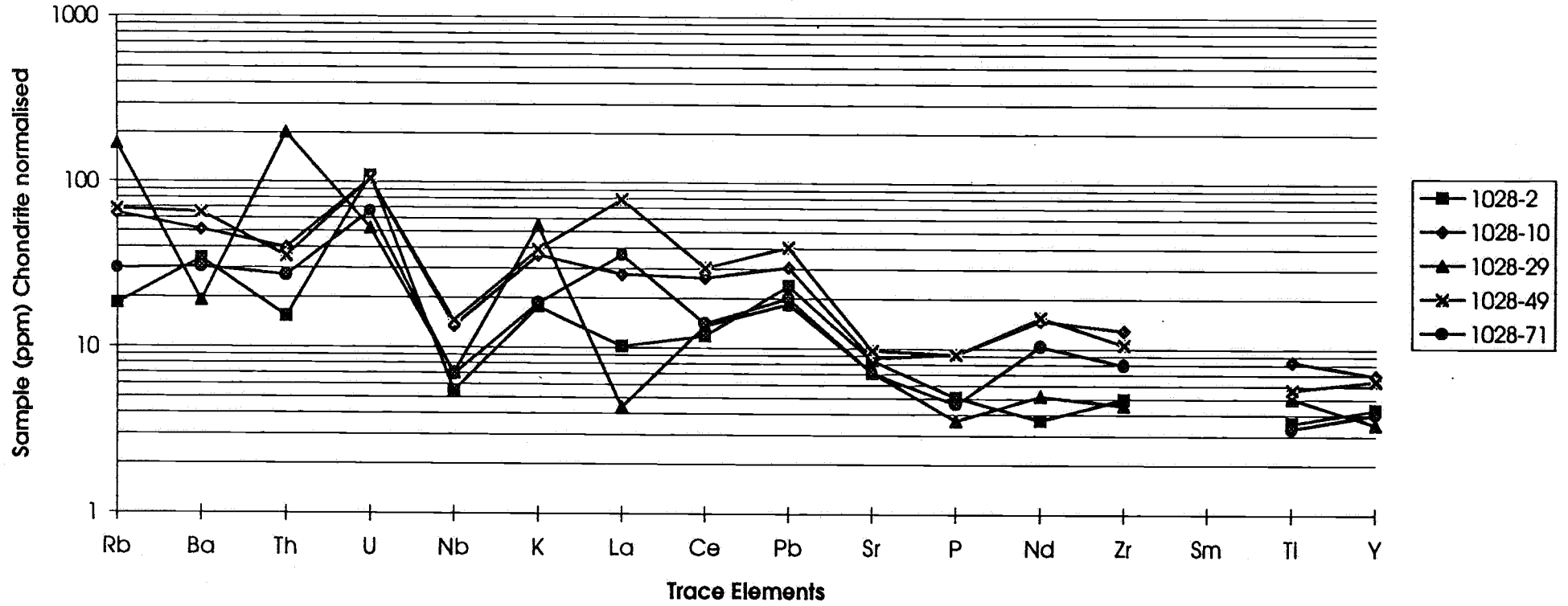
X-axis: Trace Element — Rb, Ba, Th, U, Nb, K, La, Ce, Pb, Sr, P, Nd, Zr, Sm, Ti, Y
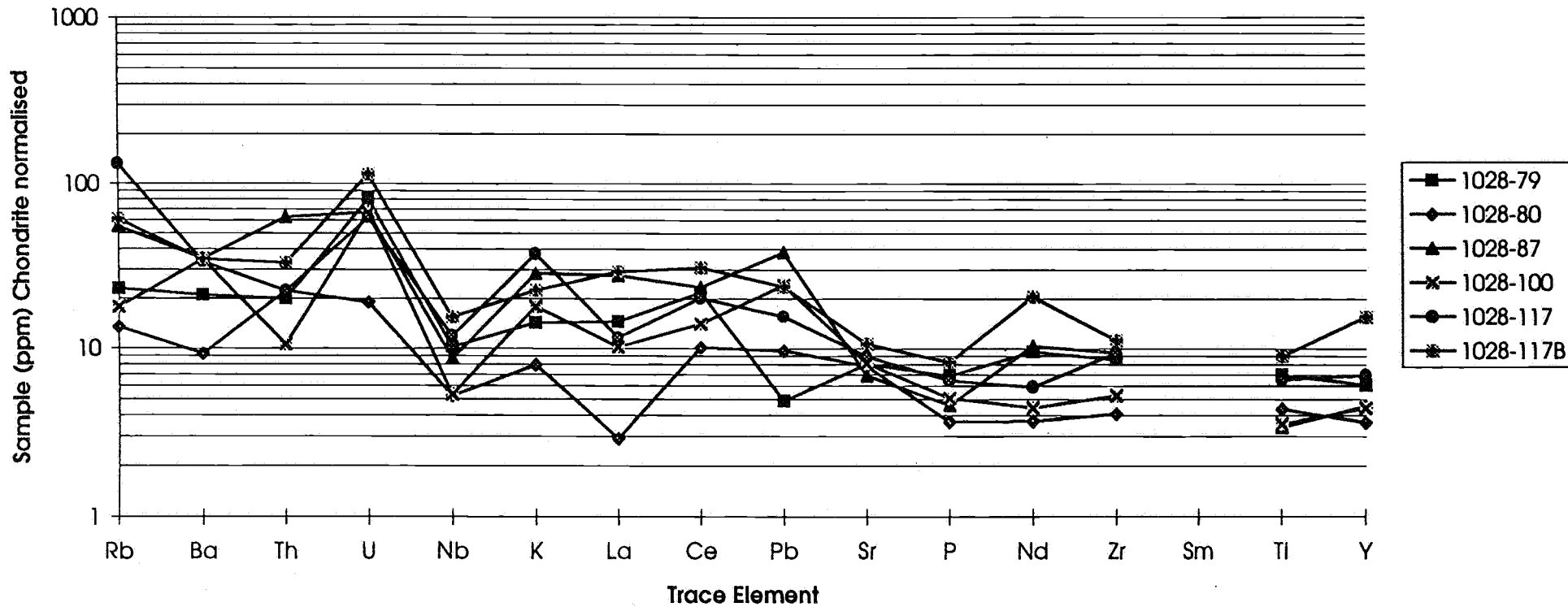
APPENDIX C

MINERAL CHEMISTRY, GEOTHERMOMETRY DATA AND AN EXAMPLE OF THERMOCALC P-T ESTIMATES

APPENDIX C

This appendix contains data referred to in section 3. Figures 1 to 3 are ternary diagrams which display the geochemistry of various minerals from selected mafic dykes sampled, as determined using a Cameca Camebax SX51 Electron Microprobe. Figures 4 to 7 are graphs of chemical zoning in garnets from garnet bearing mafic dykes, discussed in section 3.3. Figures 8 to 16 are graphs of pressure and temperature estimates for all the samples tested, as discussed in section 3.4, and derived using THERMOCALC. Figures 17 and 17a are graphs which display the results of garnet-hornblende and garnet-pyroxene geothermometry as discussed in section 3.4. An example of average pressure and average pressure-temperature calculations for one sample using THERMOCALC is included. Finally, tables of representative electron microprobe data for the equilibrium mineral assemblages of all samples calculated are included.
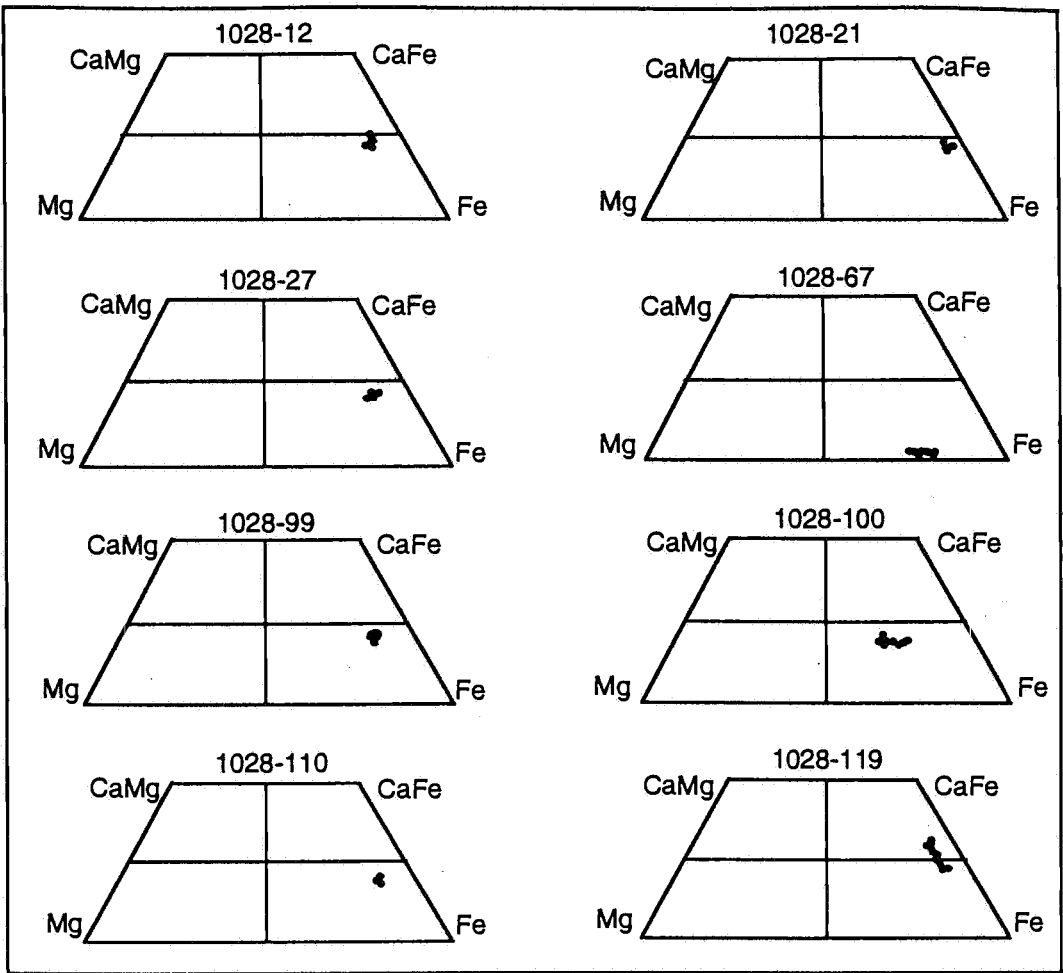
Figure 1. Geochemistry of garnets in Tournefort mafic dykes
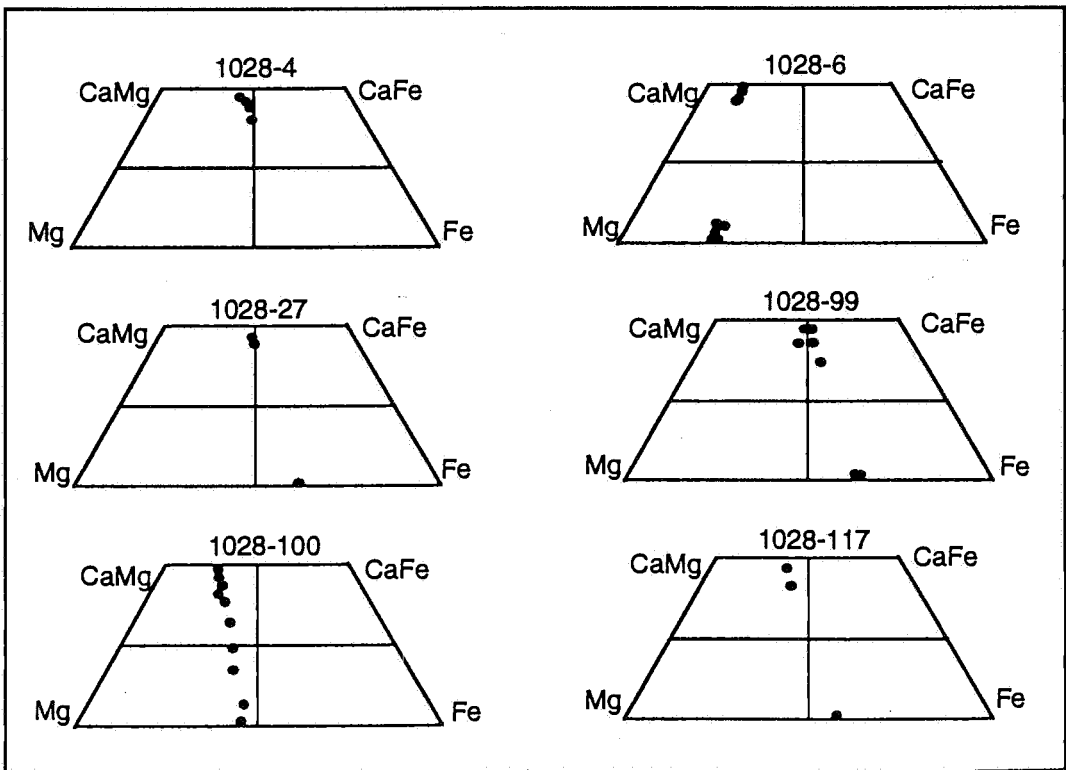
Figure 2. Geochemistry of pyroxenes in Tournefort mafic dykes
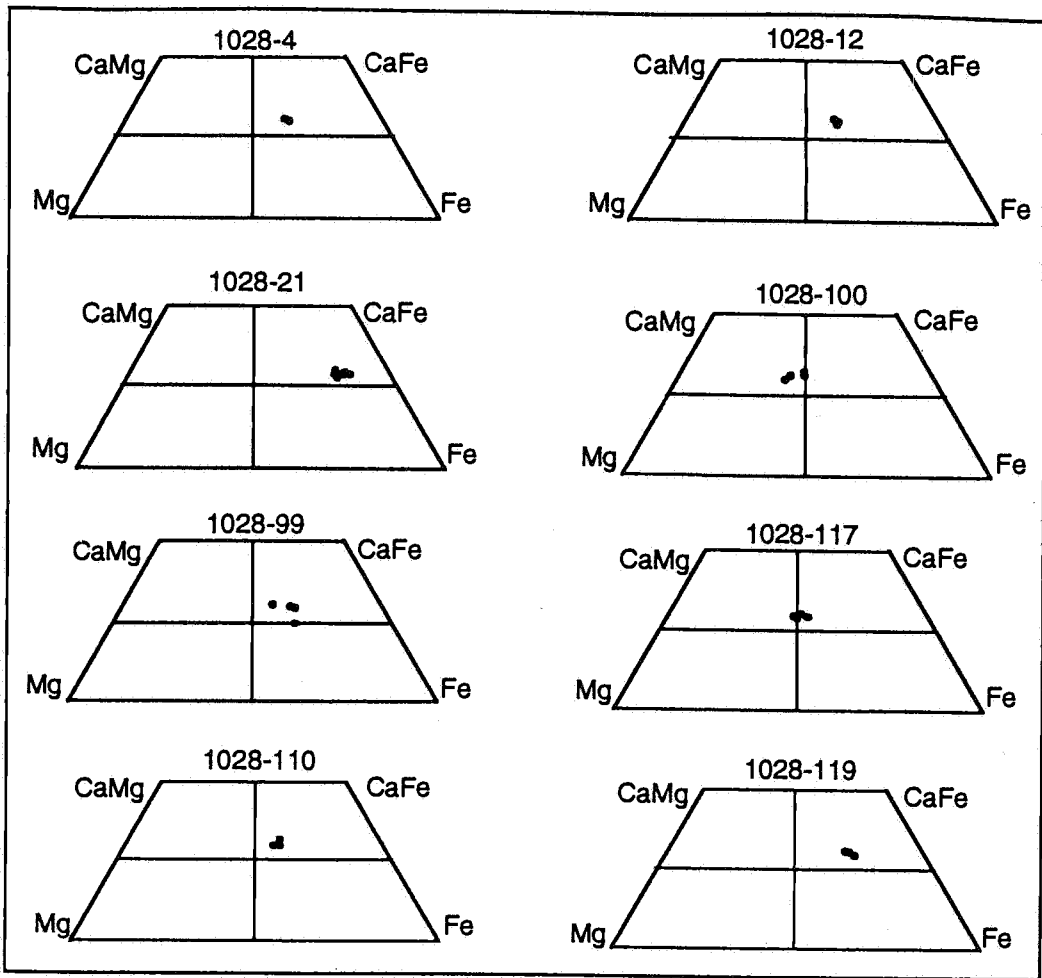
Figure 3. Geochemistry of amphiboles in Tournefort mafic dykes
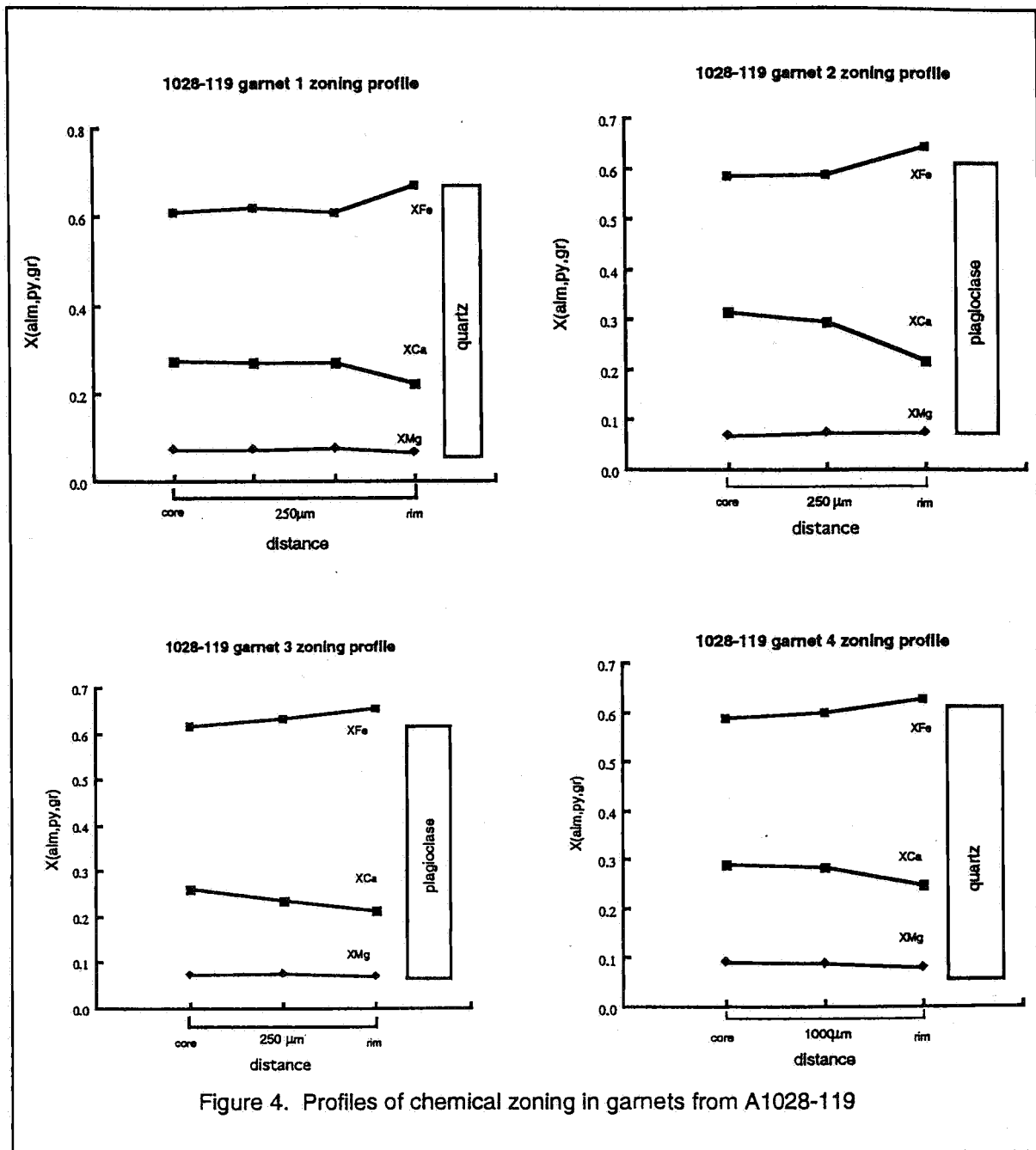
Figure 4. Profiles of chemical zoning in garnets from A1028-119
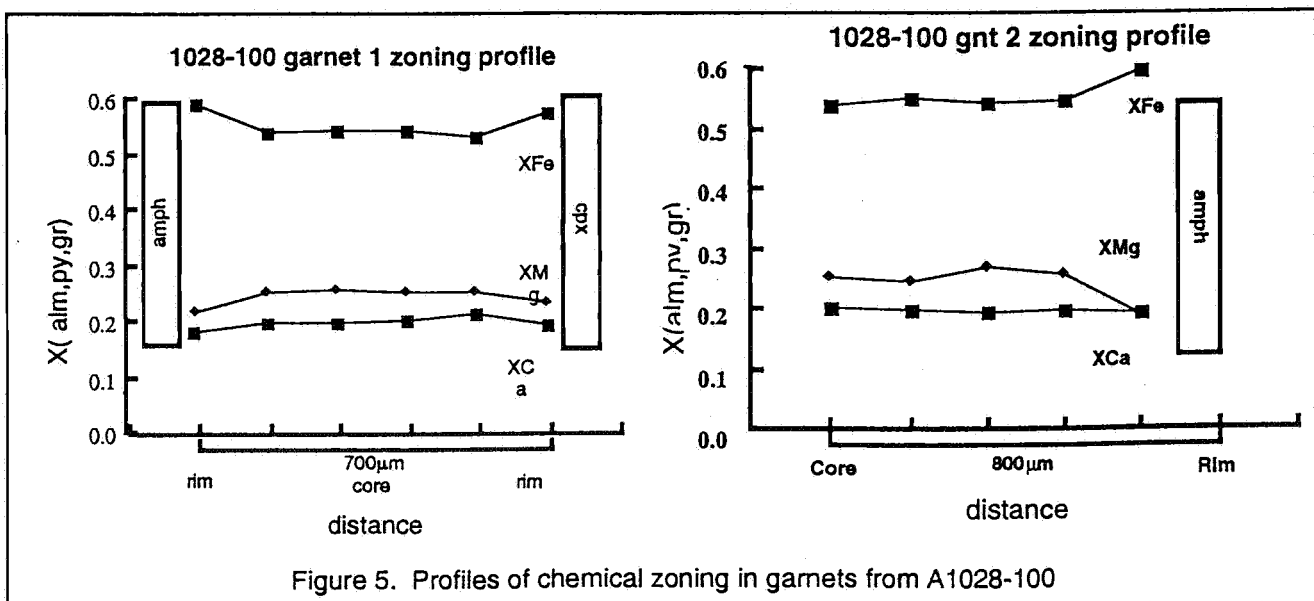
Figure 5. Profiles of chemical zoning in garnets from A1028-100

Figure 6. Profiles of chemical zoning in garnets from A1028-12

Figure 7. Profiles of chemical zoning in garnets from A1028-67
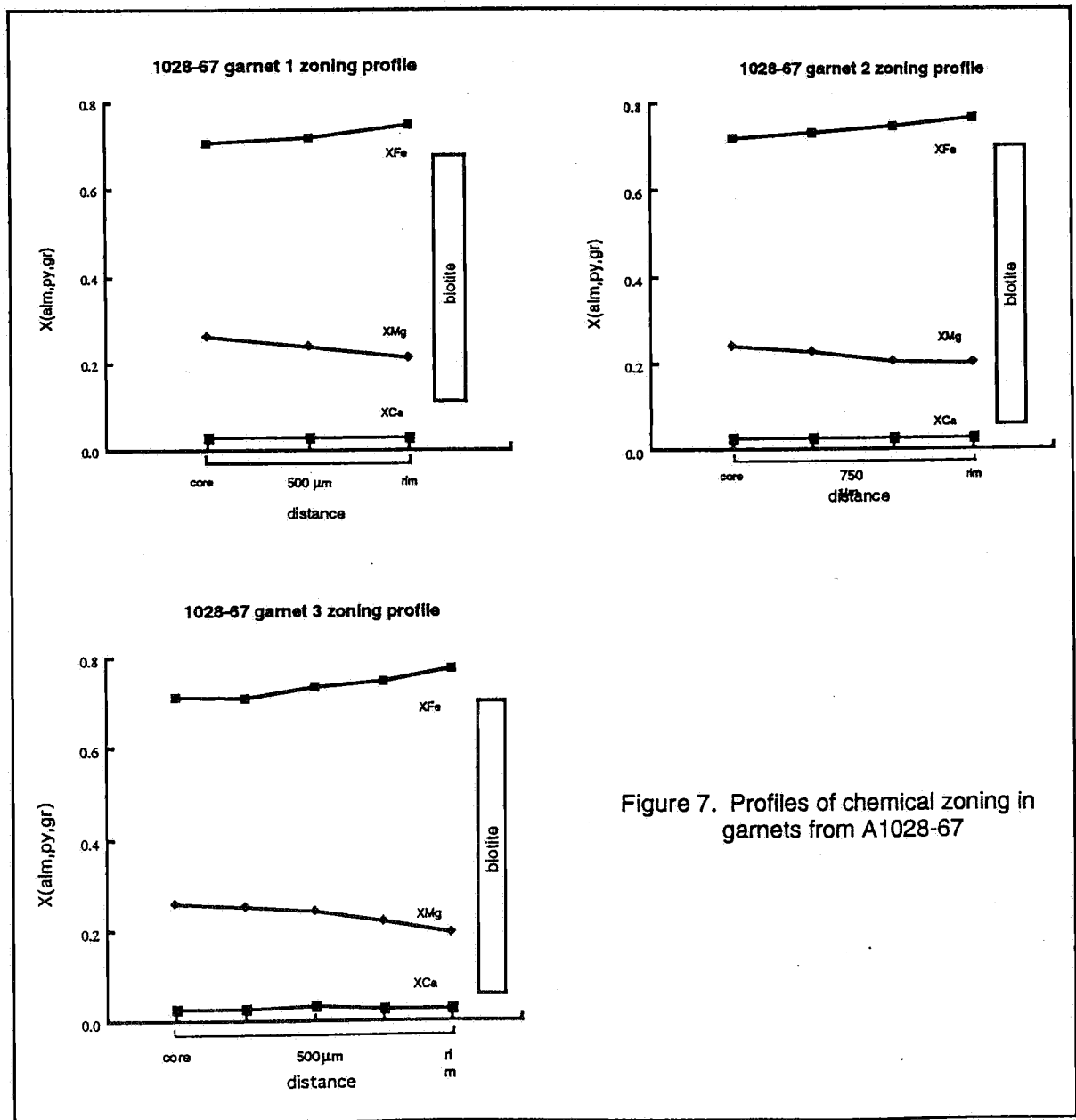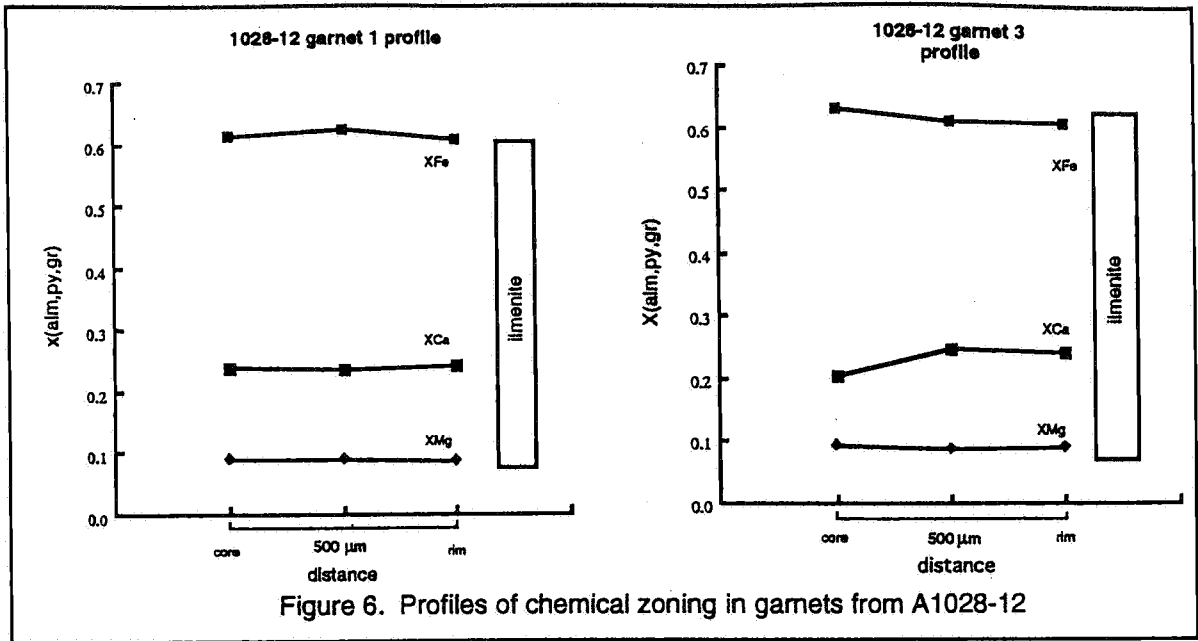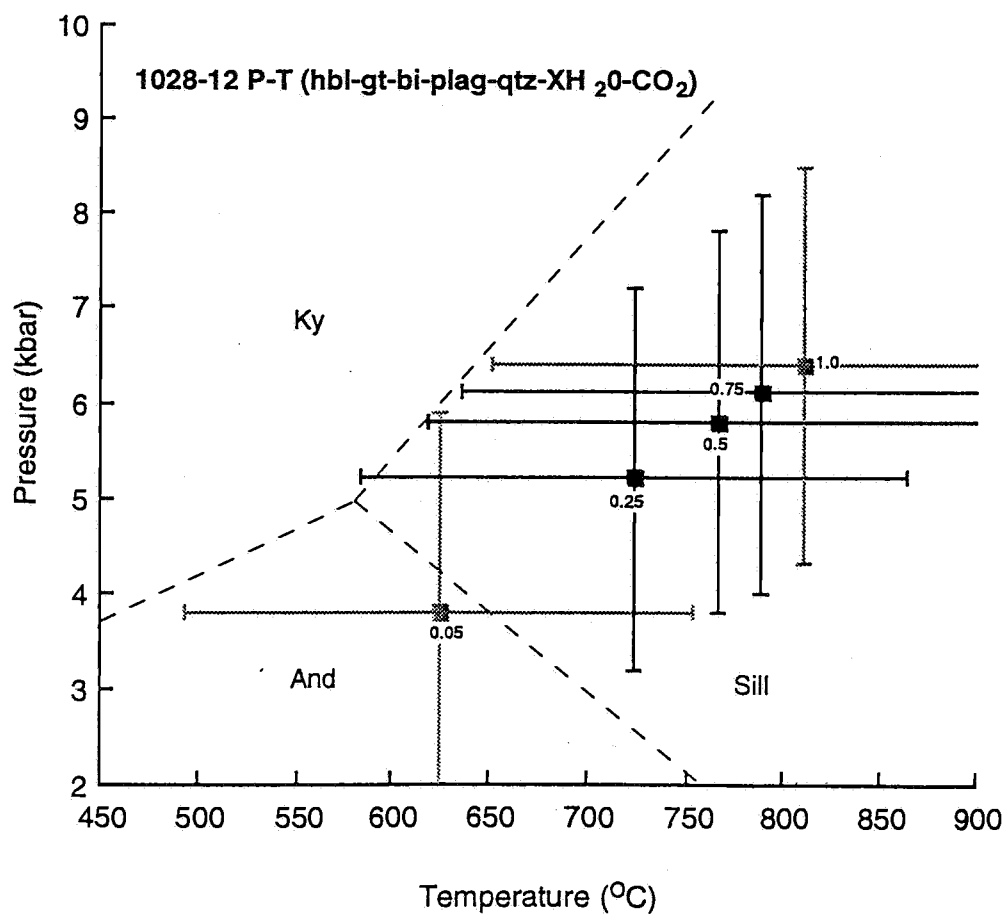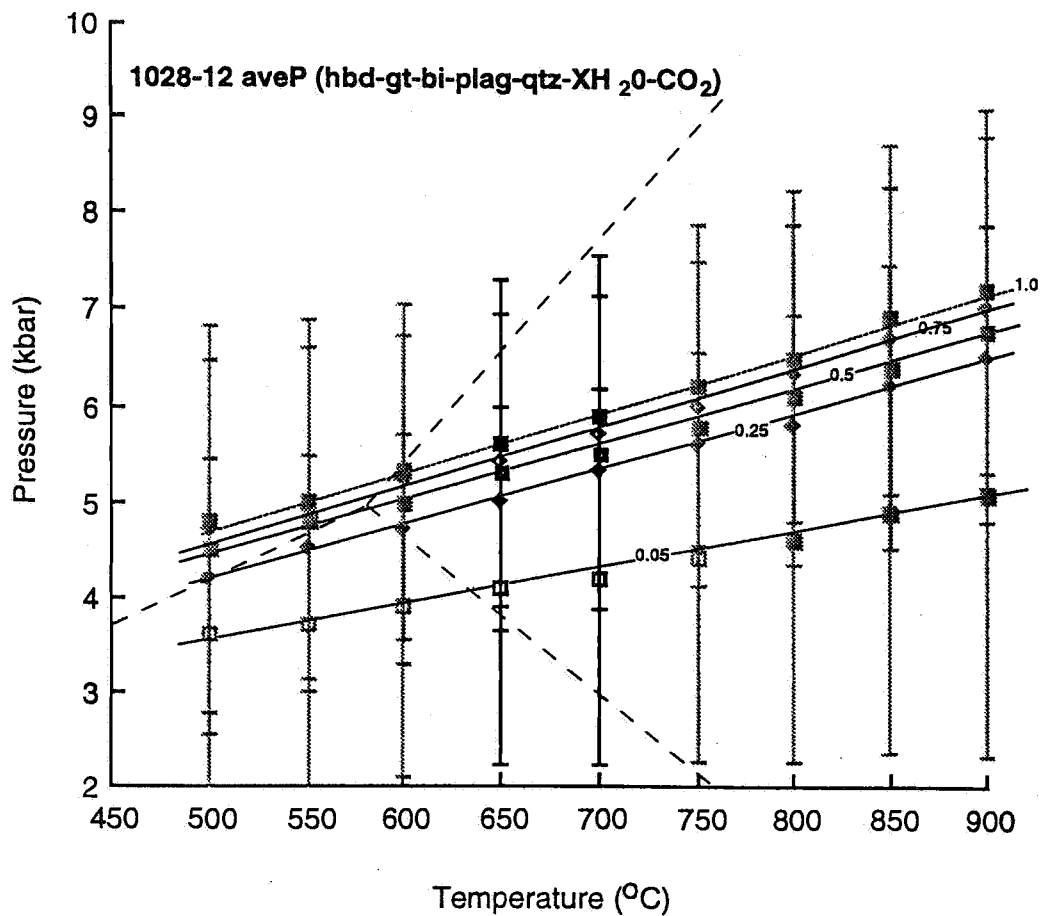
Figure 8. P-T estimates for sample A1028-12 from Lookout
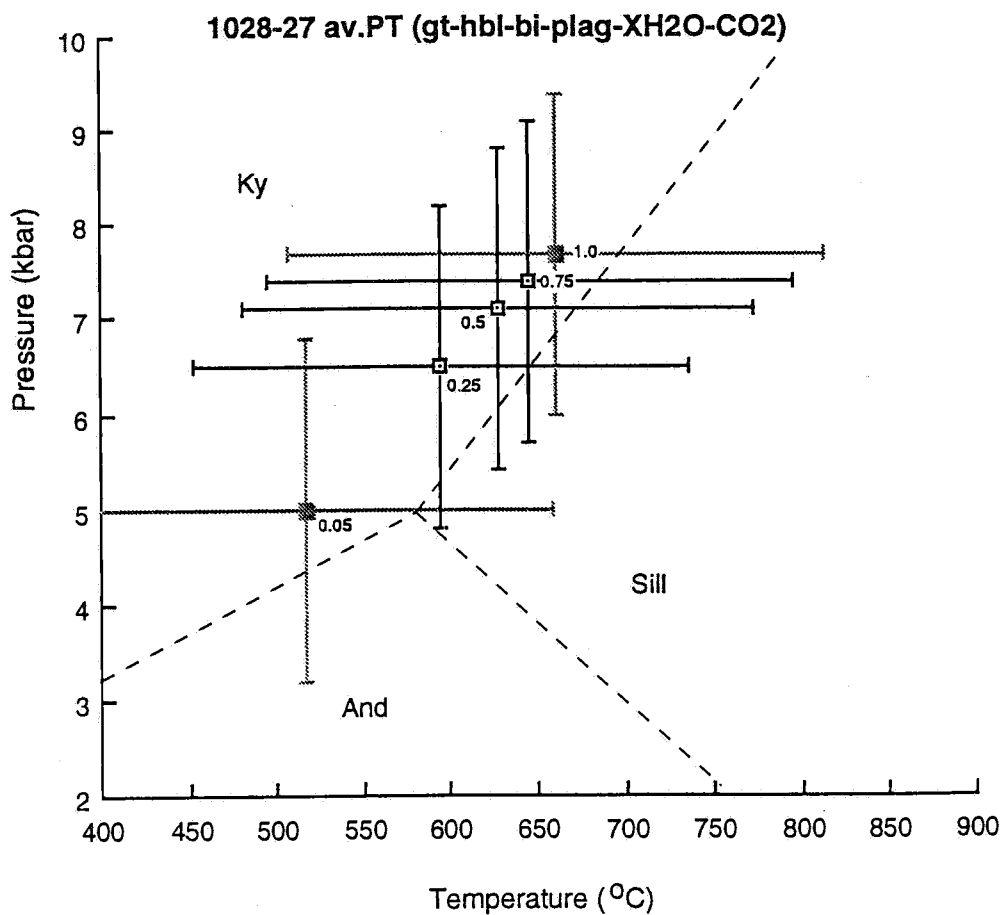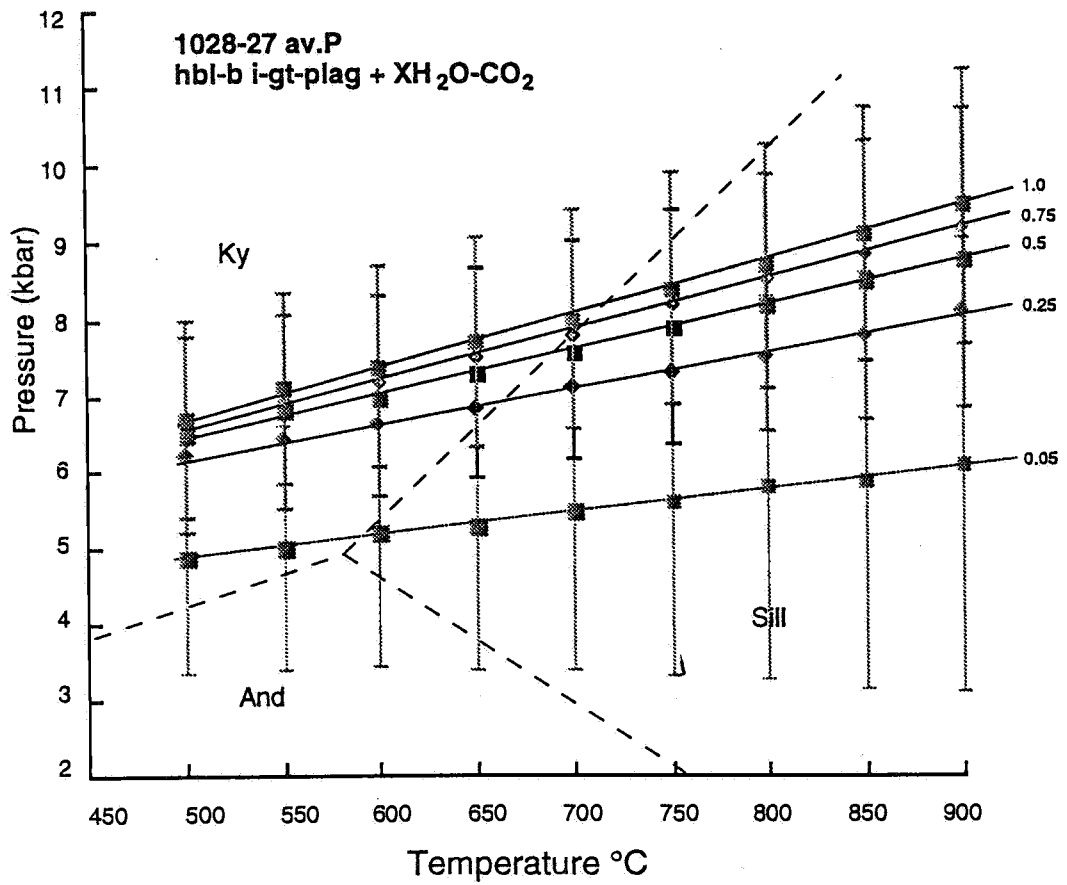
Figure 9. P-T estimates for sample A1028-27 from Louth Bay
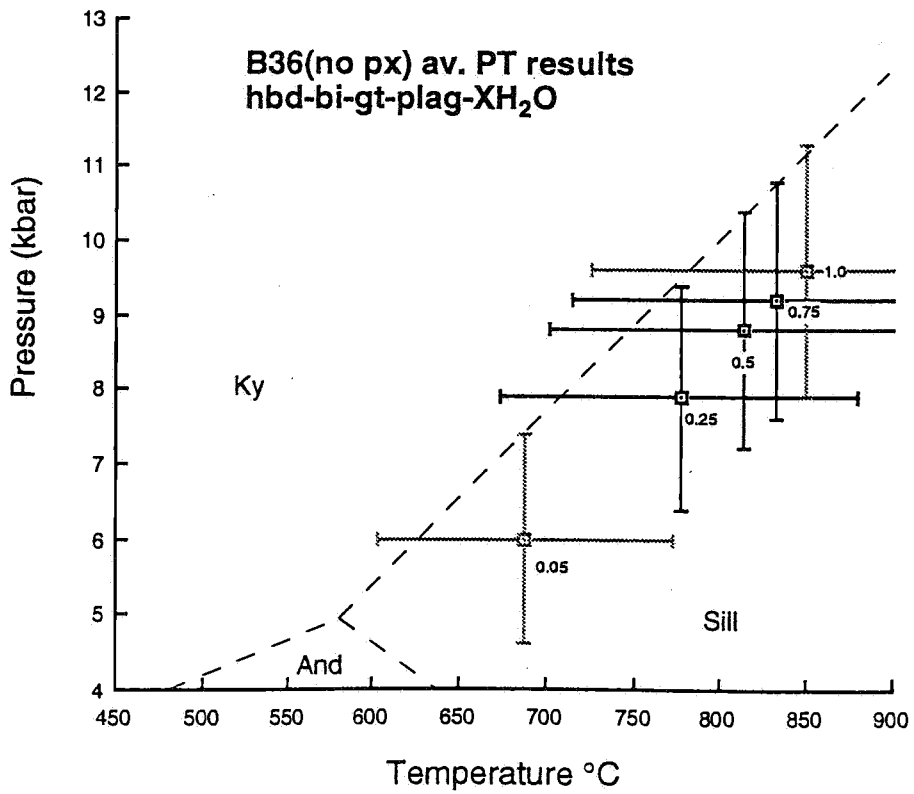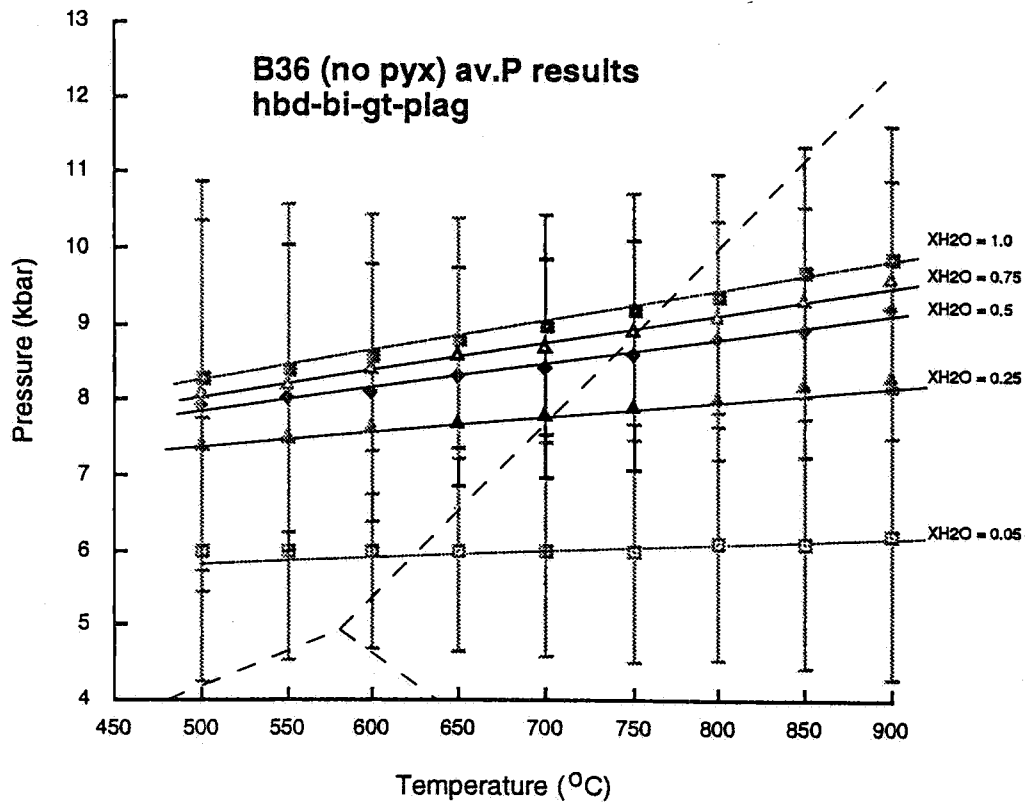
Figure 10. P-T estimates for sample B36 (Mortimer, 1984) from Surfleet Cove
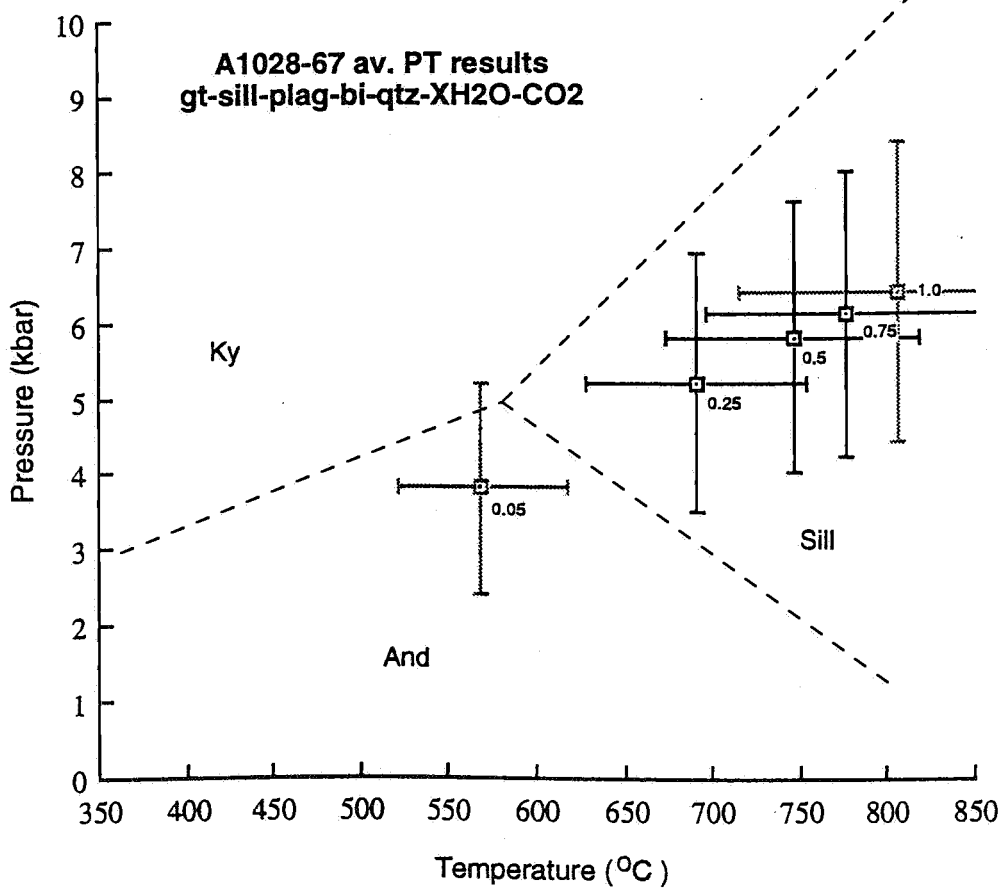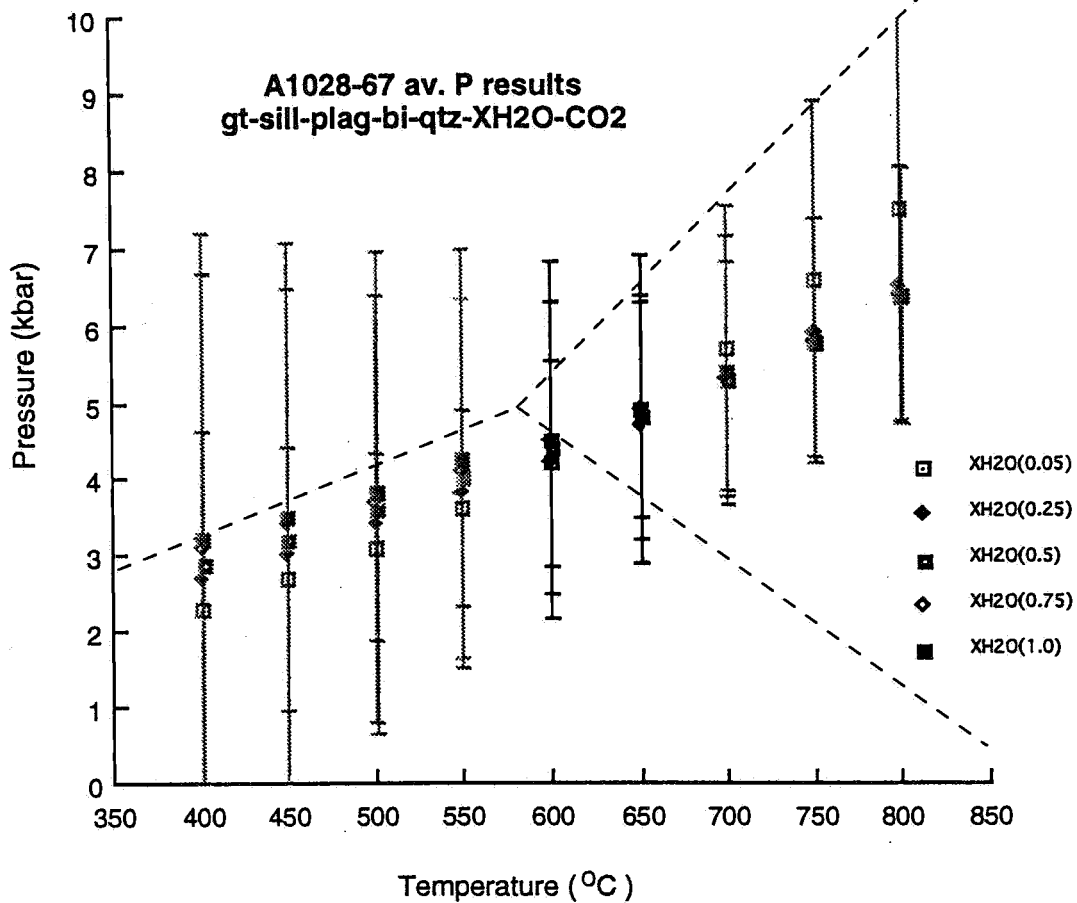
Figure 11. P-T estimates for sample A1028-67 from Mine Creek
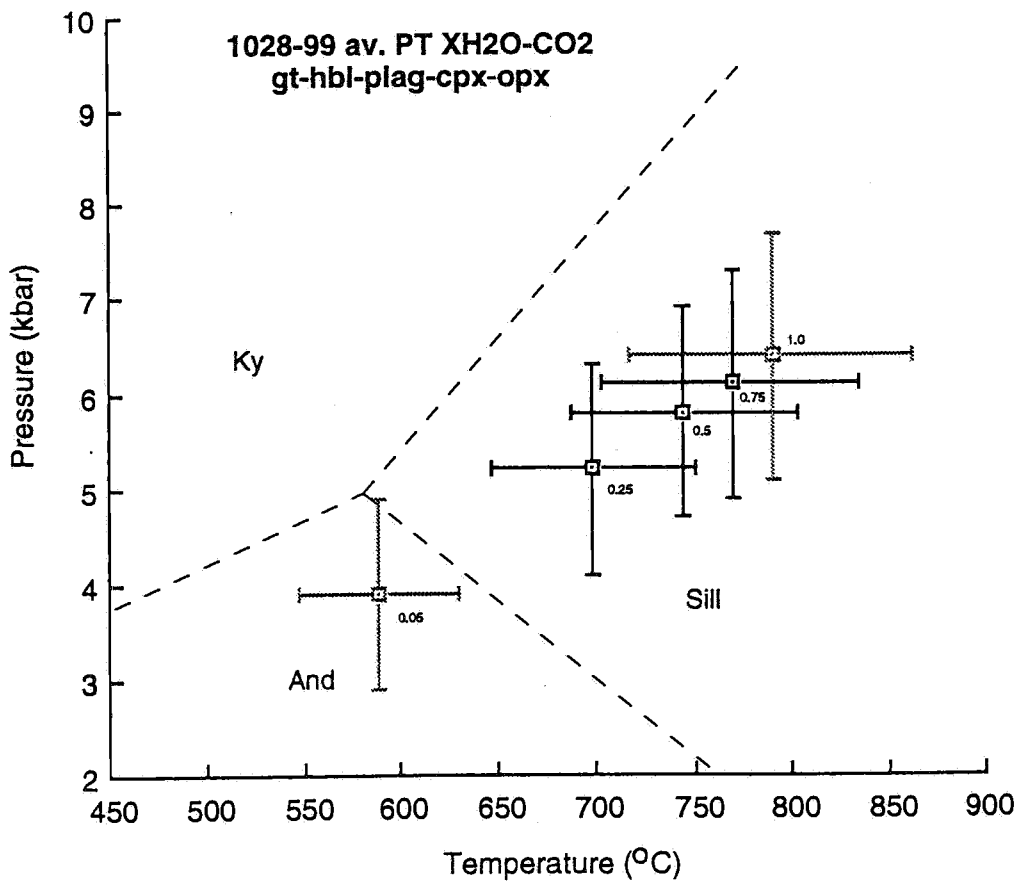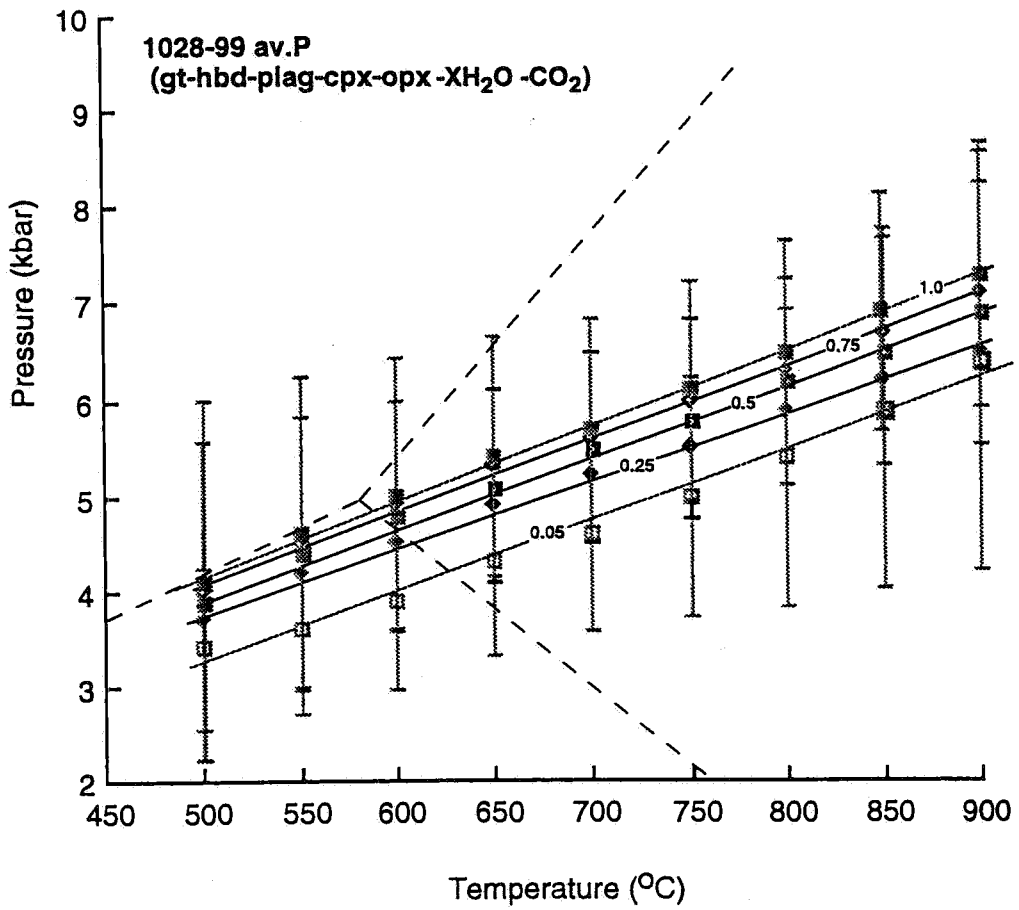
Figure 12. P-T estimates for sample A1028-99 from West Point

Figure 13. P-T estimates for sample A1028-21 from Lookout

Figure 14. P-T estimates for sample A1028-100 from West Point
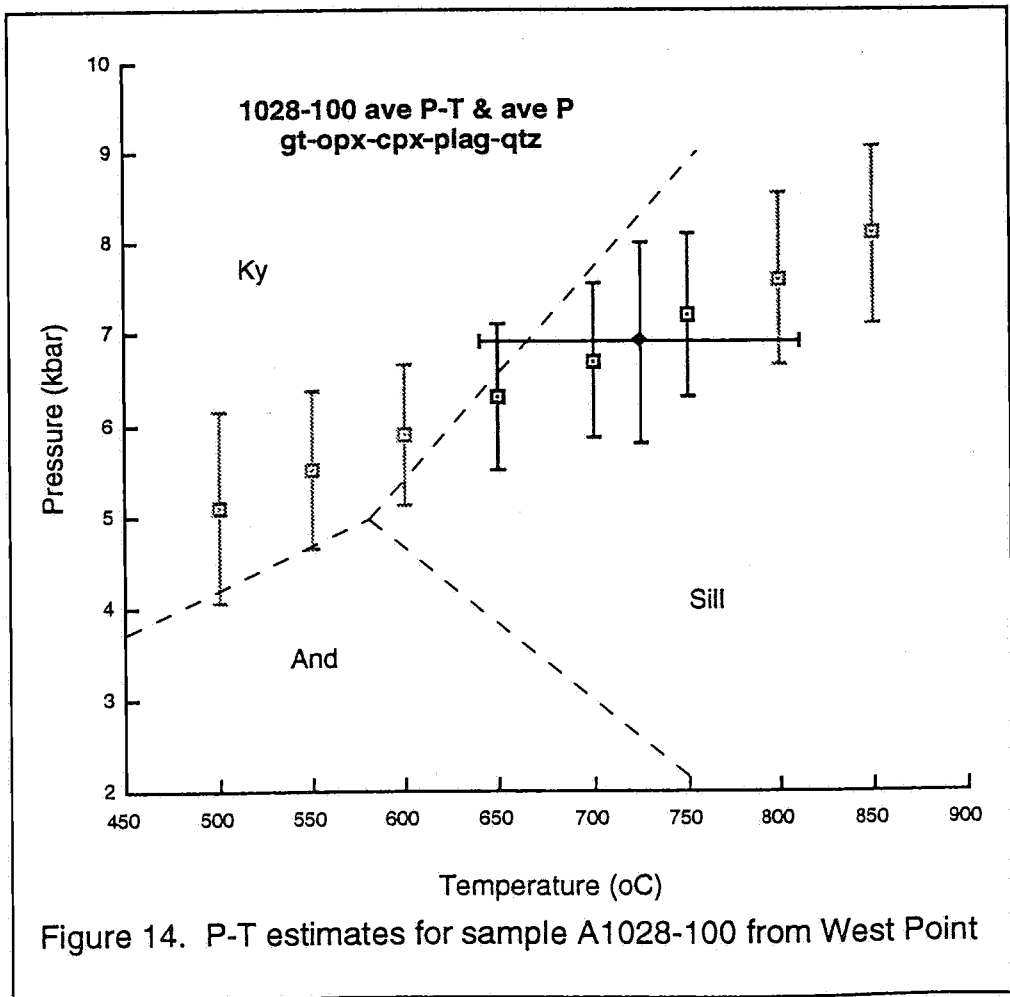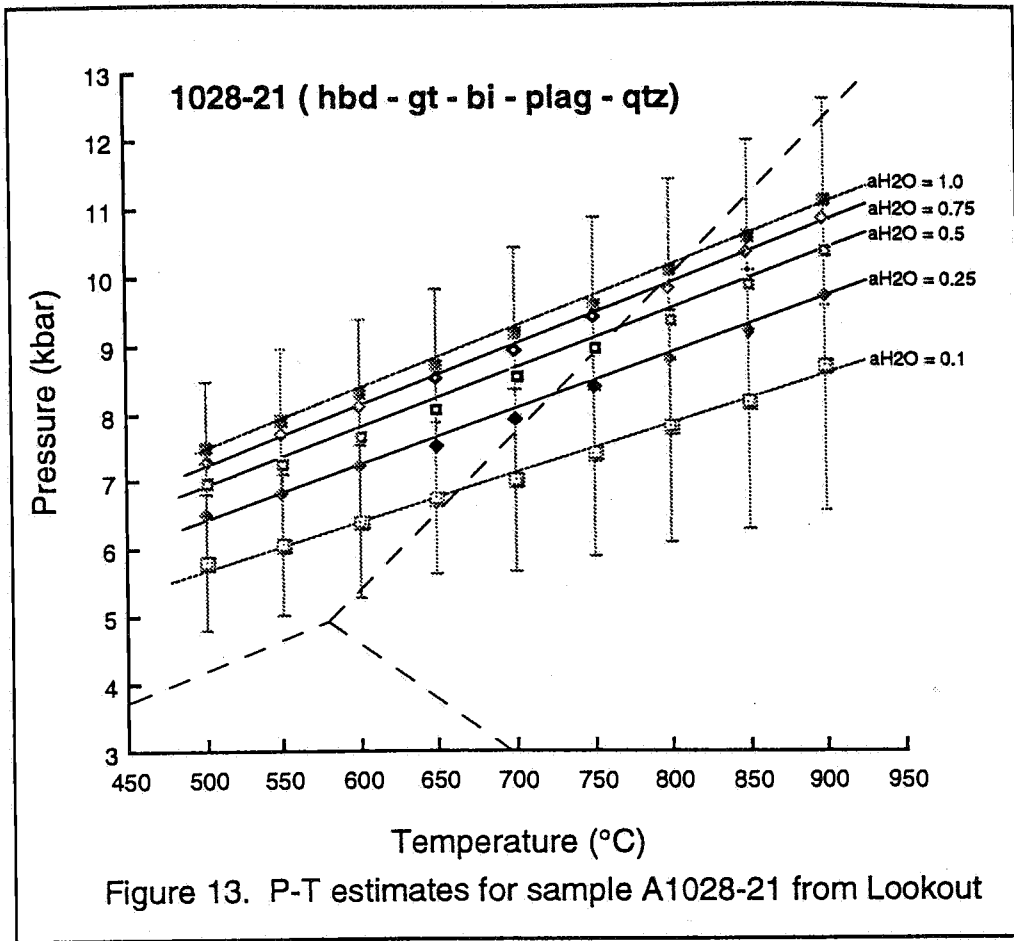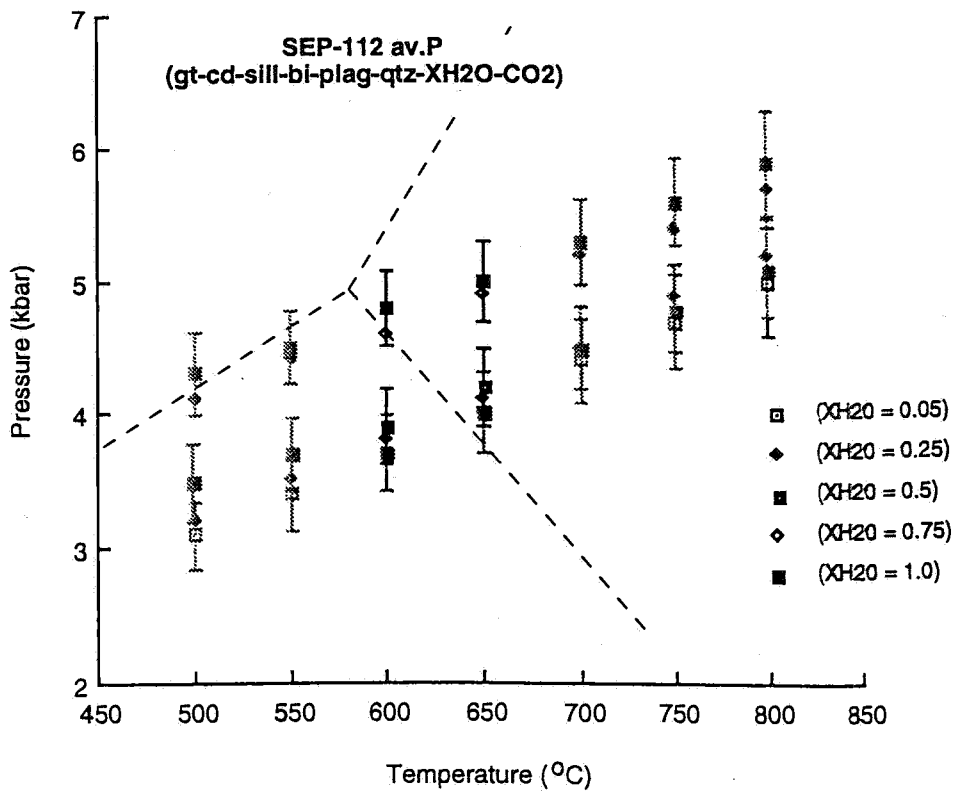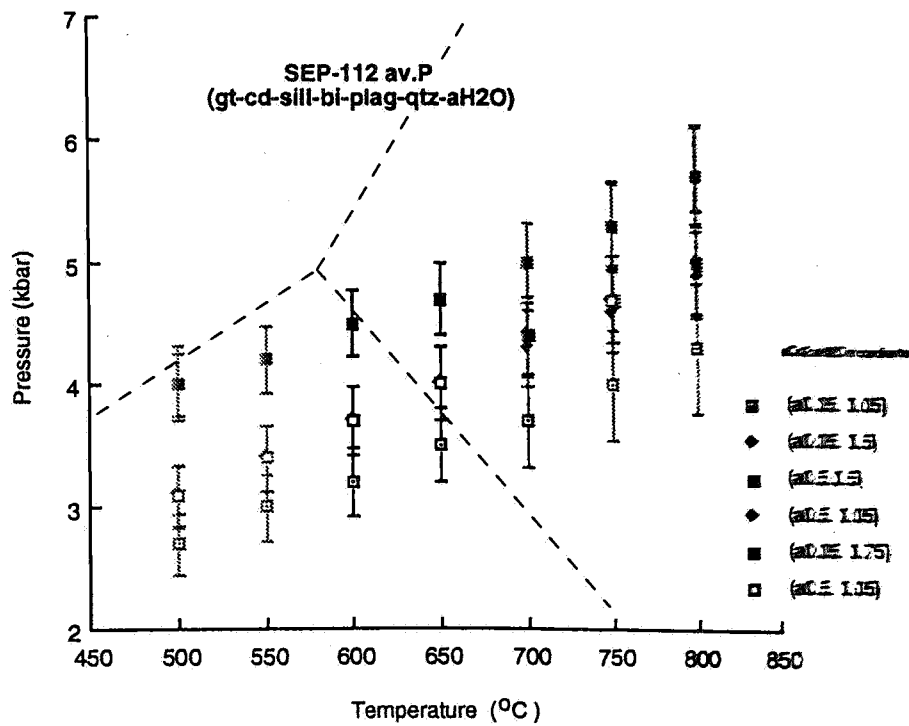
Figure 15. P-T estimates for sample SEP-112
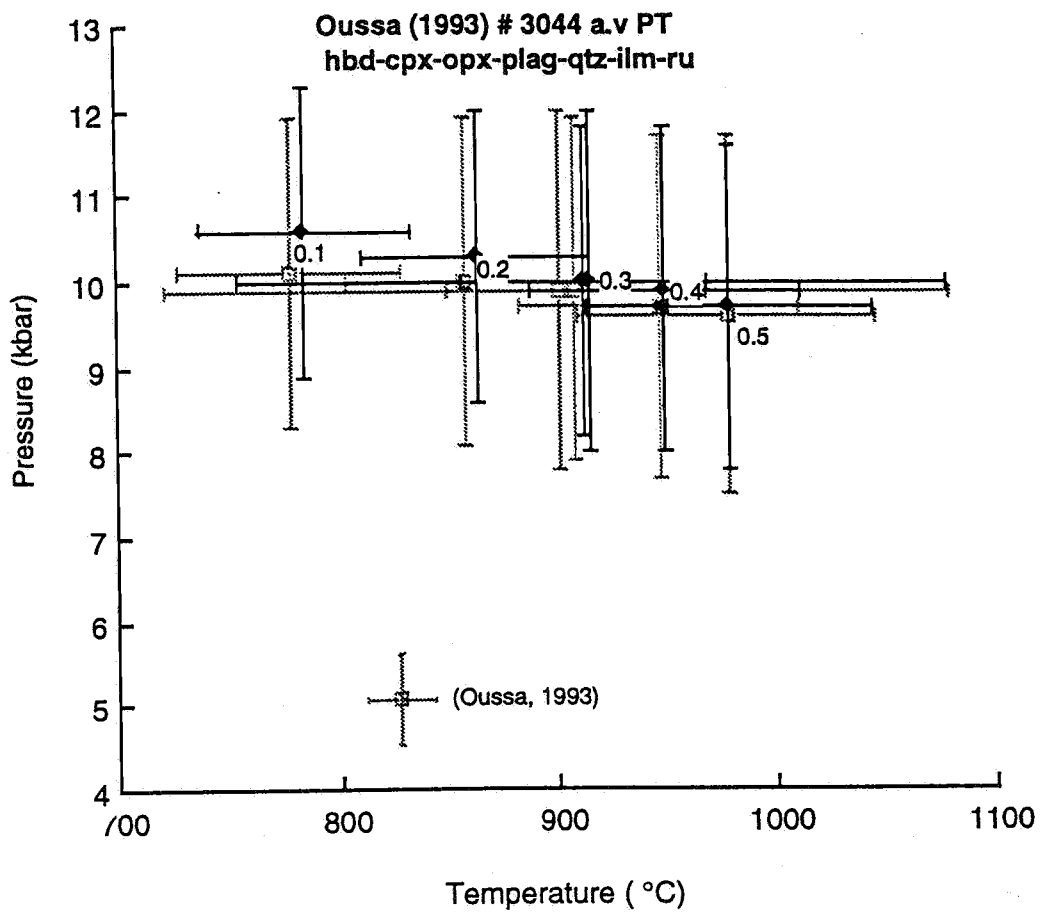
Figure 16. P-T estimates for sample 3044 (Oussa, 1993) from Pt Neill
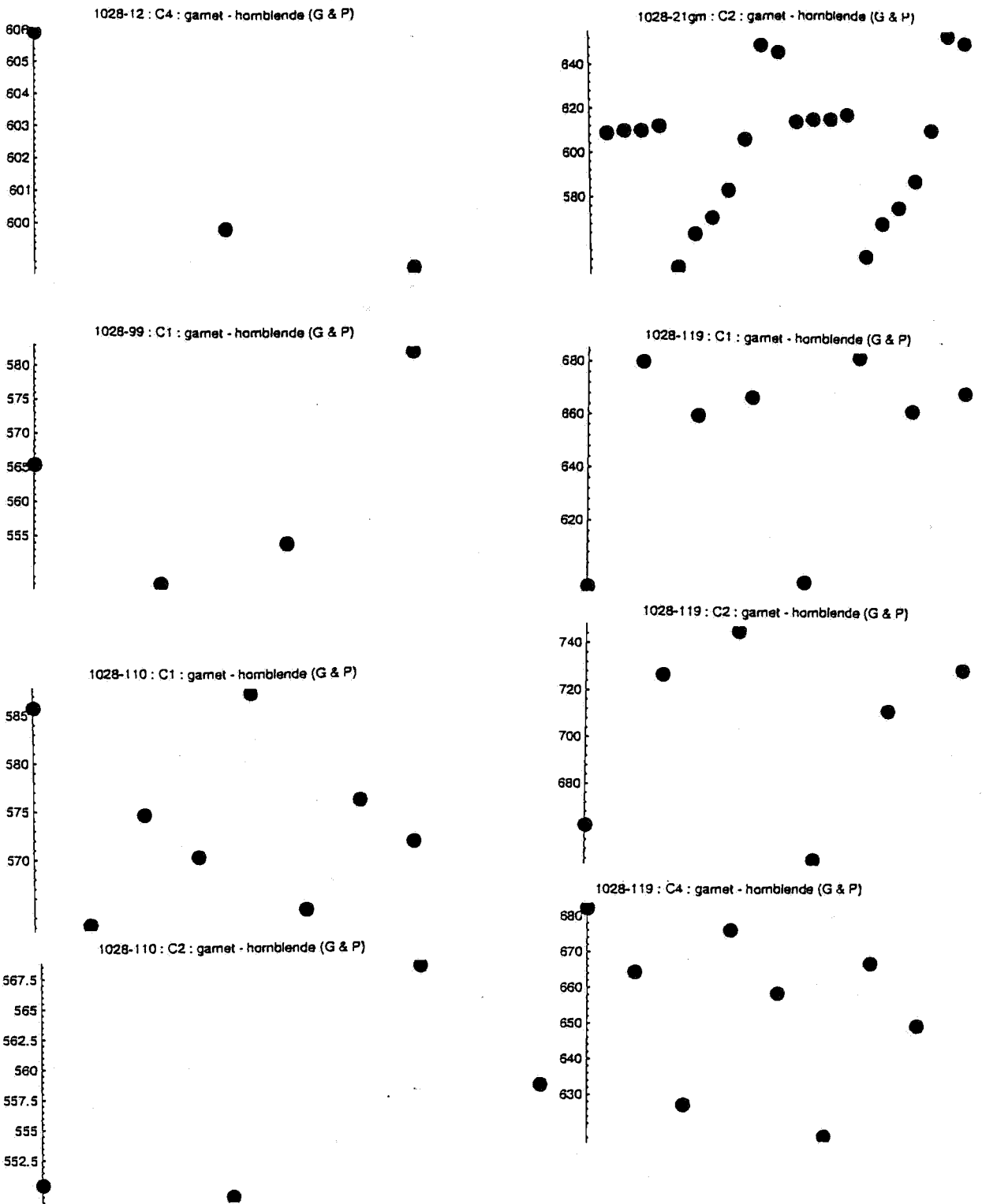
Figure 17a. Results of applied geothermometers.

Appendix C: Example of average P-T and average P calculations using THERMOCALC (Powell and Holland, 1988)

Pressure-temperature estimates can be derived using the average pressure-temperature and average pressure routines of the computer programme THERMOCALC (Powell and Holland, 1988) with the internally consistent data set of Holland and Powell (1990). Independent reactions are calculated from the equilibrium mineral assemblage, and combined to produce a weighted estimate of the desired parameter. A chi squared test is applied to the calculated answer and expressed as a sigma fit. If this value is below a critical value, the answer is accepted at 95% confidence.

THERMOCALC v2.2b1 running at 10.31 on Tue 11 Oct, 1994
(thermodynamic dataset produced at 17.20 on Tue 8 Sep, 1992)

an independent set of reactions has been calculated

Rock name : A1028-27 (suggested T = 700°C) (for x(CO2) = 0.95 and x(H2O) = 0.05)

	an	ab	gr	py	alm	phl	ann	naph
a	0.604	0.540	0.0110	0.00108	0.254	0.0267	0.113	0.00127
sd(a)/a	0.05000	0.06348	0.54440	1.16667	0.15000	0.42007	0.23950	7.86782

	tr	ftr	hb	ed	parg	H2O
a	5.60e-5	7.57e-4	0.00166	7.72e-4	0.00411	0.0500
sd(a)/a	2.67261	0.87191	0.55206	0.86978	1.00754	

reactions
1)   4an + 2ed = ab + 2gr + py + naph + hb
2)   12an + 3tr + 3ed = 3ab + 4gr + 2py + 6hb
3)   12an + 6tr + 3parg = 3ab + 4gr + 2py + 9hb
4)   12an + 10naph + 3ed = 4ab + 3py + 9parg + 4H2O
5)   12an + 3py + 3ftr + 3ed = 3ab + 4gr + 5alm + 6hb
6)   12an + 5phl + 3ftr + 3ed = 3ab + 4gr + 2py + 5ann + 6hb

Rock   : average pressures (for x(CO2) = 0.95 and x(H2O) = 0.05)

Single end-member diagnostic information

av, sd, fit are result of doubling the uncertainty on ln a :
a ln a is suspect if any are v different from lsq values.
e* are ln a residuals normalised to ln a uncertainties :
large absolute values, say >2.5, point to suspect info.
hat are the diagonal elements of the hat matrix :
large values, say >0.43, point to influential data.
For 95% confidence, fit (= sd(fit)) should be less than 1.49;
however a larger value may be OK - look at the diagnostics!

	av	sd	fit
lsq	5.45	2.08	1.41

	P	sd	fit	e*	hat
an	5.40	2.12	1.41	0.1	0.01
ab	5.45	2.09	1.41	-0.0	0.00
gr	6.06	3.15	1.40	0.2	0.45
py	5.50	2.07	1.40	0.5	0.01
alm	5.54	2.15	1.41	0.1	0.02
phl	6.31	1.87	1.19	1.3	0.08

```
       ann    5.86   1.99   1.31   -0.8  0.03
      naph    5.44   2.08   1.41    0.2  0.00
        tr    5.47   1.98   1.34    1.1  0.00
       ftr    4.88   1.88   1.23    1.2  0.04
        hb    4.75   1.49   0.98   -1.9  0.03
        ed    5.20   2.29   1.40    0.3  0.17
      parg    5.58   2.17   1.40   -0.3  0.08
       H2O    5.50   2.09   1.40    0.2  0.00
```

T°C	500	550	600	650	700	750	800	850	900
av P	4.9	5.0	5.2	5.3	5.5	5.6	5.8	5.9	6.1
sd	1.52	1.61	1.74	1.90	2.08	2.29	2.50	2.73	2.96
f	1.3	1.3	1.3	1.4	1.4	1.5	1.5	1.6	1.7

****

an independent set of reactions has been calculated

Rock name :A1028-27 (suggested T = 700°C) (for x(CO2) = 0.75 and
x(H2O) = 0.25)

```
              an       ab       gr       py      alm      phl      ann     naph
a          0.604    0.540   0.0110  0.00108    0.254   0.0267    0.113  0.00127
sd(a)/a  0.05000  0.06348  0.54440  1.16667  0.15000  0.42007  0.23950  7.86782

              tr      ftr       hb       ed     parg      H2O
a         5.60e-5  7.57e-4  0.00166  7.72e-4  0.00411    0.250
sd(a)/a   2.67261  0.87191  0.55206  0.86978  1.00754
```

reactions
1)   4an + 2ed = ab + 2gr + py + naph + hb
2)   12an + 3tr + 3ed = 3ab + 4gr + 2py + 6hb
3)   12an + 6tr + 3parg = 3ab + 4gr + 2py + 9hb
4)   11ab + 12gr + 19hb + 21parg = 52an + 32ed + 8H2O
5)   12an + 3py + 3ftr + 3ed = 3ab + 4gr + 5alm + 6hb
6)   12an + 5phl + 3ftr + 3ed = 3ab + 4gr + 2py + 5ann + 6hb

Rock : average pressures (for x(CO2) = 0.75 and x(H2O) = 0.25)

Single end-member diagnostic information

av, sd, fit are result of doubling the uncertainty on ln a :
a ln a is suspect if any are v different from lsq values.
e* are ln a residuals normalised to ln a uncertainties :
large absolute values, say >2.5, point to suspect info.
hat are the diagonal elements of the hat matrix :
large values, say >0.43, point to influential data.
For 95% confidence, fit (= sd(fit)) should be less than 1.49;
however a larger value may be OK - look at the diagnostics!

```
           av    sd    fit
lsq       7.05  1.63  1.09

                 P     sd    fit     e*    hat

        an     7.02   1.66   1.09    0.1   0.01
        ab     7.05   1.63   1.09   -0.0   0.00
        gr     7.48   2.46   1.08    0.1   0.45
        py     7.08   1.62   1.08    0.3   0.01
       alm     7.12   1.68   1.09    0.1   0.02
       phl     7.73   1.45   0.92    1.1   0.08
       ann     7.38   1.55   1.01   -0.6   0.02
```

```
          naph    7.04    1.62    1.09     0.3    0.00
            tr    7.06    1.54    1.03     0.9    0.00
           ftr    6.57    1.43    0.93     1.0    0.04
            hb    6.52    1.22    0.80    -1.4    0.03
            ed    7.15    1.80    1.09    -0.1    0.17
          parg    6.97    1.70    1.09     0.2    0.08
          H2O     7.06    1.63    1.09     0.0    0.00
```

T°C	500	550	600	650	700	750	800	850	900
av P	6.2	6.4	6.6	6.8	7.1	7.3	7.5	7.8	8.1
sd	1.40	1.39	1.43	1.51	1.63	1.76	1.92	2.08	2.26
f	1.1	1.1	1.1	1.1	1.1	1.1	1.2	1.2	1.3

****

an independent set of reactions has been calculated

Rock name : A1028-27 (suggested T = 700°C) (for x(CO2) = 0.5 and
x(H2O) = 0.5)

	an	ab	gr	py	alm	phl	ann	naph
a	0.604	0.540	0.0110	0.00108	0.254	0.0267	0.113	0.00127
sd(a)/a	0.05000	0.06348	0.54440	1.16667	0.15000	0.42007	0.23950	7.86782

	tr	ftr	hb	ed	parg	H2O
a	5.60e-5	7.57e-4	0.00166	7.72e-4	0.00411	0.500
sd(a)/a	2.67261	0.87191	0.55206	0.86978	1.00754	

reactions
1)   4an + 2ed = ab + 2gr + py + naph + hb
2)   12an + 3tr + 3ed = 3ab + 4gr + 2py + 6hb
3)   12an + 6tr + 3parg = 3ab + 4gr + 2py + 9hb
4)   11ab + 12gr + 40hb = 52an + 21tr + 11ed + 8H2O
5)   12an + 3py + 3ftr + 3ed = 3ab + 4gr + 5alm + 6hb
6)   12an + 5phl + 3ftr + 3ed = 3ab + 4gr + 2py + 5ann + 6hb

Rock : average pressures (for x(CO2) = 0.5 and x(H2O) = 0.5)

Single end-member diagnostic information

av, sd, fit are result of doubling the uncertainty on ln a :
a ln a is suspect if any are v different from lsq values.
e* are ln a residuals normalised to ln a uncertainties :
large absolute values, say >2.5, point to suspect info.
hat are the diagonal elements of the hat matrix :
large values, say >0.43, point to influential data.
For 95% confidence, fit (= sd(fit)) should be less than 1.49;
however a larger value may be OK - look at the diagnostics!

	av	sd	fit
lsq	7.60	1.44	0.99

	P	sd	fit	e*	hat
an	7.57	1.47	0.99	0.1	0.01
ab	7.60	1.44	0.99	-0.0	0.00
gr	7.84	2.20	0.99	0.1	0.45
py	7.62	1.44	0.99	0.2	0.01
alm	7.64	1.49	0.99	0.1	0.02
phl	8.20	1.53	0.84	0.9	0.08
ann	7.89	1.48	0.92	-0.5	0.03
naph	7.58	1.44	0.98	0.3	0.00

```
          tr    7.61    1.44    0.93     0.8   0.00
         ftr    7.18    1.48    0.84     0.9   0.04
          hb    7.20    1.47    0.75    -1.2   0.03
          ed    7.79    1.59    0.98    -0.3   0.16
        parg    7.42    1.51    0.97     0.3   0.09
         H2O    7.60    1.44    0.99     0.0   0.00
```

T°C	500	550	600	650	700	750	800	850	900
av P	6.5	6.8	7.0	7.3	7.6	7.9	8.2	8.5	8.8
sd	1.30	1.28	1.30	1.37	1.44	1.53	1.66	1.80	1.96
f	1.1	1.0	1.0	1.0	1.0	1.0	1.1	1.1	1.1

****

an independent set of reactions has been calculated

Rock name : A1028-27 (suggested T = 700°C) (for x(CO2) = 0.25 and x(H2O) = 0.75)

```
                an       ab       gr       py     alm       phl      ann     naph
a             0.604    0.540   0.0110  0.00108   0.254   0.0267    0.113  0.00127
sd(a)/a     0.05000  0.06348  0.54440  1.16667 0.15000 0.42007  0.23950 7.86782
```

```
                tr      ftr       hb       ed    parg      H2O
a            5.60e-5  7.57e-4  0.00166  7.72e-4 0.00411   0.750
sd(a)/a      2.67261  0.87191  0.55206  0.86978 1.00754
```

reactions
1)   4an + 2ed = ab + 2gr + py + naph + hb
2)   12an + 3tr + 3ed = 3ab + 4gr + 2py + 6hb
3)   12an + 6tr + 3parg = 3ab + 4gr + 2py + 9hb
4)   11ab + 12gr + 40hb = 52an + 21tr + 11ed + 8H2O
5)   12an + 3py + 3ftr + 3ed = 3ab + 4gr + 5alm + 6hb
6)   12an + 5phl + 3ftr + 3ed = 3ab + 4gr + 2py + 5ann + 6hb

Rock : average pressures (for x(CO2) = 0.25 and x(H2O) = 0.75)

Single end-member diagnostic information

av, sd, fit are result of doubling the uncertainty on ln a :
a ln a is suspect if any are v different from lsq values.
e* are ln a residuals normalised to ln a uncertainties :
large absolute values, say >2.5, point to suspect info.
hat are the diagonal elements of the hat matrix :
large values, say >0.43, point to influential data.
For 95% confidence, fit (= sd(fit)) should be less than 1.49;
however a larger value may be OK - look at the diagnostics!

```
            av     sd     fit
lsq       7.83   1.44    0.95
```

```
                  P      sd     fit      e*     hat

          an    7.81    1.47    0.95     0.0   0.01
          ab    7.83    1.44    0.95    -0.0   0.00
          gr    8.05    2.19    0.95     0.1   0.45
          py    7.85    1.44    0.95     0.1   0.01
         alm    7.87    1.49    0.95     0.1   0.02
         phl    8.41    1.53    0.81     0.9   0.08
         ann    8.11    1.48    0.89    -0.5   0.03
        naph    7.81    1.44    0.95     0.3   0.00
          tr    7.85    1.44    0.90     0.8   0.00
```

```
      ftr   7.43   1.48   0.81    0.9  0.04
       hb   7.46   1.46   0.74   -1.1  0.03
       ed   8.08   1.58   0.94   -0.3  0.16
     parg   7.63   1.51   0.93    0.4  0.09
      H2O   7.83   1.44   0.95    0.0  0.00
```

T°C	500	550	600	650	700	750	800	850	900
av P	6.6	6.9	7.2	7.5	7.8	8.1	8.5	8.8	9.2
sd	1.30	1.26	1.30	1.37	1.44	1.51	1.58	1.72	1.86
f	1.1	1.0	1.0	1.0	1.0	1.0	1.0	1.0	1.1

```
*************************************
```

an independent set of reactions has been calculated

Rock name : A1028-27 (suggested T = 700°C)(for x(H2O) = 1.0)

```
              an       ab       gr       py      alm      phl      ann     naph
a           0.604    0.540   0.0110  0.00108    0.254   0.0267    0.113  0.00127
sd(a)/a    0.05000  0.06348  0.54440  1.16667  0.15000  0.42007  0.23950  7.86782

              tr      ftr       hb       ed     parg      H2O
a          5.60e-5  7.57e-4  0.00166  7.72e-4  0.00411     1.00
sd(a)/a    2.67261  0.87191  0.55206  0.86978  1.00754
```

reactions
1)   4an + 2ed = ab + 2gr + py + naph + hb
2)   12an + 3tr + 3ed = 3ab + 4gr + 2py + 6hb
3)   12an + 6tr + 3parg = 3ab + 4gr + 2py + 9hb
4)   11ab + 12gr + 40hb = 52an + 21tr + 11ed + 8H2O
5)   12an + 3py + 3ftr + 3ed = 3ab + 4gr + 5alm + 6hb
6)   12an + 5phl + 3ftr + 3ed = 3ab + 4gr + 2py + 5ann + 6hb

Rock : average pressures(for x(H2O) = 1.0)

Single end-member diagnostic information

av, sd, fit are result of doubling the uncertainty on ln a :
a ln a is suspect if any are v different from 1sq values.
e* are ln a residuals normalised to ln a uncertainties :
large absolute values, say >2.5, point to suspect info.
hat are the diagonal elements of the hat matrix :
large values, say >0.43, point to influential data.
For 95% confidence, fit (= sd(fit)) should be less than 1.49;
however a larger value may be OK - look at the diagnostics!

```
          av    sd    fit
1sq      8.04  1.43  0.93

            P     sd    fit     e*    hat

      an   8.02  1.46   0.93    0.0   0.01
      ab   8.04  1.44   0.93   -0.0   0.00
      gr   8.23  2.19   0.93    0.1   0.45
      py   8.05  1.44   0.93    0.1   0.01
     alm   8.08  1.48   0.93    0.1   0.02
     phl   8.59  1.52   0.79    0.9   0.08
     ann   8.31  1.48   0.87   -0.5   0.03
    naph   8.02  1.44   0.92    0.3   0.00
      tr   8.06  1.44   0.88    0.8   0.00
     ftr   7.65  1.48   0.78    0.9   0.04
      hb   7.69  1.46   0.74   -1.1   0.03
```

```
      ed    8.33   1.58   0.91   -0.4   0.16
    parg    7.81   1.51   0.90    0.5   0.09
     H2O    8.04   1.43   0.93      0·     0
```

T°C	500	550	600	650	700	750	800	850	900
av P	6.7	7.1	7.4	7.7	8.0	8.4	8.7	9.1	9.5
sd	1.29	1.25	1.29	1.36	1.43	1.51	1.58	1.65	1.79
f	1.1	1.0	1.0	0.9	0.9	0.9	1.0	1.0	1.0

```
*************************************
```

THERMOCALC v2.2b1 running at 11.16 on Fri 14 Oct, 1994
(thermodynamic dataset produced at 17.20 on Tue 8 Sep, 1992)

an independent set of reactions has been calculated

Rock name : A1028-27 (suggested T = 700°C) (for a(H2O) = 0.25)

```
                 an       ab      gr      py      alm     phl      ann
naph
a             0.604    0.540  0.0110 0.00108   0.254  0.0267    0.113
0.00127
sd(a)/a       0.05000 0.06348 0.54440 1.16667 0.15000 0.42007 0.23950
7.86782

                 tr      ftr      hb      ed     parg     H2O
a             5.60e-5 7.57e-4 0.00166 7.72e-4 0.00411   0.250
sd(a)/a       2.67261 0.87191 0.55206 0.86978 1.00754
```

reactions
1)   4an + 2ed = ab + 2gr + py + naph + hb
2)   12an + 3tr + 3ed = 3ab + 4gr + 2py + 6hb
3)   12an + 6tr + 3parg = 3ab + 4gr + 2py + 9hb
4)   11ab + 12gr + 19hb + 21parg = 52an + 32ed + 8H2O
5)   12an + 3py + 3ftr + 3ed = 3ab + 4gr + 5alm + 6hb
6)   12an + 5phl + 3ftr + 3ed = 3ab + 4gr + 2py + 5ann + 6hb

Rock : average pressures (for a(H2O) = 0.25)

Single end-member diagnostic information

av, sd, fit are result of doubling the uncertainty on ln a :
a ln a is suspect if any are v different from lsq values.
e* are ln a residuals normalised to ln a uncertainties :
large absolute values, say >2.5, point to suspect info.
hat are the diagonal elements of the hat matrix :
large values, say >0.43, point to influential data.
For 95% confidence, fit (= sd(fit)) should be less than 1.49;
however a larger value may be OK - look at the diagnostics!

```
           av    sd    fit
lsq      6.66   1.70   1.16

             P     sd    fit    e*    hat

      an   6.62   1.73   1.15    0.1   0.01
      ab   6.66   1.71   1.16   -0.0   0.00
      gr   7.09   2.58   1.15    0.1   0.45
```

```
   py    6.69    1.70    1.15     0.3   0.01
  alm    6.73    1.75    1.15     0.1   0.02
  phl    7.38    1.52    0.97     1.1   0.08
  ann    7.01    1.62    1.07    -0.6   0.03
 naph    6.64    1.70    1.15     0.2   0.00
   tr    6.67    1.61    1.09     0.9   0.00
  ftr    6.17    1.50    0.99     1.0   0.04
   hb    6.12    1.25    0.83    -1.5   0.03
   ed    6.67    1.88    1.16    -0.0   0.17
 parg    6.63    1.78    1.16     0.1   0.08
  H2O    6.66    1.70    1.16       0      0
```

T°C	500	550	600	650	700	750	800	850	900
av P	5.7	5.9	6.2	6.4	6.7	6.9	7.2	7.4	7.7
sd	1.40	1.42	1.48	1.58	1.70	1.84	1.99	2.16	2.33
f	1.2	1.1	1.1	1.1	1.2	1.2	1.2	1.3	1.3

****

an independent set of reactions has been calculated

Rock name : A1028-27 (suggested T = 700°C) (for a(H2O) = 0.5)

	an	ab	gr	py	alm	phl	ann
naph							
a	0.604	0.540	0.0110	0.00108	0.254	0.0267	0.113
0.00127							
sd(a)/a	0.05000	0.06348	0.54440	1.16667	0.15000	0.42007	0.23950
7.86782							

	tr	ftr	hb	ed	parg	H2O
a	5.60e-5	7.57e-4	0.00166	7.72e-4	0.00411	0.500
sd(a)/a	2.67261	0.87191	0.55206	0.86978	1.00754	

reactions
1)   4an + 2ed = ab + 2gr + py + naph + hb
2)   12an + 3tr + 3ed = 3ab + 4gr + 2py + 6hb
3)   12an + 6tr + 3parg = 3ab + 4gr + 2py + 9hb
4)   11ab + 12gr + 19hb + 21parg = 52an + 32ed + 8H2O
5)   12an + 3py + 3ftr + 3ed = 3ab + 4gr + 5alm + 6hb
6)   12an + 5phl + 3ftr + 3ed = 3ab + 4gr + 2py + 5ann + 6hb

Rock : average pressures (for a(H2O) = 0.5)

Single end-member diagnostic information

av, sd, fit are result of doubling the uncertainty on ln a :
a ln a is suspect if any are v different from lsq values.
e* are ln a residuals normalised to ln a uncertainties :
large absolute values, say >2.5, point to suspect info.
hat are the diagonal elements of the hat matrix :
large values, say >0.43, point to influential data.
For 95% confidence, fit (= sd(fit)) should be less than 1.49;
however a larger value may be OK - look at the diagnostics!

	av	sd	fit
lsq	7.35	1.53	1.03

	P	sd	fit	e*	hat
an	7.32	1.56	1.03	0.1	0.01
ab	7.35	1.53	1.03	-0.0	0.00
gr	7.70	2.32	1.03	0.1	0.45
py	7.37	1.53	1.03	0.2	0.01
alm	7.41	1.58	1.03	0.1	0.02
phl	7.99	1.37	0.87	1.0	0.08
ann	7.66	1.46	0.96	-0.6	0.03
naph	7.33	1.52	1.03	0.3	0.00
tr	7.36	1.45	0.98	0.9	0.00
ftr	6.90	1.34	0.88	0.9	0.04
hb	6.87	1.17	0.77	-1.3	0.03
ed	7.51	1.69	1.03	-0.2	0.17
parg	7.22	1.59	1.03	0.3	0.08
H2O	7.35	1.53	1.03	0	0

T°C	500	550	600	650	700	750	800	850	900
av P	6.3	6.5	6.8	7.1	7.4	7.6	7.9	8.2	8.6
sd	1.37	1.35	1.37	1.43	1.53	1.65	1.78	1.93	2.09
f	1.1	1.1	1.0	1.0	1.0	1.1	1.1	1.1	1.2

an independent set of reactions has been calculated

Rock name :A1028-27 (suggested T = 700°C) (for a(H2O) = 0.75)

	an	ab	gr	py	alm	phl	ann
naph							
a	0.604	0.540	0.0110	0.00108	0.254	0.0267	0.113
0.00127							
sd(a)/a	0.05000	0.06348	0.54440	1.16667	0.15000	0.42007	0.23950
7.86782							

	tr	ftr	hb	ed	parg	H2O
a	5.60e-5	7.57e-4	0.00166	7.72e-4	0.00411	0.750
sd(a)/a	2.67261	0.87191	0.55206	0.86978	1.00754	

reactions
1)   4an + 2ed = ab + 2gr + py + naph + hb
2)   12an + 3tr + 3ed = 3ab + 4gr + 2py + 6hb
3)   12an + 6tr + 3parg = 3ab + 4gr + 2py + 9hb
4)   11ab + 12gr + 40hb = 52an + 21tr + 11ed + 8H2O
5)   12an + 3py + 3ftr + 3ed = 3ab + 4gr + 5alm + 6hb
6)   12an + 5phl + 3ftr + 3ed = 3ab + 4gr + 2py + 5ann + 6hb

Rock : average pressures (for a(H2O) = 0.75)

Single end-member diagnostic information

av, sd, fit are result of doubling the uncertainty on ln a :
a ln a is suspect if any are v different from lsq values.
e* are ln a residuals normalised to ln a uncertainties :
large absolute values, say >2.5, point to suspect info.
hat are the diagonal elements of the hat matrix :
large values, say >0.43, point to influential data.
For 95% confidence, fit (= sd(fit)) should be less than 1.49;
however a larger value may be OK - look at the diagnostics!

	av	sd	fit
lsq	7.77	1.43	0.96

	P	sd	fit	e*	hat
an	7.74	1.46	0.96	0.0	0.01
ab	7.76	1.44	0.96	-0.0	0.00
gr	7.99	2.19	0.96	0.1	0.45
py	7.78	1.44	0.96	0.1	0.01
alm	7.81	1.48	0.96	0.1	0.02
phl	8.35	1.52	0.82	0.9	0.08
ann	8.05	1.48	0.90	-0.5	0.03
naph	7.75	1.44	0.96	0.3	0.00
tr	7.78	1.43	0.91	0.8	0.00
ftr	7.36	1.48	0.81	0.9	0.04
hb	7.39	1.46	0.75	-1.1	0.03
ed	8.00	1.58	0.95	-0.3	0.16
parg	7.57	1.51	0.94	0.4	0.09
H2O	7.77	1.43	0.96	0	0

T°C	500	550	600	650	700	750	800	850	900
av P	6.5	6.8	7.1	7.5	7.8	8.1	8.4	8.8	9.1
sd	1.30	1.26	1.29	1.36	1.43	1.50	1.60	1.73	1.87
f	1.1	1.0	1.0	1.0	1.0	1.0	1.0	1.0	1.1

an independent set of reactions has been calculated

Rock name : A1028-27 (for a(H2O) = 0.25)

	an	ab	gr	py	alm	phl	ann
naph a	0.604	0.540	0.0110	0.00108	0.254	0.0267	0.113
0.00127							
sd(a)/a	0.05000	0.06348	0.54440	1.16667	0.15000	0.42007	0.23950
7.86782							

	tr	ftr	hb	ed	parg	H2O
a	5.60e-5	7.57e-4	0.00166	7.72e-4	0.00411	0.250
sd(a)/a	2.67261	0.87191	0.55206	0.86978	1.00754	

reactions
1)   3ab + 2gr + py + 9hb = 12an + 3naph + 6tr
2)   4an + 2ed = ab + 2gr + py + naph + hb
3)   12an + naph + 3ed = 4ab + 6gr + 6py + 4H2O
4)   12an + 6tr + 3parg = 3ab + 4gr + 2py + 9hb
5)   12an + 5alm + 9ed = 3ab + 8gr + 9py + 6naph + 3ftr
6)   3ab + 2gr + py + 10ann + 9hb = 12an + 10phl + 3naph + 6ftr   .

Rock : average PT (for a(H2O) = 0.25)

Single end-member diagnostic information

avP, avT, sd's, cor, fit are result of doubling the uncertainty on ln
a :
a ln a is suspect if any are v different from lsq values.
e* are ln a residuals normalised to ln a uncertainties :
large absolute values, say >2.5, point to suspect info.
hat are the diagonal elements of the hat matrix :
large values, say >0.43, point to influential data.
For 95% confidence, fit (= sd(fit)) should be less than 1.49
however a larger value may be OK - look at the diagnostics!

	avP	sd	avT	sd	cor	fit
lsq	6.0	1.8	579	152	0.364	1.28

	P	sd(P)	T	sd(T)	cor	fit	e*	hat
an	5.99	1.81	579	152	0.353	1.28	-0.05	0.01
ab	6.01	1.79	579	152	0.363	1.28	0.00	0.00
gr	6.33	2.67	582	153	0.343	1.28	-0.12	0.45
py	5.69	1.95	522	211	0.541	1.26	0.37	0.63
alm	6.09	1.81	577	151	0.340	1.27	-0.16	0.03
phl	6.64	1.51	574	123	0.340	1.04	-1.19	0.07
ann	6.31	1.67	576	139	0.352	1.17	0.68	0.02
naph	5.99	1.78	578	151	0.366	1.27	-0.27	0.01
tr	6.02	1.67	577	142	0.364	1.20	-0.99	0.00
ftr	5.70	1.59	602	134	0.326	1.12	-0.94	0.05
hb	5.84	1.40	654	127	0.314	0.97	1.28	0.12
ed	6.17	1.86	563	162	0.207	1.27	0.27	0.26
parg	5.74	1.95	558	164	0.476	1.26	-0.34	0.22
H2O	6.01	1.78	579	152	0.364	1.28	0	0

T = 579°C, sd = 152,
P = 6.0 kbars, sd = 1.8, cor = 0.364, f = 1.28
****

an independent set of reactions has been calculated

Rock name : A1028-27 (for a(H2O) = 0.5)

	an	ab	gr	py	alm	phl	ann
naph							
a	0.604	0.540	0.0110	0.00108	0.254	0.0267	0.113
0.00127							
sd(a)/a	0.05000	0.06348	0.54440	1.16667	0.15000	0.42007	0.23950
7.86782							

	tr	ftr	hb	ed	parg	H2O
a	5.60e-5	7.57e-4	0.00166	7.72e-4	0.00411	0.500
sd(a)/a	2.67261	0.87191	0.55206	0.86978	1.00754	

reactions
1)   3ab + 2gr + py + 9hb = 12an + 3naph + 6tr
2)   4an + 2ed = ab + 2gr + py + naph + hb
3)   12an + naph + 3ed = 4ab + 6gr + 6py + 4H2O
4)   12an + 6tr + 3parg = 3ab + 4gr + 2py + 9hb
5)   12an + 5alm + 9ed = 3ab + 8gr + 9py + 6naph + 3ftr
6)   3ab + 2gr + py + 10ann + 9hb = 12an + 10phl + 3naph + 6ftr

Rock : average PT (for a(H2O) = 0.5)

Single end-member diagnostic information

avP, avT, sd's, cor, fit are result of doubling the uncertainty on ln
a :
a ln a is suspect if any are v different from 1sq values.
e* are ln a residuals normalised to ln a uncertainties :
large absolute values, say >2.5, point to suspect info.
hat are the diagonal elements of the hat matrix :
large values, say >0.43, point to influential data.
For 95% confidence, fit (= sd(fit)) should be less than 1.49
however a larger value may be OK - look at the diagnostics!

	avP	sd	avT	sd	cor	fit
1sq	6.8	1.8	618	152	0.436	1.17

	P	sd(P)	T	sd(T)	cor	fit	e*	hat
an	6.80	1.78	618	152	0.424	1.17	-0.04	0.01
ab	6.82	1.76	618	152	0.434	1.17	0.00	0.00
gr	7.11	2.59	621	153	0.392	1.16	-0.10	0.45
py	6.58	1.99	580	214	0.612	1.16	0.22	0.63
alm	6.88	1.78	616	151	0.411	1.16	-0.12	0.03
phl	7.39	1.56	612	130	0.409	0.96	-1.06	0.07
ann	7.10	1.65	615	140	0.422	1.07	0.60	0.02
naph	6.79	1.75	616	151	0.437	1.16	-0.29	0.01
tr	6.82	1.65	616	143	0.436	1.10	-0.89	0.00
ftr	6.53	1.54	642	133	0.399	1.01	-0.90	0.05
hb	6.73	1.50	691	139	0.393	0.90	1.16	0.12
ed	7.01	1.79	595	160	0.289	1.15	0.35	0.27
parg	6.44	1.92	589	162	0.538	1.14	-0.42	0.22
H2O	6.82	1.75	618	152	0.436	1.17	0	0

T = 618°C, sd = 152,
P = 6.8 kbars, sd = 1.8, cor = 0.436, f = 1.17
****

an independent set of reactions has been calculated

Rock name : A1028-27 (for a(H2O) = 0.25)

	an	ab	gr	py	alm	phl	ann
naph							
a	0.604	0.540	0.0110	0.00108	0.254	0.0267	0.113
0.00127							
sd(a)/a	0.05000	0.06348	0.54440	1.16667	0.15000	0.42007	0.23950
7.86782							

	tr	ftr	hb	ed	parg	H2O
a	5.60e-5	7.57e-4	0.00166	7.72e-4	0.00411	0.250
sd(a)/a	2.67261	0.87191	0.55206	0.86978	1.00754	

reactions
1)   3ab + 2gr + py + 9hb = 12an + 3naph + 6tr
2)   4an + 2ed = ab + 2gr + py + naph + hb
3)   12an + naph + 3ed = 4ab + 6gr + 6py + 4H2O
4)   12an + 6tr + 3parg = 3ab + 4gr + 2py + 9hb
5)   12an + 5alm + 9ed = 3ab + 8gr + 9py + 6naph + 3ftr
6)   3ab + 2gr + py + 10ann + 9hb = 12an + 10phl + 3naph + 6ftr   .

Rock : average PT (for a(H2O) = 0.25)

Single end-member diagnostic information

avP, avT, sd's, cor, fit are result of doubling the uncertainty on ln
a :
a ln a is suspect if any are v different from lsq values.
e* are ln a residuals normalised to ln a uncertainties :
large absolute values, say >2.5, point to suspect info.
hat are the diagonal elements of the hat matrix :
large values, say >0.43, point to influential data.
For 95% confidence, fit (= sd(fit)) should be less than 1.49
however a larger value may be OK - look at the diagnostics!

	avP	sd	avT	sd	cor	fit
lsq	6.0	1.8	579	152	0.364	1.28

	P	sd(P)	T	sd(T)	cor	fit	e*	hat
an	5.99	1.81	579	152	0.353	1.28	-0.05	0.01
ab	6.01	1.79	579	152	0.363	1.28	0.00	0.00
gr	6.33	2.67	582	153	0.343	1.28	-0.12	0.45
py	5.69	1.95	522	211	0.541	1.26	0.37	0.63
alm	6.09	1.81	577	151	0.340	1.27	-0.16	0.03
phl	6.64	1.51	574	123	0.340	1.04	-1.19	0.07
ann	6.31	1.67	576	139	0.352	1.17	0.68	0.02
naph	5.99	1.78	578	151	0.366	1.27	-0.27	0.01
tr	6.02	1.67	577	142	0.364	1.20	-0.99	0.00
ftr	5.70	1.59	602	134	0.326	1.12	-0.94	0.05
hb	5.84	1.40	654	127	0.314	0.97	1.28	0.12
ed	6.17	1.86	563	162	0.207	1.27	0.27	0.26
parg	5.74	1.95	558	164	0.476	1.26	-0.34	0.22
H2O	6.01	1.78	579	152	0.364	1.28	0	0

T = 579°C, sd = 152,
P = 6.0 kbars, sd = 1.8, cor = 0.364, f = 1.28
****

an independent set of reactions has been calculated

Rock name : A1028-27 (for a(H2O) = 0.5)

	an	ab	gr	py	alm	phl	ann	naph
a	0.604	0.540	0.0110	0.00108	0.254	0.0267	0.113	0.00127
sd(a)/a	0.05000	0.06348	0.54440	1.16667	0.15000	0.42007	0.23950	7.86782

	tr	ftr	hb	ed	parg	H2O
a	5.60e-5	7.57e-4	0.00166	7.72e-4	0.00411	0.500
sd(a)/a	2.67261	0.87191	0.55206	0.86978	1.00754	

reactions
1)   3ab + 2gr + py + 9hb = 12an + 3naph + 6tr
2)   4an + 2ed = ab + 2gr + py + naph + hb
3)   12an + naph + 3ed = 4ab + 6gr + 6py + 4H2O
4)   12an + 6tr + 3parg = 3ab + 4gr + 2py + 9hb
5)   12an + 5alm + 9ed = 3ab + 8gr + 9py + 6naph + 3ftr
6)   3ab + 2gr + py + 10ann + 9hb = 12an + 10phl + 3naph + 6ftr

Rock : average PT (for a(H2O) = 0.5)

Single end-member diagnostic information

avP, avT, sd's, cor, fit are result of doubling the uncertainty on ln
a :
a ln a is suspect if any are v different from 1sq values.
e* are ln a residuals normalised to ln a uncertainties :
large absolute values, say >2.5, point to suspect info.
hat are the diagonal elements of the hat matrix :
large values, say >0.43, point to influential data.
For 95% confidence, fit (= sd(fit)) should be less than 1.49
however a larger value may be OK - look at the diagnostics!

	avP	sd	avT	sd	cor	fit
1sq	6.8	1.8	618	152	0.436	1.17

	P	sd(P)	T	sd(T)	cor	fit	e*	hat
an	6.80	1.78	618	152	0.424	1.17	-0.04	0.01
ab	6.82	1.76	618	152	0.434	1.17	0.00	0.00
gr	7.11	2.59	621	153	0.392	1.16	-0.10	0.45
py	6.58	1.99	580	214	0.612	1.16	0.22	0.63
alm	6.88	1.78	616	151	0.411	1.16	-0.12	0.03
phl	7.39	1.56	612	130	0.409	0.96	-1.06	0.07
ann	7.10	1.65	615	140	0.422	1.07	0.60	0.02
naph	6.79	1.75	616	151	0.437	1.16	-0.29	0.01
tr	6.82	1.65	616	143	0.436	1.10	-0.89	0.00
ftr	6.53	1.54	642	133	0.399	1.01	-0.90	0.05
hb	6.73	1.50	691	139	0.393	0.90	1.16	0.12
ed	7.01	1.79	595	160	0.289	1.15	0.35	0.27
parg	6.44	1.92	589	162	0.538	1.14	-0.42	0.22
H2O	6.82	1.75	618	152	0.436	1.17	0	0

T = 618°C, sd = 152,
P = 6.8 kbars, sd = 1.8, cor = 0.436, f = 1.17
****

an independent set of reactions has been calculated

Rock name :A1028-27 (for x(CO2) = 0.95 and x(H2O) = 0.05)

	an	ab	gr	py	alm	phl	ann
naph							
a	0.604	0.540	0.0110	0.00108	0.254	0.0267	0.113
0.00127							
sd(a)/a	0.05000	0.06348	0.54440	1.16667	0.15000	0.42007	0.23950
7.86782							

	tr	ftr	hb	ed	parg	H2O
a	5.60e-5	7.57e-4	0.00166	7.72e-4	0.00411	0.0500
sd(a)/a	2.67261	0.87191	0.55206	0.86978	1.00754	

reactions
1)   3ab + 2gr + py + 9hb = 12an + 3naph + 6tr
2)   4an + 2ed = ab + 2gr + py + naph + hb
3)   12an + naph + 3ed = 4ab + 6gr + 6py + 4H2O
4)   12an + 6tr + 3parg = 3ab + 4gr + 2py + 9hb
5)   12an + 5alm + 9ed = 3ab + 8gr + 9py + 6naph + 3ftr
6)   3ab + 2gr + py + 10ann + 9hb = 12an + 10phl + 3naph + 6ftr

Rock : average PT (for x(CO2) = 0.95 and x(H2O) = 0.05)

Single end-member diagnostic information

avP, avT, sd's, cor, fit are result of doubling the uncertainty on ln a :
a ln a is suspect if any are v different from lsq values.
e* are ln a residuals normalised to ln a uncertainties :
large absolute values, say >2.5, point to suspect info.
hat are the diagonal elements of the hat matrix :
large values, say >0.43, point to influential data.
For 95% confidence, fit (= sd(fit)) should be less than 1.49
however a larger value may be OK - look at the diagnostics!

	avP	sd	avT	sd	cor	fit
lsq	5.0	1.8	518	140	0.192	1.45

	P	sd(P)	T	sd(T)	cor	fit	e*	hat
an	4.97	1.88	518	140	0.183	1.45	-0.06	0.01
ab	5.00	1.85	518	140	0.192	1.45	0.00	0.00
gr	5.39	2.78	522	141	0.246	1.45	-0.16	0.44
py	4.68	1.85	441	184	0.330	1.39	0.68	0.59
alm	5.11	1.88	515	139	0.173	1.44	-0.22	0.02
phl	5.70	1.55	518	112	0.185	1.16	-1.39	0.07
ann	5.33	1.72	518	127	0.189	1.32	0.79	0.02
naph	4.98	1.85	517	140	0.195	1.45	-0.24	0.01
tr	5.00	1.73	517	131	0.192	1.36	-1.13	0.00
ftr	4.62	1.70	538	127	0.149	1.30	-0.97	0.06
hb	4.61	1.43	592	116	0.113	1.11	1.41	0.13
ed	5.14	2.01	507	151	0.012	1.45	0.21	0.27
parg	4.84	1.98	504	154	0.321	1.44	-0.25	0.22
H2O	5.05	1.87	520	140	0.206	1.45	-0.13	0.01

T = 518°C, sd = 140,
P = 5.0 kbars, sd = 1.8, cor = 0.192, f = 1.45
****

an independent set of reactions has been calculated

Rock name : A1028-27 (for x(CO2) = 0.75 and x(H2O) = 0.25)

	an	ab	gr	py	alm	phl	ann
naph
a	0.604	0.540	0.0110	0.00108	0.254	0.0267	0.113
0.00127
sd(a)/a	0.05000	0.06348	0.54440	1.16667	0.15000	0.42007	0.23950
7.86782

	tr	ftr	hb	ed	parg	H2O
a	5.60e-5	7.57e-4	0.00166	7.72e-4	0.00411	0.250
sd(a)/a	2.67261	0.87191	0.55206	0.86978	1.00754

reactions
1)   3ab + 2gr + py + 9hb = 12an + 3naph + 6tr
2)   4an + 2ed = ab + 2gr + py + naph + hb
3)   12an + naph + 3ed = 4ab + 6gr + 6py + 4H2O
4)   12an + 6tr + 3parg = 3ab + 4gr + 2py + 9hb
5)   12an + 5alm + 9ed = 3ab + 8gr + 9py + 6naph + 3ftr
6)   3ab + 2gr + py + 10ann + 9hb = 12an + 10phl + 3naph + 6ftr

Rock : average PT (for x(CO2) = 0.75 and x(H2O) = 0.25)

Single end-member diagnostic information

avP, avT, sd's, cor, fit are result of doubling the uncertainty on ln
a :
a ln a is suspect if any are v different from lsq values.
e* are ln a residuals normalised to ln a uncertainties :
large absolute values, say >2.5, point to suspect info.
hat are the diagonal elements of the hat matrix :
large values, say >0.43, point to influential data.
For 95% confidence, fit (= sd(fit)) should be less than 1.49
however a larger value may be OK - look at the diagnostics!

	avP	sd	avT	sd	cor	fit
lsq	6.5	1.7	594	142	0.340	1.21

	P	sd(P)	T	sd(T)	cor	fit	e*	hat
an	6.49	1.75	594	142	0.329	1.21	-0.04	0.01
ab	6.51	1.73	594	142	0.339	1.21	0.00	0.00
gr	6.82	2.59	598	143	0.337	1.20	-0.11	0.45
py	6.25	1.85	547	193	0.503	1.19	0.34	0.60
alm	6.58	1.75	592	141	0.318	1.20	-0.14	0.02
phl	7.12	1.49	594	117	0.324	0.99	-1.11	0.07
ann	6.80	1.62	594	130	0.332	1.11	0.63	0.02
naph	6.48	1.72	593	141	0.342	1.20	-0.29	0.01
tr	6.51	1.62	594	133	0.340	1.13	-0.93	0.00
ftr	6.18	1.53	617	125	0.299	1.05	-0.90	0.06
hb	6.32	1.43	668	127	0.281	0.93	1.18	0.13
ed	6.73	1.79	573	151	0.172	1.19	0.35	0.28
parg	6.17	1.86	567	153	0.459	1.18	-0.41	0.23
H2O	6.52	1.73	595	142	0.342	1.21	-0.04	0.00

T = 594°C, sd = 142,
P = 6.5 kbars, sd = 1.7, cor = 0.340, f = 1.21
****

an independent set of reactions has been calculated

Rock name : A1028-27 (for x(CO2) = 0.5 and x(H2O) = 0.5)

```
                 an       ab       gr       py      alm      phl      ann
naph
a               0.604    0.540   0.0110  0.00108    0.254   0.0267    0.113
0.00127
sd(a)/a        0.05000  0.06348  0.54440  1.16667  0.15000  0.42007  0.23950
7.86782
```

```
                 tr      ftr       hb       ed     parg      H2O
a             5.60e-5  7.57e-4  0.00166  7.72e-4  0.00411    0.500
sd(a)/a        2.67261  0.87191  0.55206  0.86978  1.00754
```

reactions
1)   3ab + 2gr + py + 9hb = 12an + 3naph + 6tr
2)   4an + 2ed = ab + 2gr + py + naph + hb
3)   12an + naph + 3ed = 4ab + 6gr + 6py + 4H2O
4)   12an + 6tr + 3parg = 3ab + 4gr + 2py + 9hb
5)   12an + 5alm + 9ed = 3ab + 8gr + 9py + 6naph + 3ftr
6)   3ab + 2gr + py + 10ann + 9hb = 12an + 10phl + 3naph + 6ftr

Rock : average PT (for x(CO2) = 0.5 and x(H2O) = 0.5)

Single end-member diagnostic information

avP, avT, sd's, cor, fit are result of doubling the uncertainty on ln
a :
a ln a is suspect if any are v different from lsq values.
e* are ln a residuals normalised to ln a uncertainties :
large absolute values, say >2.5, point to suspect info.
hat are the diagonal elements of the hat matrix :
large values, say >0.43, point to influential data.
For 95% confidence, fit (= sd(fit)) should be less than 1.49
however a larger value may be OK - look at the diagnostics!

```
             avP     sd     avT     sd    cor     fit
      lsq    7.1     1.7     627    146  0.420    1.13

              P    sd(P)      T   sd(T)    cor     fit      e*     hat

       an   7.09    1.74     627    146   0.408    1.13   -0.04    0.01
       ab   7.11    1.72     627    146   0.419    1.13    0.00    0.00
       gr   7.40    2.55     630    147   0.386    1.13   -0.10    0.45
       py   6.90    1.92     594    203   0.590    1.12    0.20    0.61
      alm   7.17    1.75     625    146   0.396    1.13   -0.11    0.03
      phl   7.67    1.58     624    129   0.398    0.94   -1.01    0.07
      ann   7.38    1.62     625    135   0.409    1.04    0.58    0.02
     naph   7.08    1.71     625    145   0.422    1.12   -0.30    0.01
       tr   7.11    1.61     626    138   0.420    1.06   -0.86    0.00
      ftr   6.81    1.54     651    131   0.382    0.98   -0.87    0.06
       hb   7.00    1.52     700    139   0.373    0.88    1.10    0.12
       ed   7.33    1.74     601    154   0.266    1.10    0.40    0.27
     parg   6.69    1.86     594    156   0.528    1.10   -0.46    0.22
      H2O   7.11    1.72     627    146   0.421    1.13   -0.02    0.00
```

T = 627°C, sd = 146,
P = 7.1 kbars, sd = 1.7, cor = 0.420, f = 1.13
****

an independent set of reactions has been calculated

Rock name : A1028-27 (for x(CO2) = 0.25 and x(H2O) = 0.75)

	an	ab	gr	py	alm	phl	ann
naph							
a	0.604	0.540	0.0110	0.00108	0.254	0.0267	0.113
0.00127							
sd(a)/a	0.05000	0.06348	0.54440	1.16667	0.15000	0.42007	0.23950
7.86782							

	tr	ftr	hb	ed	parg	H2O
a	5.60e-5	7.57e-4	0.00166	7.72e-4	0.00411	0.750
sd(a)/a	2.67261	0.87191	0.55206	0.86978	1.00754	

reactions
1)   3ab + 2gr + py + 9hb = 12an + 3naph + 6tr
2)   4an + 2ed = ab + 2gr + py + naph + hb
3)   12an + naph + 3ed = 4ab + 6gr + 6py + 4H2O
4)   12an + 6tr + 3parg = 3ab + 4gr + 2py + 9hb
5)   12an + 5alm + 9ed = 3ab + 8gr + 9py + 6naph + 3ftr
6)   3ab + 2gr + py + 10ann + 9hb = 12an + 10phl + 3naph + 6ftr

Rock : average PT (for x(CO2) = 0.25 and x(H2O) = 0.75)

Single end-member diagnostic information

avP, avT, sd's, cor, fit are result of doubling the uncertainty on ln a :
a ln a is suspect if any are v different from lsq values.
e* are ln a residuals normalised to ln a uncertainties :
large absolute values, say >2.5, point to suspect info.
hat are the diagonal elements of the hat matrix :
large values, say >0.43, point to influential data.
For 95% confidence, fit (= sd(fit)) should be less than 1.49
however a larger value may be OK - look at the diagnostics!

	avP	sd	avT	sd	cor	fit
lsq	7.4	1.7	645	150	0.472	1.10

	P	sd(P)	T	sd(T)	cor	fit	e*	hat
an	7.40	1.76	645	150	0.460	1.10	-0.04	0.01
ab	7.42	1.74	645	150	0.471	1.10	0.00	0.00
gr	7.69	2.55	648	151	0.419	1.09	-0.09	0.45
py	7.26	2.00	622	212	0.645	1.09	0.13	0.63
alm	7.47	1.76	643	150	0.448	1.09	-0.10	0.03
phl	7.95	1.64	640	137	0.446	0.92	-0.96	0.07
ann	7.68	1.63	642	139	0.459	1.01	0.55	0.02
naph	7.39	1.72	643	149	0.474	1.09	-0.31	0.01
tr	7.42	1.63	643	142	0.472	1.03	-0.83	0.00
ftr	7.14	1.60	669	139	0.437	0.94	-0.86	0.05
hb	7.37	1.58	717	147	0.433	0.85	1.07	0.12
ed	7.63	1.74	616	157	0.331	1.07	0.41	0.27
parg	6.95	1.88	609	159	0.570	1.06	-0.48	0.22
H2O	7.42	1.73	645	150	0.472	1.10	-0.01	0.00

T = 645°C, sd = 150,
P = 7.4 kbars, sd = 1.7, cor = 0.472, f = 1.10

PROBE DATA

Garnet analysis

	1028-12	1028-21	1028-27	1028-67	1028-99	1028-100	1028-119	SEP-112
SiO2	37.460	37.280	37.210	37.310	37.190	39.111	37.540	37.120
TiO2	0.120	0.060	0.040			0.069	0.170	0.037
Al2O3	20.320	19.970	20.620	20.840	20.030	20.843	19.490	21.116
Cr2O3	0.000			0.010	0.140	0.000		0.037
MgO	2.380	0.920	2.220	4.990	2.360	6.847	1.800	3.696
CaO	7.240	7.870	7.440	0.920	1.570	7.218	9.560	0.918
MnO	3.150	3.690	1.700	1.010	1.570	0.815	2.670	1.492
FeO	28.250	30.000	29.860	34.480	29.620	25.772	28.140	37.104
Fe2O3	1.450	1.990	0.820	0.630	1.560		3.160	
NiO						0.017		0.024
ZnO						0.043		0.000
Na2O	0.020	0.040				0.053	0.020	0.054
K2O	0.010	0.010			0.010	0.025	0.010	0.016
F						0.012		0.000
Cl						0.000		0.001
TOTAL	100.400	101.830	99.910	100.190	94.050	100.825	102.560	101.615
Si	2.990	2.980	2.990	2.980	2.990	6.037	2.960	5.918
Ti	0.010	0.000	0.000			0.008	0.010	0.004
Al	1.910	1.880	1.950	1.960	1.900	3.792	1.810	3.968
Cr	0.000			0.000	0.010	0.000		0.005
Mg	0.280	0.110	0.270	0.590	0.280	1.575	0.210	0.878
Ca	0.620	0.670	0.640	0.080	0.650	1.194	0.810	0.157
Mn	0.210	0.250	0.120	0.070	0.110	0.107	0.180	0.201
Fe3	0.090	0.120	0.050	0.040	0.090		0.190	
Fe2	1.890	2.000	2.000	2.300	1.990	3.327	1.860	4.947
Ni						0.002		0.003
Zn						0.005	-	0.000
Na	0.000	0.010				0.016	0.000	0.017
K2	0.000	0.000			0.000	0.005	0.000	0.003
F								0.000
Cl						0.000		0.000
TOTAL	8.000	8.020	8.020	8.020	8.020	16.068	8.030	16.101

PROBE DATA

Plagioclase analysis

	1028-12	1028-21	1028-27	1028-67	1028-99	1028-100	1028-119	SEP-112
SiO2	58.580	62.600	58.360	63.920	55.130	55.561	58.500	62.952
TiO2	0.010	0.050	0.010	0.000		0.000	0.010	0.035
Al2O3	26.620	24.760	26.860	24.400	28.360	28.062	26.690	23.897
Cr2O3			0.010	0.040	0.020	0.013	0.010	0.004
MgO						0.000		0.000
CaO	9.070	6.760	9.240	5.820	11.470	10.979	9.000	5.842
MnO	0.030			0.010	0.040	0.014	0.000	0.000
FeO						0.084		0.247
Fe2O3	0.310			0.010	0.200		0.100	
NiO						0.000		0.000
ZnO						0.000		0.006
Na2O	5.990	7.010	5.970	7.240	4.870	5.179	6.150	7.669
K2O	0.120	0.230	0.230	0.170	0.170	0.085	0.200	0.100
F						0.043		0.000
Cl						0.003		0.000
TOTAL	100.730	101.410	100.680	101.610	100.260	100.023	100.660	100.752
Si	2.600	2.730	2.590	2.770	2.480	7.502	2.600	8.293
Ti	0.000	0.000	0.000	0.000		0.000	0.000	0.003
Al	1.390	1.270	1.410	1.250	1.500	4.466	11.400	3.710
Cr			0.000	0.000	0.000	0.001	0.000	0.000
Mg						0.000		0.000
Ca	0.430	0.320	0.440	0.270	0.550	1.588	0.430	0.825
Mn	0.000			0.000	0.000	0.002	0.000	0.000
Fe3			0.000	0.000	0.010		0.000	
Fe2						0.009		0.027
Ni						0.000		0.000
Zn						0.000		0.001
Na	0.520	0.590	0.510	0.610	0.420	1.356	0.530	1.959
K2	0.010	0.010	0.010	0.010	0.010	0.015	0.010	0.017
F								0.000
Cl								0.000
TOTAL	4.950	4.920	4.960	4.910	4.970	14.939	14.970	14.835

PROBE DATA

Clinopyroxene analysis

	1028-27	1028-99	1028-100
SiO2	50.780	51.490	52.019
TiO2	0.170	0.140	0.324
Al2O3	1.940	1.450	2.773
Cr2O3			0.038
MgO	9.460	9.300	12.653
CaO	21.230	21.580	21.926
MnO	0.240	0.200	0.223
FeO	14.830	15.690	10.205
NiO			0.017
ZnO			0.043
Fe2O3	1.130		
Na2O	0.370	0.310	0.504
K2O	0.000	0.020	0.000
TOTAL	100.150	100.180	100.725
Si	1.950	1.980	7.750
Ti	0.000	0.000	0.036
Al	0.090	0.070	0.487
Cr			0.004
Mg	0.540	0.530	2.810
Ca	0.870	0.890	3.500
Mn	0.010	0.010	0.028
Fe3	0.030		
Fe2	0.480		1.271
Ni			0.008
Zn			0.001
Na	0.030	0.020	0.146
K2	0.000	0.000	0.000
TOTAL	4.000	3.500	16.041

K-Feldspar analysis

	SEP-112
SiO2	63.738
TiO2	0.048
Al2O3	18.640
Cr2O3	0.000
MgO	0.000
CaO	0.000
MnO	0.014
FeO	0.029
NiO	0.088
ZnO	0.019
Na2O	0.986
K2O	13.276
F	0.073
Cl	0.011
TOTAL	96.922
Si	8.989
Ti	0.005
Al	3.098
Cr	0.000
Mg	0.000
Ca	0.000
Mn	0.002
Fe2	0.003
Ni	0.010
Zn	0.002
Na	0.270
K2	2.388
TOTAL	14.767

PROBE DATA

Biotite analysis

	1028-12	1028-21	1028-27	1028-67	SEP-112
SiO2	35.660	34.150	35.790	37.050	35.004
TiO2	4.900	5.000	5.560	4.530	3.128
Al2O3	13.900	13.470	14.060	16.870	18.341
Cr2O3	0.040	0.000		0.080	0.044
MgO	8.780	4.260	8.340	13.030	9.153
CaO	0.010	0.010	0.020	0.010	0.009
MnO	0.090	0.150	0.010	0.120	0.000
FeO	19.680	25.710	20.480	12.300	20.314
Fe2O3	3.860	5.040	4.020	2.410	
NiO					0.000
ZnO					0.107
Na2O	0.020	0.080	0.050	0.160	0.080
K2O	9.120	8.720	8.690	9.220	8.696
F					0.302
Cl					0.100
H2O	3.900	3.790	3.940	4.070	
TOTAL	99.960	100.380	100.960	99.850	95.278
Si	2.740	2.700	2.720	2.730	5.830
Ti	0.280	0.300	0.320	0.250	0.392
Al	1.260	1.260	1.260	1.460	3.600
Cr	0.000	0.000		0.000	0.006
Mg	1.010	0.500	0.950	1.430	2.272
Ca	0.000	0.000	0.000	0.000	0.002
Mn	0.010	0.010	0.000	0.010	0.000
Fe3	0.220	0.300	0.230	0.130	
Fe2	1.270	1.700	1.300	0.760	2.830
Ni		0.000			0.000
Zn		0.010			0.013
Na	0.020	0.080	0.010	0.020	0.026
K2	0.890	0.880	0.840	0.870	1.847
OH	2.000	2.000	2.000	2.000	
TOTAL	9.700	9.740	9.630	9.660	16.818

PROBE DATA

Amphibole analysis

	1028-12	1028-21	1028-27	1028-99	1028-100	1028-119
SiO2	41.540	39.110	39.930	41.100	40.459	40.220
TiO2	1.810	1.630	2.590	2.200	3.334	2.700
Al2O3	11.180	11.340	12.170	11.550	13.325	11.500
Cr2O3	0.020		0.000	0.030	0.045	0.010
MgO	7.910	3.230	6.770	8.140	9.684	5.570
CaO	11.580	11.110	12.120	11.650	11.862	11.520
MnO	0.160	0.170	0.170	0.060	0.155	0.170
FeO	17.260	23.340	17.280	16.590	16.035	20.220
Fe2O3	3.380	4.580	3.390	3.250		3.970
ZnO					0.000	
Na2O	1.250	1.500	1.370	1.300	1.941	1.400
K2O	1.400	1.560	1.800	1.790	1.555	1.730
H2O	1.960	1.890	1.950	1.960		1.950
F					0.117	
CL					0.046	
TOTAL	99.450	99.460	99.540	99.620	98.558	100.960
Si	6.360	6.220	6.150	6.280	6.330	6.190
Ti	0.210	0.200	0.300	0.250	0.392	0.310
Al	2.020	2.120	2.210	2.080	2.457	2.090
Cr	0.000		0.000	0.000	0.006	0.000
Mg	1.800	0.770	1.550	1.850	2.258	1.280
Ca	1.900	1.890	12.120	1.910	1.988	1.900
Mn	0.020	0.020		0.010	0.021	0.020
Fe3	0.390	0.550	0.390	0.370		0.460
Fe2	2.210	3.100	2.230	2.120	2.098	2.600
Zn					0.000	
Na	0.370	0.460	0.410	0.380	0.589	0.420
K2	0.270	0.320	0.350	0.350	0.310	0.340
OH	2.000	2.000	2.000	2.000		2.000
TOTAL	17.550	17.650	27.710	17.600	16.449	17.610

PROBE DATA

Orthpyroxene analysis

	1028-27	1028-99	1028-100
SiO2	49.960	49.510	52.203
TiO2	0.030	0.090	0.087
Al2O3	0.560	0.860	1.028
Cr2O3	0.000	0.000	0.019
MgO	12.870	11.520	19.294
CaO	0.520	0.650	0.397
MnO	0.630	0.540	0.527
FeO	35.360	37.130	27.923
Fe2O3	0.500	0.070	
NiO			0.055
ZnO			0.139
Na2O	0.020	0.030	0.019
K2O	0.020	0.030	0.004
F			0.000
Cl			0.008
TOTAL	100.470	100.430	101.703
Si	1.980	1.980	7.853
Ti	0.000	0.000	0.010
Al	0.030	0.040	0.182
Cr	0.000	0.000	0.002
Mg	0.760	0.690	4.326
Ca	0.020	0.030	0.064
Mn	0.020	0.020	0.067
Fe3	0.020	0.000	
Fe2	1.170	1.240	3.513
Ni			0.007
Zn			0.015
Na	0.000	0.000	0.006
K2	0.000	0.000	0.001
F			0.000
TOTAL	4.000	4.000	16.046

Cordierite analysis

	SEP-112
SiO2	48.555
TiO2	0.000
Al2O3	32.177
Cr2O3	0.000
MgO	8.080
CaO	0.040
MnO	0.108
FeO	8.682
NiO	0.007
ZnO	0.052
Na2O	0.157
K2O	0.011
F	0.129
Cl	0.000
Total	97.998
Si	6.703
Ti	0.000
Al	5.236
Cr	0.000
Mg	1.663
Ca	0.006
Mn	0.013
Fe2	1.002
Ni	0.001
Zn	0.005
Na	0.042
K2	0.002
F	
Cl	0.000
TOTAL	14.673

APPENDIX D

SUMMARY OF ISOTOPIC DATA

APPENDIX D

This appendix includes a table of all isotopic data collected for the two samples analysed, as discussed in section 4.2.
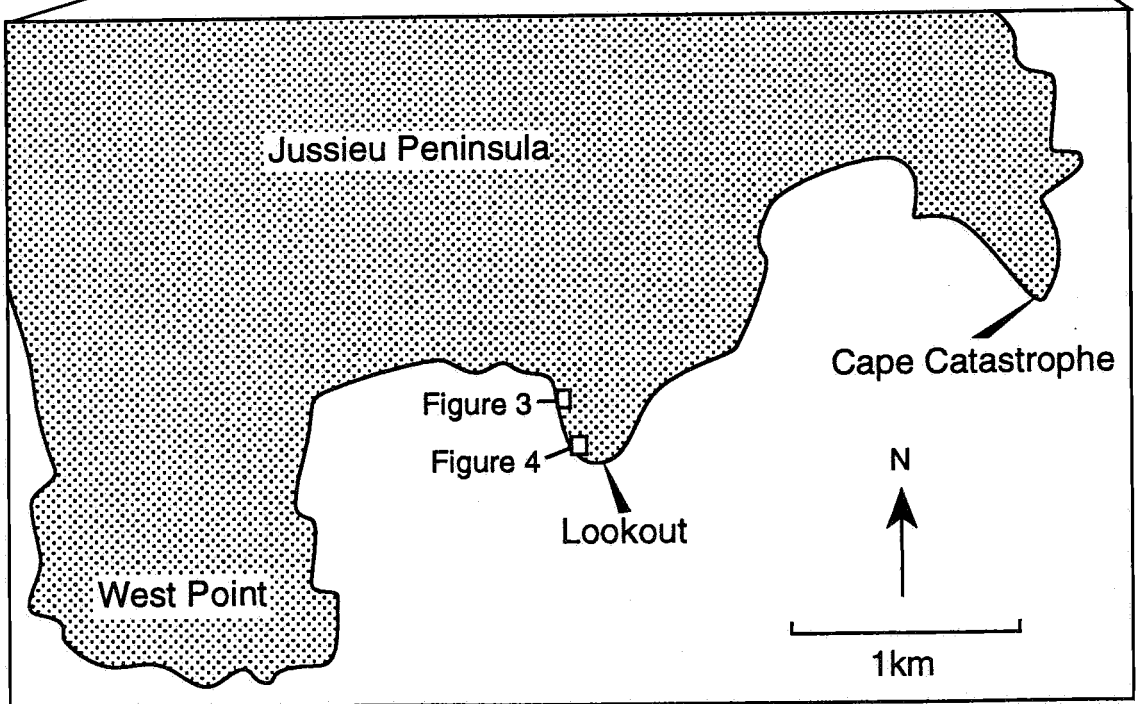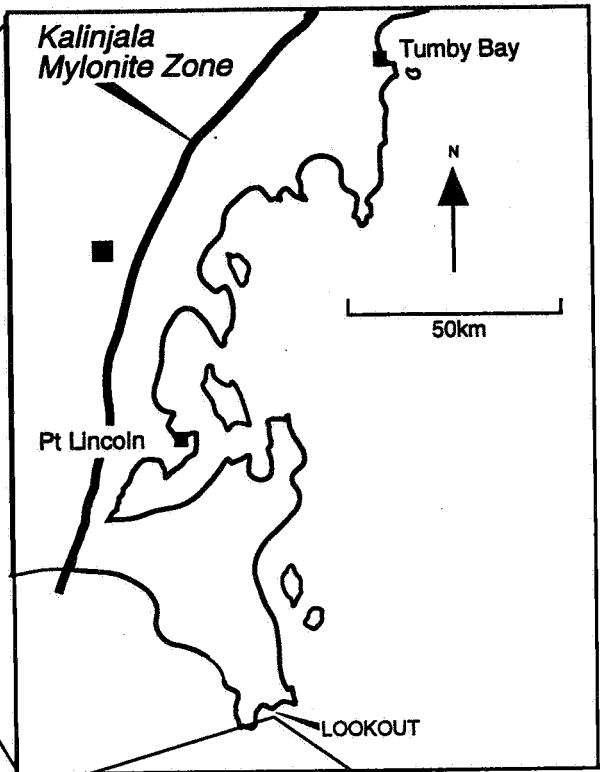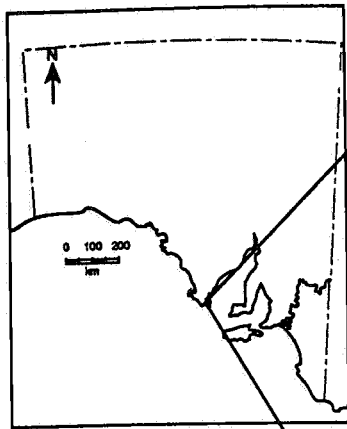
SUMMARY OF ISOTOPE DATA

| Sample No.	1028-110 Whole Rock	1028-110 Garnet	1028-110 Hornblende	1028-99 Whole Rock	1028-99 Garnet	1028-99 Hornblende
Nd ppm	25.016	6.101	35.972	31.912	10.339	46
Sm ppm	5.782	2.631	15.934	6.999	4.997	11
143/144 Nd	0.511876	0.513131	0.513346	0.511627	0.513442	0.511791
2 sigma	0.000059	0.000059	0.000059	0.000059	0.000059	0.000059
Sm/Nd	0.2311	0.4313	0.2193	0.2193	0.4833	0.2391
147 Sm/144 Nd	0.1398	0.2609	0.1327	0.1327	0.2923	0.1447
143/144 Nd ch	0.512638	0.512638	0.512638	0.512638	0.512638	0.512638
143/144 Nd dep	0.513108	0.513108	0.513108	0.513108	0.513108	0.513108
T mod: chur	2.03	1.17	1.51	2.39	1.28	2.47
T mod: dep	2.46	0.08	0.69	2.7	0.67	2.81
eps Nd (0)	-14.8642902	9.616923	13.81091	-19.71762	15.683582	-16.52238
age (T)	1.56	1.56	1.56	1.56	1.56	1.56
143/144 (T)	0.510442	0.510456	0.510598	0.510267	0.510444	0.510308
143/144 ch T	0.510621	0.510621	0.510621	0.5102621	0.510621	0.510621
eps Nd chT	-3.5	-3.23	-0.44	-6.94	-3.46	-6.13
Sr 87/86	0.751932	0.784197	0.73819	0.726084	0.745927	0.7393
2 sigma	0.000049	0.000049	0.000049	0.000049	0.000049	0.000049
Sr ppm	150.898	3.617	35.35	208.945	13.266	28.52
Rb ppm	95.62	4.0015	3.288	56.898	3.8391	3.225
Rb/Sr	0.6337	1.1063	0.093	0.2723	0.2894	0.1131
frac 87	1.215937	1.21979	1.214296	1.212851	1.2152198	1.2144286
at wt Sr	87.61378	87.61155	87.61473	87.61557	87.614195	87.614655
87 Rb/86 Sr	1.84131	3.22477	0.269912	0.789282	0.8404214	0.32817633
87/86 (T)	0.710688	0.71197	0.73214	0.708405	0.727102	0.731949
87/86/300	0.744071	0.77043	0.737038	0.7227145	0.7423392	0.73789899
87/86/400	0.741444	0.765828	0.736653	0.721588	0.7411398	0.73743066
87 Rb/86 Sr	1.84131	3.22477	0.26991	0.789282	0.840421	0.328176
Sr 87/86	0.751932	0.784197	0.73819	0.726084	0.74593	0.7393

APPENDIX E

GEOLOGICAL MAPS

APPENDIX E

This appendix includes three maps. The first is a location map indicating the positions of the two geological maps which follow it. The geological maps are two grid maps which were drawn at Lookout in the Lincoln National Park at Jussieu Peninsula, in order to demonstrate the complex nature of deformation in areas far from the Kalinjala Mylonite Zone, as discussed in section 2.4.

Kalinjala
Mylonite Zone

Tumby Bay

N

50km

Pt Lincoln

LOOKOUT

Jussieu Peninsula

Cape Catastrophe

Figure 3

Figure 4

N

Lookout

West Point

1km

Location of areas mapped at Lookout

FIGURE 3
GEOLOGICAL MAP
OF LOOKOUT

1m
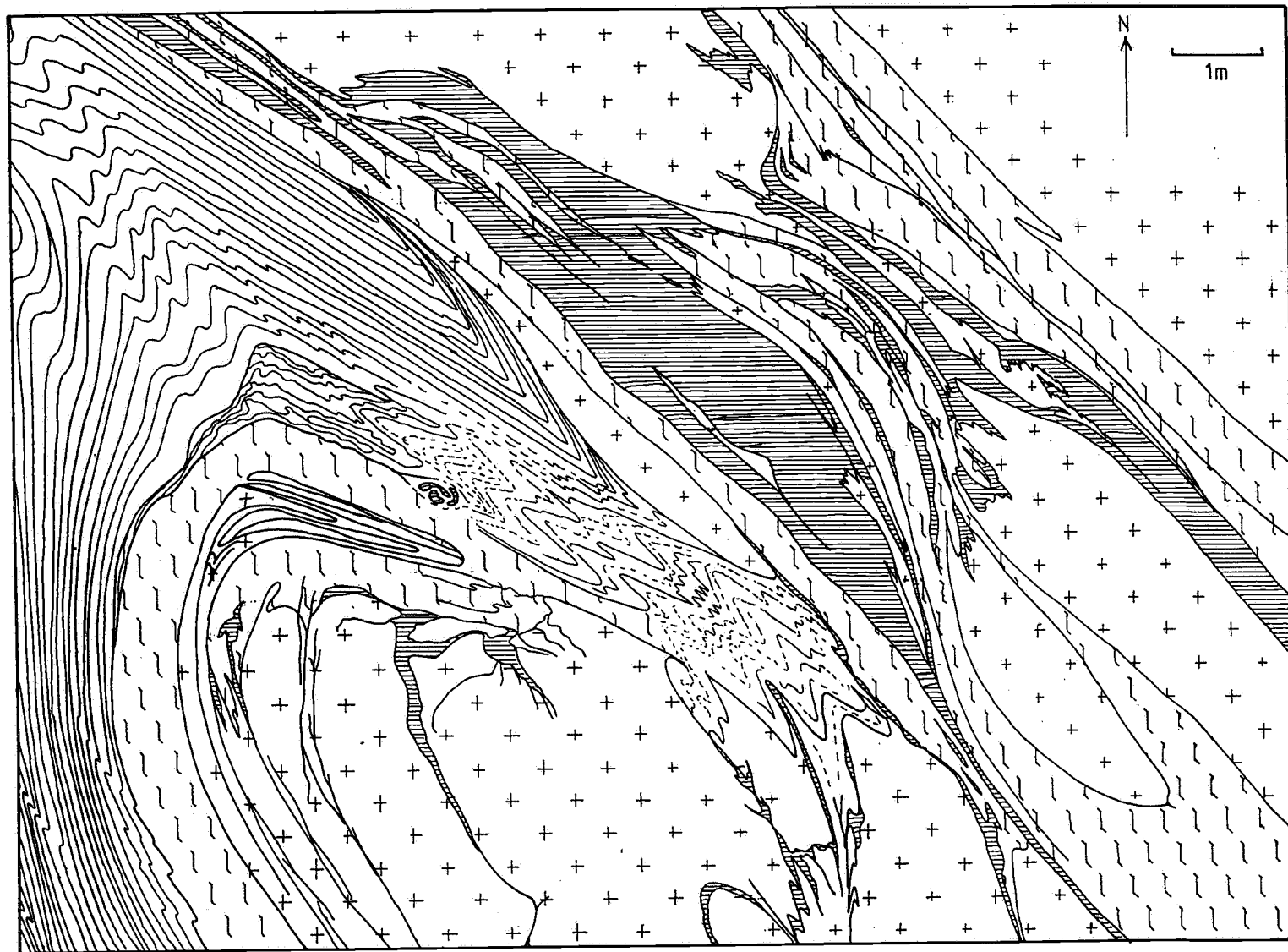
QUARTZOFELDSPATHIC GNEISS WITH
LEUCOCRATIC SEGREGATIONS

MAFIC DYKE

PORPHYROBLASTIC MAFIC

PEGMATITE

LITHOLOGICAL BOUNDARY

FOLIATION TREND